

AD-A217 437

DOCUMENTATION PAGE

Form Approved
OMB No. 0704-0188

1a. REPORT SECURITY CLASSIFICATION UNCLASSIFIED		1b. RESTRICTIVE MARKINGS NONE	
2a. SECURITY CLASSIFICATION AUTHORITY		3. DISTRIBUTION / AVAILABILITY OF REPORT APPROVED FOR PUBLIC RELEASE; DISTRIBUTION UNLIMITED.	
2b. DECLASSIFICATION / DOWNGRADING SCHEDULE			
4. PERFORMING ORGANIZATION REPORT NUMBER(S)		5. MONITORING ORGANIZATION REPORT NUMBER(S) AFIT/CI/CIA-88-20 0	
6a. NAME OF PERFORMING ORGANIZATION AFIT STUDENT AT COLORADO STATE UNIVERSITY	6b. OFFICE SYMBOL (If applicable)	7a. NAME OF MONITORING ORGANIZATION AFIT/CIA	
6c. ADDRESS (City, State, and ZIP Code)		7b. ADDRESS (City, State, and ZIP Code) Wright-Patterson AFB OH 45433-6583	
8a. NAME OF FUNDING / SPONSORING ORGANIZATION	8b. OFFICE SYMBOL (If applicable)	9. PROCUREMENT INSTRUMENT IDENTIFICATION NUMBER	
8c. ADDRESS (City, State, and ZIP Code)		10. SOURCE OF FUNDING NUMBERS	
		PROGRAM ELEMENT NO.	PROJECT NO.
		TASK NO.	WORK UNIT ACCESSION NO.
11. TITLE (Include Security Classification) (UNCLASSIFIED) OBSERVATIONAL EVALUATION OF SNOW COVER EFFECTS ON THE GENERATION AND MODIFICATION OF MESOSCALE CIRCULATIONS			
12. PERSONAL AUTHOR(S) JAMES CRAMER			
13a. TYPE OF REPORT THESIS/DISSERTATION	13b. TIME COVERED FROM TO	14. DATE OF REPORT (Year, Month, Day) 1988	15. PAGE COUNT 155
16. SUPPLEMENTARY NOTATION APPROVED FOR PUBLIC RELEASE IAW AFR 190-1 ERNEST A. HAYGOOD, 1st Lt, USAF Executive Officer, Civilian Institution Programs			
17. COSATI CODES		18. SUBJECT TERMS (Continue on reverse if necessary and identify by block number)	
FIELD	GROUP		
19. ABSTRACT (Continue on reverse if necessary and identify by block number)			
20. DISTRIBUTION / AVAILABILITY OF ABSTRACT <input checked="" type="checkbox"/> UNCLASSIFIED/UNLIMITED <input type="checkbox"/> SAME AS RPT. <input type="checkbox"/> DTIC USERS			
22a. NAME OF RESPONSIBLE INDIVIDUAL ERNEST A. HAYGOOD, 1st Lt, USAF		22b. TELEPHONE (Include Area Code) (513) 255-2259	22c. OFFICE SYMBOL AFIT/CI

DTIC
ELECTE
FEB 01 1990
S D
90 01 31 004 00 E

THESIS

OBSERVATIONAL EVALUATION OF SNOW COVER EFFECTS ON THE
GENERATION AND MODIFICATION OF MESOSCALE CIRCULATIONS



Submitted by
Captain James Cramer
Department of Atmospheric Science

Accession For	
NTIS GRA&I	<input checked="" type="checkbox"/>
DTIC TAB	<input type="checkbox"/>
Unannounced	<input type="checkbox"/>
Justification	
By	
Distribution/	
Availability Codes	
Dist	Avail and/or Special
A-1	

In partial fulfillment of the requirements
for the degree of Master of Science
Colorado State University
Fort Collins, Colorado
Fall 1988

COLORADO STATE UNIVERSITY

July 25, 1988

We hereby recommend that the Thesis OBSERVATIONAL EVALUATION OF SNOW COVER EFFECTS ON THE GENERATION AND MODIFICATION OF MESOSCALE CIRCULATIONS, prepared under our supervision by Captain James Cramer be accepted as fulfilling in part requirements for the degree of Master of Science.

Committee on Graduate Work

Committee Member

Committee Member

Committee Member

Adviser

Department Head

ABSTRACT OF THESIS

OBSERVATIONAL EVALUATION OF SNOW COVER EFFECTS ON THE GENERATION AND MODIFICATION OF MESOSCALE CIRCULATIONS

This thesis presents results from an observational evaluation of the impacts of snow cover on mesoscale flow due to the relatively small thermal forcing of snow cover. Specifically, the suppression of daytime upslope flow due to the presence of widespread snow cover, and the generation of thermally-direct mesoscale circulations caused by variable snow cover are examined.

Thermally direct circulations caused by variable snow cover are examined in some detail through aircraft observations. Four case study presentations from the results of an aircraft field experiment are shown.

Captain James Cramer
Department of Atmospheric Science
Colorado State University
Fort Collins, Colorado 80523
Fall 1988

ACKNOWLEDGEMENTS

This study was supported by the National Science Foundation (NSF) under Grant # ATM-8616662. Aircraft observations were carried out by the National Center for Atmospheric Research (NCAR) King Air N312D¹. The SSBLIM project was managed and supported by the NCAR Research Aviation Facility. Processing of the flight data was carried out by NCAR on the NCAR Cray Computer. GOES satellite imagery and forecasting support was primarily provided by the CSU RAMSDATA Weather Laboratory. This included the PROFS-SERS workstation at the Cooperative Institute for Research in the Atmosphere, Colorado State University, and the NOAA/NESDIS/RAMM Branch VAS Data Utilization Center (VDUC). Additional image processing support was provided by the CSU COMTAL image processing system.

Special appreciation is extended to the staff of the NCAR RAF facility for their professionalism and personal assistance well beyond what was required. In particular, I thank the SSBLIM project manager, A. Schanot. From the initial planning of the SSBLIM project, to the research flights (on most of which he served as data manager and airborne scientist), through the final processing of the plotted data, his knowledge, flexibility, and hard work were instrumental in the quick and accurate execution of the flight portion of this research. The combined assistance of the NCAR RAF staff speeded the completion of this thesis by many months.

I thank P. Hildebrand (NCAR) for sharing his extensive experience in boundary layer aircraft measurements, and in particular the interpretation of flux measurements. Also, D. Wolff (NOAA ERL) is thanked for loaning the research effort much BAO Tower data for an extended period of time.

¹NCAR is sponsored by the NSF.

I cannot overstress the importance of the leading role played by M. Segal, my primary advisory point of contact through this research. His knowledge, patience, understanding, and accessibility were crucial to the direction, scope, and soundness of the work. His years of experience gained studying NCMC's provided a strong foundation for the research. As my academic advisor and instructor, R.A. Pielke is thanked for teaching me how to think about mesoscale weather, for editing the manuscript drafts, and for his input to the final thesis as committee chairman. The flexibility and input of the other committee members, D. Johnson and B. Bienkiewicz, are also appreciated. Assistance was also provided by R. Avissar, R. Zehr, and J. Weaver.

Sincere gratitude is extended to Dallas McDonald and Bryan Critchfield for their rapid turn-around time on the word processing of the manuscript. Worth special mention are the extra hours and assistance given by Dallas McDonald, well beyond what was expected or required. I thank Judy Sorbie for the timely drafting of the figures, and Fredi Boston for letting me use her library as a workshop and for guiding me toward valuable resources.

I thank the U.S. Air Force for assigning me to Colorado State University, for funding my education, and for providing much-needed support from the first day Gina and I arrived in Fort Collins. In particular, I thank F. Kelly for always being there when I had questions.

Finally, I thank my wife, Gina. Through the pregnancies of our two beautiful boys, Andrew and Nathan, she persisted with less support than she deserved. Her continued love and encouragement through this time will never be forgotten.

TABLE OF CONTENTS

1 INTRODUCTION	1
2 PHYSICAL ANALYSIS AND HYPOTHESIS	5
2.1 Surface Sensible Heat Flux	5
2.1.1 Energy balance equation	5
2.1.2 Bare soil	6
2.1.3 Snow cover	7
2.1.4 Numerical model results	9
2.1.5 Observations	9
2.2 Scale Analysis	11
2.2.1 Snow breeze scaling of the circulation	11
2.2.2 Scaling of daytime upslope flow	16
2.2.3 Hypothesis	18
3 PRELIMINARY OBSERVATIONS OF THE IMPACTS OF SNOW COVER	19
3.1 Modification of Surface and Boundary Layer Temperatures	19
3.1.1 Surface temperature	20
3.1.2 Shelter-height temperatures	20
3.1.3 PBL structure	23
3.2 Suppression of Daytime Upslope Flow	23
3.2.1 Location of observations	27
3.2.2 Surface flow suppression	29
3.2.3 Upslope suppression above the surface	29
3.3 Generation of the Snow Breeze	33
4 AIRCRAFT FIELD EXPERIMENT	38
4.1 Introduction	38
4.2 Experiment Design	38
4.2.1 Aircraft and instrumentation	38
4.2.2 Flight plan	39
4.2.3 Operations decisions	42
4.3 Flight #1	43
4.3.1 Situation	43
4.3.2 Measurements	46
4.3.3 Cross section analysis and summary	61
4.4 Flight #7	62
4.4.1 Situation	62
4.4.2 Measurements	62

4.4.3	Cross sectional analysis and summary	74
4.5	Flight #8	81
4.5.1	Situation	81
4.5.2	Measurements	81
4.5.3	Cross section analysis and summary	99
4.6	Flight #9	99
4.6.1	Situation	99
4.6.2	Measurements	99
4.6.3	Cross section analysis and summary	113
4.7	Summarization and Generalization of the Field Experiment	113
5	SUMMARY AND CONCLUDING REMARKS	118
	APPENDIX A: SNOW COVER CLIMATOLOGY	127
	APPENDIX B: SYNOPTIC MAPS	129
	APPENDIX C: SNOW COVER MAPS	139
	APPENDIX D: PROCEDURE TO PRODUCE THE HEAT FLUX PLOTS IN CHAPTER 4	144

LIST OF FIGURES

2.1	Schematic illustration of the integration path for scale analysis of the snow breeze circulation	12
2.2	Schematic illustration of the integration path for the evaluation of thermally induced daytime upslope flow.	17
3.1	Skin temperature analysis for 1300 MST	21
3.2	Observed maximum temperatures and snow depths for 20 December, 1986 . . .	22
3.3	Air temperature profiles from BAO 300 m meteorological tower	24
3.4	Same as in Fig. 3.3	25
3.5	National Weather Service (NWS) radiosonde temperature soundings for Amarillo, Texas	26
3.6	PROFS mesonetwork stations and surrounding conventional stations	28
3.7	Surface streamline composite analysis from July, 1981	30
3.8	Plots of surface wind speeds and direction for PROFS stations	31
3.9	Wind plots from the BAO tower data	32
3.10	Daytime profiles of temperature and plot of cloud cover and surface wind for CID and ALO	34
3.11	Vertical cross sections of simulated snow breezes	36
3.11	Continued	37
4.1	Schematic diagram illustrating the basic flight plan for the SSBLIM project . .	41
4.2	GOES satellite imagery from 12 February, 1988, photographed from NOAA SERS workstations	44
4.3	Surface synoptic weather analysis for 12 February, 1988, 0500 MST	45
4.4	(a) GOES IR satellite image for 12 February, 1988, 1301 MST and (b) isotherm analysis	47
4.5	(a-e). Vertical profile measurements from flight #1	48
4.5	Continued	49
4.5	Continued	50
4.6	(a). Plotted aircraft measurements from horizontal transects for flight #1 . . .	51
4.6	(b)	52
4.6	(c)	53
4.6	(d)	54
4.6	(e)	55
4.6	(f)	56
4.6	(g)	57
4.6	(h)	58
4.6	(i)	59
4.7	Cross section analyses for flight #1 based on the horizontal transect presented in Fig. 4.6	63

4.8	As in 4.3 except for 18 March, 1988	64
4.9	As in Fig. 4.2 except for 18 March, 1988	65
4.10	As in Fig. 4.4 except for 18 March, 1988, 1501 CST	67
4.11	(a-e). Vertical profile measurements from flight # 7	68
4.11	Continued	69
4.11	Continued	70
4.12	(a-k). 90 m flight transect data	71
4.12	Continued	72
4.12	Continued	73
4.13	(a-j) As in Fig. 4.12 except for 14:21:30 - 14:36:23 CST	75
4.13	Continued	76
4.13	Continued	77
4.14	(a-h). 90 m flight data measured from 14:35:00-14:53:00 CST	78
4.14	Continued	79
4.15	Cross section analysis for flight #7 based on horizontal transect measurements	80
4.16	As in Fig. 4.2 except for 19 March, 1988	82
4.17	As in Fig. 4.3 except for 19 March, 1988	83
4.18	As in Fig. 4.4 except for 19 March, 1988, 1331 CST	84
4.19	(a-e). Vertical profile measurements from flight #8	85
4.19	Continued	86
4.19	Continued	87
4.20	(a). Plotted aircraft measurements for flight #8	88
4.20	(b)	89
4.20	(c)	90
4.20	(d)	91
4.20	(e)	92
4.20	(f)	93
4.20	(g)	94
4.20	(h)	95
4.20	(i)	96
4.21	Cross section analyses for flight #8 based on plotted measurements in Fig. 4.20	98
4.22	As in Fig. 4.3 except for 20 March, 1988	100
4.23	As in Fig. 4.2 except for 20 March, 1988, 1501 CST	101
4.24	As in Fig. 4.4 except for 20 March, 1988, 1501 CST	103
4.25	(a). Plotted aircraft measurements from flight #9	104
4.25	(b)	105
4.25	(c)	106
4.25	(d)	107
4.25	(e)	108
4.25	(f)	109
4.25	(g)	110
4.25	(h)	111
4.25	(i)	112
4.26	Cross section analyses for flight #9 based on plotted measurements in Fig. 4.25	114
A.1	Average annual date of first and last snow cover of 2.5 cm or more, 1950-1960.	128
B.1	Surface synoptic weather analysis for 0500 MST, 12 December, 1986.	130

B.2	As in Fig. B-1 except for 26 December, 1986	131
B.3	As in Fig. B-1 except for 9 February, 1987	132
B.4	As in Fig. B-1 except for 21 February, 1987	133
B.5	70 kPa analysis valid at 0500 MST, 12 December, 1986	134
B.6	As in Fig. B-5 except for 1700 MST, 26 December, 1986	135
B.7	As in Fig. B-5 except for 1700 MST, 8 February, 1987	136
B.8	As in Fig. B-5 except for 0500 MST, 10 February, 1987	137
B.9	As in Fig. B-5 except for 1700 MST, 21 February, 1987	138
C.1	Observed snow depth (cm) for 12 December, 1986	140
C.2	As in Fig. C-1 except for 20 December, 1986.	141
C.3	As in Fig. C-1 except for 9 February, 1987	142
C.4	As in Fig. C-1 except for 21 February, 1987	143

LIST OF TABLES

2.1	Evaluations of the magnitudes of surface line circulations for snow and sea breezes at various times of the year.	15
4.1	NCAR RAF Instrument Performance Specifications	40
4.2	Summarization of case studies.	116

Chapter 1

INTRODUCTION

The sea breeze and slope/valley flow and their local and mesoscale weather implications are generally well-known. These "classical" thermally induced mesoscale circulations have been studied observationally since prior to the turn of the century, analyzed theoretically since as early as the 1920's, and modeled numerically beginning in the 1950's (Atkinson, 1981). Among the important weather implications of these circulations are enhanced and preferred zones of convective cloud formation and pollutant transport.

Thermally induced flows forced by other types of differential terrain heating (such as contrasts associated with wet/dry soil, cloud-covered/clear sky regions, vegetation covered ground/bare soil, snow cover/bare soil, soil type discontinuities, high albedo/low albedo surfaces, etc.), referred to as "non-classical" mesoscale circulations (NCMCs) (Segal, 1986), however, have been relatively unexamined until more recent years. Furthermore, the impacts of modifications of the surface thermal forcing associated with the classical circulations, such as considering the sea breeze and slope flows when the soil is wet instead of dry, or when cloud cover prevails as opposed to clear skies, were also generally not evaluated until relatively recent years. (The generation of NCMCs and the modification of the classical thermally induced mesoscale flows due the presence of characteristics which modify surface sensible heat fluxes will hereafter be referred to as "non-classical effects".)

Within about the last ten years there has been a growing interest in the role that non-classical effects may play in forcing local weather. Numerical model evaluations have primarily been used to simulate some of these effects.

The results from numerical model studies have shown that non-classical effects can be quite significant. The impact of heating modifications due to soil wetness, cloud shading,

and vegetation have been most commonly examined. The studies demonstrate that when the surface heating is modified by the presence of wet soil, dense vegetation, or overcast cloud cover, the development of the classical sea breeze and upslope flow is substantially reduced. Intensity reductions of nearly a factor of two are common (McCumber, 1980, Physick, 1980, Ookouchi *et al.*, 1984, Segal *et al.*, 1986, Segal *et al.*, 1987, Yan and Anthes, 1988). Investigations have also shown that, in favorable situations, the differential surface heating caused by unmodified bare soil lying adjacent to an extensive wet soil, cloud covered, or densely vegetated region can induce NCMCs of typical sea breeze intensity (Segal *et al.*, 1986, Segal *et al.*, 1987, Yan and Anthes, 1988). The low-level convergence associated with such circulations can play a key role in the initiation or enhancement of convective precipitation (Bailey *et al.*, 1981, Anthes, 1984, McNider *et al.*, 1984, Yan and Anthes, 1988). Additionally, Mahfouf *et al.* (1987) modeled a NCMC of sea breeze intensity generated by a sand/clay contrast. Mahrer and Pielke (1978) simulated noticeable NCMC effects caused by an albedo contrast of 0.2. Theoretical and conceptual evaluations have accompanied and supported some of these numerical modeling efforts (Anthes, 1984, Ookouchi *et al.*, 1984, Segal *et al.*, 1986, Segal *et al.*, 1987). Although the number of theoretical and numerical modeling studies examining non-classical effects is growing, few observational experiments designed to evaluate such effects have been undertaken.

Segal *et al.* (1988) noted that an observational study during the early 1950's in the semi-arid Trans Volga steppe in the Soviet Union suggested the existence of NCMCs involved with an irrigated area, (Dzerdzeevskii, 1963). Segal *et al.* (1988) employed aircraft observations in evaluating NCMCs associated with irrigated crop regions in northeast Colorado. Although they noticed significant differences in the thermodynamic structure of the planetary boundary layer (PBL) over the wet and dry regions, only mild NCMC effects were observed coupled with the complicated background flow. Despite the increased interest in studying non-classical effects over the past ten years, there are still potentially important situations that have been left relatively unexamined.

Snow cover has not been systematically evaluated by any methodology regarding its impact on mesoscale flow due to surface thermal forcing modifications. This is perhaps

unexpected since snow cover is common over a large portion of the Earth, and its horizontal extent is frequently patchy throughout the land surfaces of the mid-latitudes during winter months. (See Appendix A for a climatology of snow cover for the contiguous United States.) Furthermore, the presence of snow cover is known to have a significant influence on the atmosphere above it.

Observational and modeling studies have shown that daytime surface sensible heat flux over snow cover is generally small, (see Section 2.1). It is also known that daytime meteorological shelter height temperatures, with other factors being roughly equal, are lower where there is snow cover as opposed to bare soil (Wash *et al.*, 1981, Schlatter *et al.*, 1983, Johnson *et al.*, 1984). Mesoscale weather anomalies and modifications of the entire boundary layer have been attributed to the effects of snow cover (Wash *et al.*, 1981, Bluestein, 1982, Johnson *et al.*, 1984). Non-classical effects have also been suggested.

Although no systematic evaluation has focused on the non-classical effects of snow cover, Ohata *et al.* (1981) did perform a year-long investigation of the slope/valley wind system in the Khumbu Himal, East Nepal. They related 14 occurrences of unusually light upslope winds to the presence of snow cover. A 30 - 90% intensity reduction was observed by a limited observational network. Additionally, Johnson *et al.* (1984) documented and discussed an interesting weather event that implied the possible generation of what they called a "snow breeze" (a non-classical analog of the sea breeze).

The present study is aimed at observing and evaluating the effects of snow cover on the generation and modification of thermally induced mesoscale circulations. As such it is intended to be an extension of the present understanding of non-classical thermally induced mesoscale flow effects. A brief overview of the physical considerations involved with the snow-atmosphere interaction and scale analyses of the hypothesized mesoscale flow implications are presented in Section 2. A presentation of some recent observations that demonstrate the impact of snow cover on the boundary layer and that suggest its suppression of the thermally induced upslope flow is given in Section 3. Section 4 presents a description and extensive results from a field experiment that employed aircraft observations to focus on an evaluation of the snow breeze. Four separate case studies from the

experiment are examined in detail. An attempt to generalize the results is also included. A summarization and conclusion follow in Chapter 5.

Chapter 2

PHYSICAL ANALYSIS AND HYPOTHESIS

Prior to discussing observations of the mesoscale flow impacts of snow cover, it is appropriate to discuss the physical reasons for such impacts and to estimate their expected magnitudes. Snow cover is expected to have mesoscale flow impacts because it is known to heat the lower atmosphere little during the day (relative to daytime lower atmospheric heating by dry, bare ground surfaces). This section discusses why the surface sensible heat flux of snow cover is small, how small it is, and to what degree mesoscale flow might be impacted by such thermal modification.

2.1 Surface Sensible Heat Flux

Boundary layer heating generally depends primarily on the magnitude of the turbulent sensible heat exchange between the surface and the atmosphere. The consideration of surface sensible heat flux is, therefore, fundamentally important to a discussion of non-classical mesoscale flow impacts. The hypothesis that snow cover will cause noticeable non-classical effects is based upon the presumption that the daytime surface sensible heat flux associated with snow cover is generally substantially smaller than that associated with bare soil. Qualitative understanding of why the fluxes associated with these surfaces should differ can be gained through a consideration of the energy balance equations involved.

2.1.1 Energy balance equation

The various components of the energy balance equations are, of course, dependent upon environmental conditions. For brevity and simplicity, this comparative discussion will be limited to considerations of energy balances involved with clear-sky, light wind environments. These are the conditions in which non-classical effects are expected to be

most noticeable. Only vertical fluxes are considered also. Atmospheric advection and precipitation processes are ignored. The effects of horizontal temperature gradients and the bulk motion of air within the snowpack are neglected.

2.1.2 Bare soil

Since bare soil is very nearly opaque to solar radiation, it is convenient to consider the energy balance equation for the soil surface, which can be expressed as

$$H_{RS} + H_{RL} + H_S + H_L + H_G = 0 \quad (2.1)$$

where

H_{RS} = absorbed solar radiation

$$H_{RS} = (1 - A)R_I \quad (2.2)$$

where

A = albedo (0.05 - 0.45) (Sellers, 1965 pg. 21)
 R_I = solar radiation incident upon the surface
 H_{RL} = net longwave radiation
 H_S = sensible heat flux exchange with the atmosphere

$$H_S = \rho_a C_p k_c \frac{\partial T}{\partial z} \quad (2.3)$$

where

ρ_a = air density
 C_p = specific heat of air at constant pressure
 k_c = transfer coefficient
 $\partial T / \partial z$ = vertical temperature gradient
 H_L = latent heat flux
 H_G = heat conduction between the surface and soil below the surface

To illustrate why the daytime sensible heat flux (H_S) associated with such a surface is typically large and directed toward the atmosphere, consider a simplified conceptual description of the daytime energy balance involved with a relatively dry soil (albedo 0.2) at a mid latitude site during the spring. Most of the incident solar radiation is absorbed by the soil surface (Eq. 2.1). This large net radiative energy surplus results in a surface temperature increase. Through the temperature gradient term in Eq. (2.3), this results

in a large negative (from the surface to the atmosphere) value of H_S . Segal *et al.* (1986) used 1-D model simulations to determine the linear relationship between H_S and R_I . (See Section 2.2.1). Sensible heat flux is also conducted downward into the soil ($-H_G$) due to the establishment of a downward temperature gradient, but primarily the large radiative energy surplus is balanced by the upward turbulent transfer of sensible heat to the atmosphere. Typical afternoon values are on the order of several hundred W m^{-2} .

2.1.3 Snow cover

An important difference between snow cover and bare soil is snow cover's ability to transmit solar radiation through considerable depths (≥ 50 cm, Schlatter, 1972). Also, the change of phase within a melting snowpack is an important energy consideration. For these reasons it is convenient to consider the energy balance through the depth of a snowpack, where the upper boundary is the snow - air interface (the "surface"), and the lower boundary is the snow - ground interface. The energy balance equation can be written

$$H_{RS} + H_{RL} + H_S + H_L + H_T + H_G = H_M \quad (2.4)$$

where

H_{RS} = solar radiation absorbed by the snowpack

$$H_{RS} = (1 - A)R_I(1 - e^{-\alpha h}) \quad (2.5)$$

where

R_I = solar radiation incident upon the surface

A = albedo (0.40 - 0.95) (Sellers, 1965, pg. 21)

α = extinction coefficient involved with snow and solar radiation (0.105 - 0.357)
(Kuzmin, 1961, pg. 77)

h = depth of snowpack

H_{RL} = net longwave radiation

H_S = surface sensible heat flux which can again be expressed as in Eq. (2.3)

H_L = latent heat flux

H_T = internal energy within the snowpack

H_G = heat conduction between the snowpack and the ground

H_M = heat involved with snowmelt

(After the U.S. Army Corps of Engineers, 1956, Chapter 5.) Note that H_{RL} , H_S and H_L can be considered as surface fluxes. H_{RS} , H_T and H_M are distributed throughout the depth of the snowpack, and H_G is a flux involved with the base of the snowpack.

The radiative and thermodynamic characteristics of snow cover are responsible for its typically small daytime surface sensible heat flux. A qualitative enumeration of the main energy balance implications of these characteristics is provided below:

1) Little solar radiation is absorbed by the snow surface. This is because of snow's typically high albedo, and the transmission of a substantial amount of radiation below the snow surface. Since cooling due to longwave radiation is confined to the snow surface, a temperature maximum can frequently occur at a considerable depth below the snow surface (Schlatter, 1972).

2) The sensible heat increase of sub-surface snow is poorly transferred to the snow surface. An expression for the upward conduction of heat within the snowpack can be written

$$H_{TC} = -k_s \frac{\partial T}{\partial z} \quad (2.6)$$

The thermal conductivity of snow, k_s , is typically much smaller, for example, than the thermal conductivity of bare soil (Berry, 1981, p. 49).

Furthermore, the magnitude of the temperature gradient in Eq. (2.6) is limited, since the temperature of the snowpack cannot exceed 0°C. Any additional energy input results in snowmelt, not snow temperature increase.

3) The surface temperature of the snow also cannot exceed 0°C. If the atmosphere overlying the snow is warmer than 0°C, then according to Eq. (2.3) the sensible heat flux will be directed toward the snow surface. When the snow surface temperature is 0°C, any additional energy surplus will result in snowmelt. The direction of the sensible heat flux can be toward the atmosphere only when the overlying air is cooler than the snow surface. Daytime occurrences of substantially negative temperature gradients at the snow surface would seem most likely to be involved with cold air advection.

Modifications to the energy balance must be made when considering patchy snow cover and snow with protruding vegetation. In such situations sensible heat fluxes, although still relatively small, should more commonly be directed toward the atmosphere.

2.1.4 Numerical model results

Apparently, the number of numerical modeling studies aimed at simulating the diurnal snow - air energy interactions is small. Simple parameterizations of snow cover are included in large scale models to evaluate its effect on seasonal and long term climate (e.g., Williams, 1975; Schneider and Gal-Chen, 1973). Anderson (1976) developed a snow - air interaction model which included a surface energy balance but was designed to model the energy and mass balance of snow cover over a fairly long time period (the model results were compared against six years of data).

Halberstam and Melendez (1979), however, developed a 1-D numerical model that included a surface energy balance and was designed to study the evolution of the boundary layer in the presence of snow cover. The daytime surface sensible heat fluxes that resulted from a simulation with the model are consistent with the previous conceptual discussions. The simulation involved a snowpack with an initial depth of 60 cm at 45°N during early April. The initial atmospheric temperature profile was neutral in the surface layer and stable in the upper layer. Light winds were initialized and apparently characterized the entire simulation period. The model was run for a simulated 5 1/3 day period, beginning at noon. The effects of clouds were not considered. The resulting daytime surface sensible heat fluxes are negligibly small. Much of the daytime radiative energy surplus of the snowpack was involved with snowmelt. A total of nearly 12 cm of the snowpack had melted by the end of the simulation due to daytime melting each day.

2.1.5 Observations

An extensive set of field measurements of daytime surface sensible heat fluxes involved with snow cover and clear-sky light wind environments apparently does not exist. The investigations that have undertaken such measurements have all reported difficulties in measuring these fluxes due to the small magnitudes involved and the damping of turbulent

energy transfer in the generally stably stratified air over snow cover (Halberstam and Schieldge, 1981). It is believed that, especially in such difficult conditions, the most accurate method of determining vertical fluxes into the atmosphere is to measure them directly in conjunction with eddy correlation techniques (Hicks and Martin, 1971; McKay and Thurtell, 1978). Hicks and Martin (1971), and McKay and Thurtell (1978) applied this methodology and each team provided single day measurements of surface sensible heat flux over snow cover for clear-sky light wind environments. Their measurements show that on the days examined, the surface sensible heat fluxes were, indeed, small relative to bare soil values.

Hicks and Martin (1971) collected measurements over a four-hour period in the afternoon on snow-covered Lake Mendota in Wisconsin on 26 March, 1971. The near surface air was very stable throughout the period and the snow surface was slowly melting with a measured surface temperature of 0°C . The average sensible heat transfer was 9 W m^{-2} directed toward the snow surface.

McKay and Thurtell (1978) reported measurements from eleven days; only one of which involved a clear-sky and light winds. The measurement site was the Edora Research Station near Ontario, Canada ($43^{\circ} 39' \text{N}$). The date 14 February, 1976, was described as a day with clear skies and cold temperatures. The maximum surface temperature of the snow was approximately -2.5°C , and it was estimated that sub-surface snow was melting during the day. From approximately 1030 to 1530 EST the sensible heat flux was directed toward the atmosphere with a peak (not an average) magnitude of approximately 18 W m^{-2} .

Approaches other than the eddy correlation technique have also been attempted. Granger and Male (1978) measured temperature and wind above the snow and subsequently calculated the sensible heat flux using Thornthwaite - Holzman (1939) type aerodynamic formulas. The measurement site was the Bad Lake Research Watershed (51.3°N) in southeast Saskatchewan, Canada. The observation date 28 March, 1976 was characterized by clear skies and very light winds. From approximately 1000-1600 CST the surface sensible heat flux was directed toward the atmosphere with a peak magnitude of approximately 16 W m^{-2} .

The observational evidence provided by these studies, though extremely limited in quantity and involved with some degree of error, suggests that the surface sensible heat flux over snow cover in light wind clear-sky environments is generally relatively small. The observations are thus consistent with the conceptual considerations and the numerical model results previously discussed (Sections 2.1.1 and 2.1.2).

2.2 Scale Analysis

Section 2.1 provides some understanding of the expected magnitude of the difference between the sensible heat fluxes of bare soil and snow cover. Using this insight it is possible to estimate the impacts of snow cover on mesoscale flow. Using the analytical scaling procedures as derived from the circulation theorem by Ookouchi *et al.* (1984) and Segal *et al.* (1986), magnitudes of the hypothesized snow breeze and daytime upslope suppression due to snow cover may be calculated.

2.2.1 Snow breeze scaling of the circulation

Fig. 2.1 illustrates the path of integration for the scale analysis of the snow breeze. The circulation path is assumed to occur between the surface and the top of the PBL. Note that the schematic illustration implies that the circulation has a narrow zone of relatively rapid ascent, and a broad zone of relatively slow sinking. This is consistent with present understanding of such circulations. Wind speed is assumed to be zero along the circulation segment at the PBL top since the PBL top grossly delimits the opposing flows of the circulation (after Anthes, 1978). Contribution to the circulation from the lateral vertical wind segments are ignored, and the vertical advection of θ is not considered. The horizontal length scale of the circulation, which is a function of time is represented by the segment A-B.

Assuming that $\int_A^B u_s dl$ (and also u_s) changes linearly with time, then for the flat terrain case:

$$\int_A^B u_s dl \cong \frac{kt}{\left(1 + \frac{1}{2}\alpha t\right)} \frac{g}{\theta} (\rho_a C_p)^{-1} \int_0^t (R_{G_1} - R_{G_2}) d\tau \quad (2.7)$$

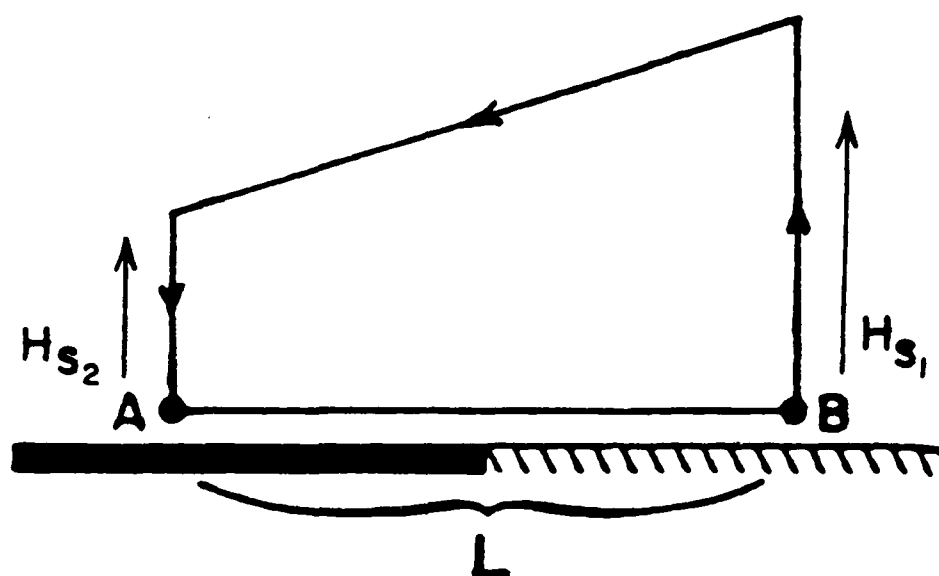


Figure 2.1: Schematic illustration of the integration path for the scale analysis of the snow breeze circulation. (The hatched surface indicates bare soil). HS_1 and HS_2 refer to the surface sensible heat fluxes of the bare soil and snow cover surfaces (or water in the sea breeze analysis), respectively. (Reproduced from Ookouchi *et al.*, 1984).

where

- u_s = surface wind component along A-B
 g = gravitational acceleration
 θ = potential temperature
 ρ_a = air density
 C_p = specific heat of air at constant pressure
 t = time after the initiation of the circulation
 α = frictional coefficient from the Rayleigh form of the friction term
 $F(u_s) = -\alpha u_s$.
 k = factor through which the absorbed solar radiation (R_G relates linearly to the surface sensible heat flux toward the atmosphere (see discussion below).
 R_{G_1} and R_{G_2} = the solar radiation absorbed by the bare soil and snow-covered (or water surfaces for sea breeze evaluation), respectively.

Segal *et al.* (1986) compared analytical results from Eq. (2.7) (and Eq. (2.10) in Section 2.2.2) with numerical results and established the validity and usefulness of the analytical evaluation.

The flat terrain, thermally-direct circulation is forced by differential surface heating of the atmosphere. Therefore, the differential surface sensible heat flux term is the primary scaling consideration in this analysis. In Eq. (2.7), the differential surface sensible heat flux is implied linearly through the radiation term.

Segal *et al.* (1986) used 1-D sensitivity simulations to show that the surface sensible heat flux can be linearly related to the absorbed shortwave radiation through

$$H_S \cong k(R_G - r) \quad (2.8)$$

where $R_G > r$. In Eq. (2.8), r is a minimal radiation required to produce a sensible heat flux directed from the surface toward the atmosphere (shown to be 100 W m^{-2} for very dry soil and 200 W m^{-2} for wet soil), and k is a factor linearly relating the absorbed radiation (R_G) in excess of r to the surface sensible heat flux (H_S) (k was shown by Segal *et al.* to be 0.5 for very dry soil and 0.16 for wet soil). Since this analysis is concerned with estimating the magnitude of the snow breeze generally, a soil moisture availability roughly between very dry and wet soil will be assumed, so $r = 150 \text{ W m}^{-2}$ and $k = 0.3$.

The magnitude of the snow breeze will be compared, in this analysis, with the magnitude of the well-known sea breeze under various typical clear-sky radiative scenarios. As discussed in Section 2.1, the surface sensible heat flux over snow cover is negligible compared to that over soil surfaces (typical clear-sky surface sensible heat fluxes over bare ground will attain noon-time magnitudes $\sim 100 \text{ W m}^{-2}$). Observations have also shown that the sensible heat flux over water surfaces may be considered as negligible for this scale analysis (e.g., Pond *et al.*, (1971), Müller-Glewe and Hinzpeter (1973), and Dunckel *et al.* (1973)). It is assumed, therefore, that the R_G term in Eq. (2.7) is equal to zero for the snow/water surface (that is, $R_{G_2} = 0$), and the evaluation of Eq. (2.7) becomes straightforward once the distribution of solar radiation over the bare ground (R_{G_1}) is known.

For this analysis R_{G_1} is approximated by,

$$R_{G_1} = B \sin \frac{\pi t'}{T}$$

where the amplitude

- B = the noon value of R_G as discussed in Pielke (1984), chapter 8
- t' = time after sunrise
- T = length of day

Since it is assumed that the surface sensible heat fluxes of both the water surface and snow cover are zero, the scale magnitudes of the sea breeze and the snow breeze will be equal assuming common radiative atmospheric, and frictional conditions. But since snow cover is a cold-season feature (see Appendix A), the snow breeze will typically be associated with weaker radiational forcing than warm season sea breezes. Since the purpose of this scale analysis is to estimate the possible impacts of snow cover on mesoscale flow, various snow breeze circulations will be scaled relative to a circulation known to often be of primary importance on the mesoscale – the mid-summer, subtropical sea breeze. The results are presented in Table 2.1.

The table shows that under favorable conditions, the snow breeze can range from relatively minor circulation (at mid-latitudes near the winter solstice) to a circulation nearly as strong as the well-developed sea breeze (at mid-latitudes at the end of the snow

Table 2.1: Evaluations of the magnitudes of surface line circulations for snow and sea breezes at various times of the year. $\int_A^B u_s dl$ is evaluated using Eq. (2.7) and describes the magnitudes of the circulations at 1400 LST; that is, at a time t seconds following the initiation of the circulation (the circulation begins when a surface sensible heat flux toward the atmosphere begins). Rough estimates of θ and ρ_a are assigned in order to attempt to include the relative effects of air temperature on the circulations.

Case	Date	Latitude (°N)	$t(s)$	θ (K)	ρ_a (kg m ⁻³)	$\int_A^B u_s dl$ (m ² s ⁻¹ × 10 ⁵)
Sea breeze	7 Aug	30	29,100	300	1.16	4.7
Snow/sea breeze	22 Dec	40	20,720	270	1.23	1.5
Snow/sea breeze	22 Jan/Nov	40	21,820	270	1.23	1.8
Snow/sea breeze	22 Feb/Oct	40	24,230	275	1.20	2.5
Snow/sea breeze	22 Mar	40	26,650	277	1.19	3.4
Snow/sea breeze	22 Apr	40	29,280	280	1.18	4.4

season). This wide range of possible impacts of the snow breeze on mesoscale weather is likely to be even further pronounced by the relative moisture content of the air at various times during the snow season. Near January, the air should generally be cold and dry, while in the early spring the air may be expected to have substantial water vapor content. The impact of a late snow-season snow breeze on the development of convective weather is potentially large (R.A. Pielke, 1988, personal communication) (e.g. Johnson *et al.*, 1984).

2.2.2 Scaling of daytime upslope flow

Fig. 2.2 illustrates the path of integration for the scale analysis of the upslope flow. The basic evaluation assumptions are the same here as in the flat terrain analysis (Section 2.2.1).

For the upslope circulation,

$$\int_A^B u_s dl \cong \left[\frac{kt}{\left(1 + \frac{1}{2}\alpha t\right)} \left(\frac{g}{\theta} \frac{\partial z_G}{\partial x} \right) \right] \times \left[k \frac{\partial \theta_0}{\partial z} (\rho_a C_p)^{-1} \int_0^t R_G d\tau \right]^{1/2} L \quad (2.10)$$

where

- $\frac{\partial z_G}{\partial x}$ = slope steepness
- $\frac{\partial \theta_0}{\partial z}$ = environmental potential temperature lapse rate.
- L = horizontal scale of the circulation
(fixed from the base of the slope to the ridge top)

The other symbols are as in Eq. (2.7).

As in the previous section, the daytime sensible heat flux for the snow surface, H_S , is assumed to be zero (thus R_G is assumed equal to zero for scaling purposes). This assumption results in: $\int_A^B u_s dl = 0$, and no detailed evaluation of the terms in Eq. (2.10) is necessary since no upslope develops. Even the ($\sim 10 \frac{W}{m^2}$) small sensible heat flux toward the atmosphere that can be associated with snow cover should still result in a strongly suppressed upslope circulation. A small surface heat flux toward the snow should result in a weak drainage flow, similar to the well-known nocturnal situation.

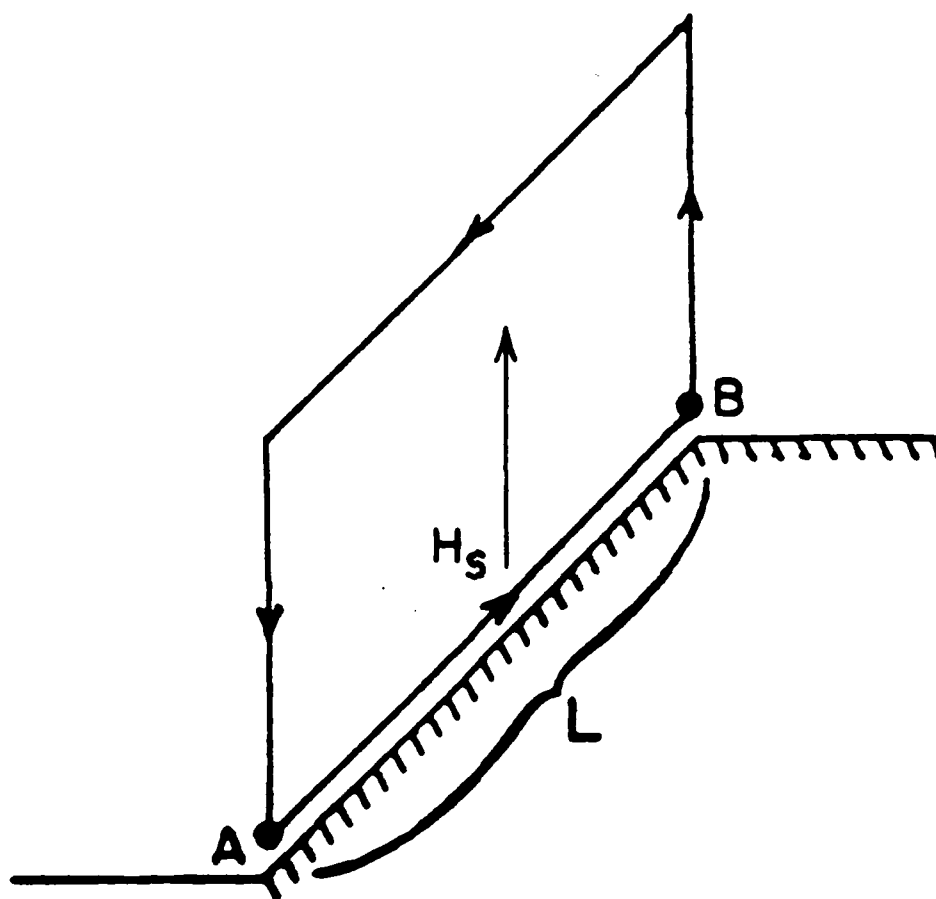


Figure 2.2: Schematic illustration of the integration path chosen for the evaluation of the thermally - induced daytime upslope flow. H_s is the surface sensible heat flux. (Reproduced from Ookouchi *et al.*, 1984.)

2.2.3 Hypothesis

Based on the previous discussion and analyses, the primary hypothesis associated with the observational evaluation of this study is that mesoscale gradients of snow cover/bare soil cause daytime horizontal gradients of surface sensible heat fluxes strong enough to induce measurable mesoscale circulations on the same scale of intensity as sea breezes. Additionally, an attempt will be made to provide further support for the hypothesis previously supported by Ohata *et al.* (1981); that is, that widespread snow cover changes the surface sensible heat flux such that a region which typically experiences daytime upslope flow (on synoptically unperturbed days with clear skies and bare soil) will experience a measurable suppression of the development of the daytime upslope flow when snow cover prevails. An effort to observe the vertical structures of both types of circulations will also be included.

Chapter 3

PRELIMINARY OBSERVATIONS OF THE IMPACTS OF SNOW COVER

This section presents some observational evidence of the ideas discussed in Chapter 2. In that chapter, it was discussed and shown that the physical characteristics of snow cover resulted in small surface sensible heat fluxes. The presence of snow cover should, therefore, modify surface and lower atmospheric temperatures. Observations of such modifications are presented and discussed in Section 3.1. These temperature modifications should result in mesoscale flow impacts, as shown in Section 2.2. Some observations of the suppression of daytime upslope flow are presented in Section 3.2, and observational hints and a preliminary model simulation of the snow breeze are presented in Section 3.3.

The presentation of the material in this chapter is not intended to provide a rigorous general quantitative evaluation. Rather, the purpose is to present representative examples of the suggested effects of snow cover in relatively favorable environments. Unless otherwise noted the examples presented are from days characterized by weak synoptic flow and mostly clear skies. Appendix B provides National Meteorological Center (NMC) synoptic analyses for these examples. Pertinent snow cover maps for dates on or about the dates of the examples (12 and 20 December, 1986 and 9 and 21 February, 1987) are provided in Appendix C.

3.1 Modification of Surface and Boundary Layer Temperatures

The theoretical discussion in Chapter 2 presents snow cover as a surface that should substantially modify the typical daytime temperature behavior of the surface and PBL. (Ideally, "typical" refers to the surface and PBL temperature behavior associated with the daytime heating of dry, bare soil). Indeed, the cooling effects of snow cover are clearly observed.

3.1.1 Surface temperature

As discussed in Chapter 2, the physical characteristics of snow cover result in low daytime surface temperatures. Most importantly, the temperature of the snow surface cannot exceed 0°C due to change of phase at that temperature. Fig. 3.1 shows an analysis of surface (skin) temperatures over northeast Colorado. Processing of an infra-red (IR) Geostationary Orbiting Earth Satellite (GOES) - East image by Colorado State University's (CSU's) COMTAL image processing system allowed for this computer analysis of surface isotherms. The gradient along A-B is about 0.3°C km⁻¹. Also note the increased satellite observed temperatures in the Denver-metro area (around DEN) and in the Pike Forest region just west of a line from DEN - COS.

3.1.2 Shelter-height temperatures

Small surface sensible heat flux implies little heating of the air overlying the surface. Wash *et al.* (1981), Schlatter *et al.* (1983) and Johnson *et al.* (1984) observed that snow cover modified meteorological shelter height temperatures. They found that daytime shelter-height temperatures were about 5°C cooler over mesoscale regions of snow cover than were the temperatures over adjacent snow free regions. Fig. 3.2 shows a more recent contrast in maximum shelter height temperatures associated with variable snow cover observed in northeast Colorado. The southeast quadrant of this figure shows that the maximum temperatures were observed to be about 5°C cooler where the ground was snow covered. Since the cooler air exists over higher terrain in this example, the horizontal temperature difference from the air over the snow to the air over the bare ($\Delta T|_z$) ground should be slightly less than 5°C. The elevation changes involved with this example are small relative to this effect, however. The same effect was not observed on this day near Denver and the adjacent South Platte River Valley to the north. The temperatures there were apparently complicated by the urban effect, valley cold pooling, and perhaps wet soil from recent snow melt.

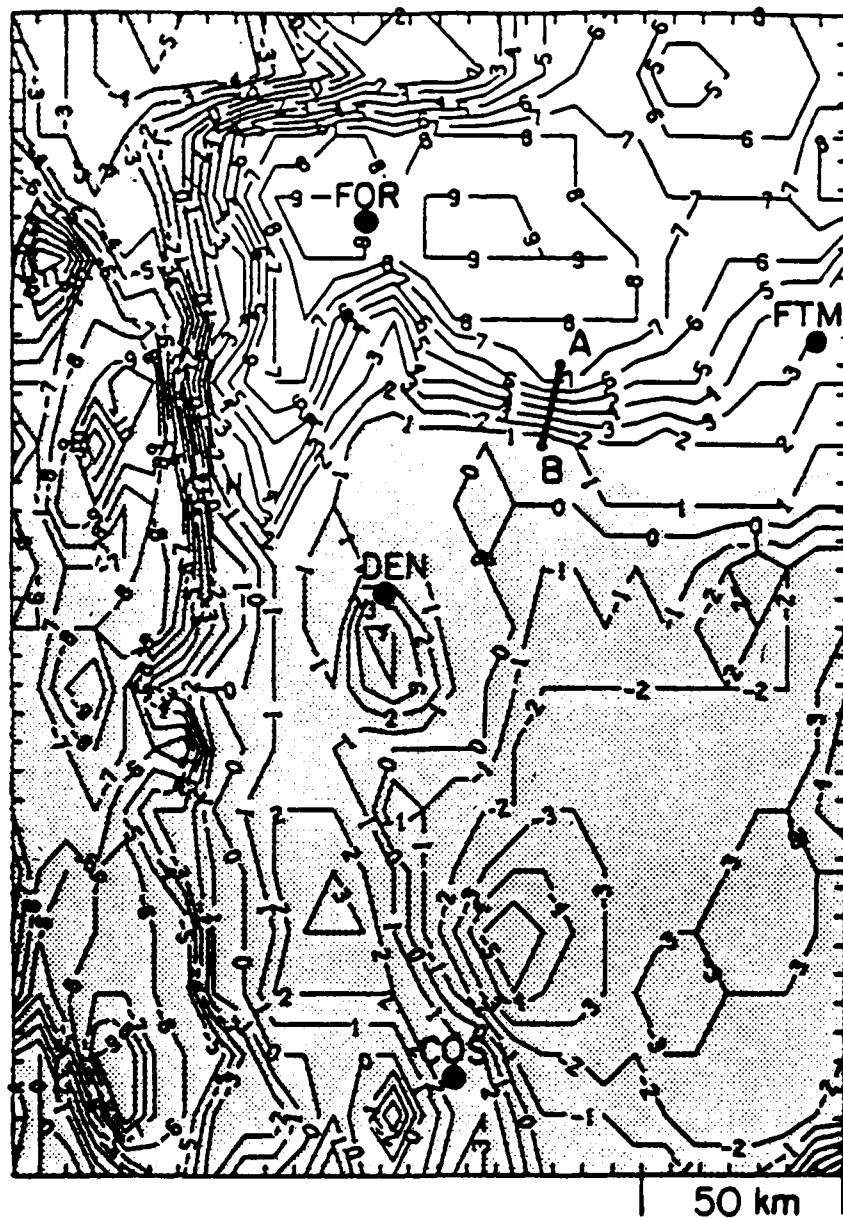


Figure 3.1: Skin temperature ($^{\circ}\text{C}$) analysis for 1300 MST, 10 January, 1987. The stipled area indicates snow cover as seen by GOES visible imagery. (Contour interval is 1°C).

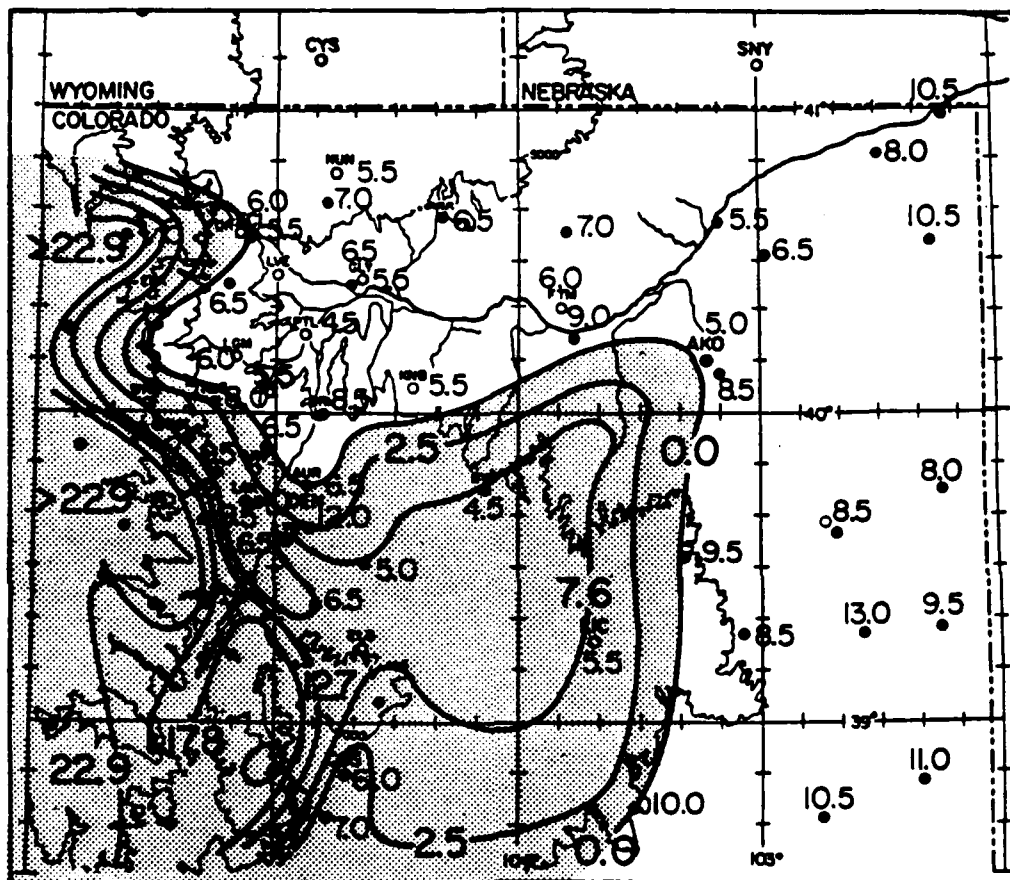


Figure 3.2: Observed maximum temperatures ($^{\circ}\text{C}$) and snow depth (cm) for 20 December, 1986. (Snow depth is contoured at an irregular interval). The stipled region indicates the areal extent of the snow cover (analyzed with the aid of 23 December, 1986 GOES visible imagery). (Large numbers are snow depth contour labels; small numbers are maximum temperature observations in $^{\circ}\text{C}$). (Data courtesy of the Colorado Climate Center located at CSU in Fort Collins, Colorado).

3.1.3 PBL structure

In the absence of the substantial upward turbulent transfer of sensible heat that is common over non-snow covered surfaces, the thermal structure of the entire PBL over snow cover is greatly modified. Figs. 3.3 and 3.4 compare the boundary layer structure over bare ground and snow covered ground at the Boulder Atmospheric Observatory (BAO) (Kaimal and Gaynor, 1983). Note the development of a relatively deep neutrally or near neutrally stratified layer by 1400 LST over the bare ground. Contrast this with the noticeably more stable stratification over the snow cover. Also note the shallow superadiabatic layer associated with a snow cover near 0°C and a relatively cold air mass (Fig. 3.4.b). This situation implies some upward surface sensible heat flux. PBL thermal structure modifications can be observed through even greater depths by conventional radiosonde data. Fig. 3.5 shows several temperature soundings of the lower atmosphere over bare ground and snow cover. The days were all characterized by the absence of persistent strong ($> 8 \text{ m s}^{-1}$) winds and by clear, partly cloudy, or occasionally thin broken skies. The soundings were taken a little more than one-hour after sunset each day. The unstable temperature profiles of the PBL over bare soil are still evident at that time; stable stratifications, however, exist over the snow cover.

3.2 Suppression of Daytime Upslope Flow

As mentioned in the introduction, Ohata *et al.* (1981) associated unusually light daytime upslope winds with the presence of snow cover. Using two 2 m anemometers positioned along a single slope/valley, they noticed a 30-90% reduction in typical upslope wind speeds when snow cover was present. Results such as this are generally consistent with the scale analysis in Section 2.2. In the report, however, they give no indication of snow cover's effect on the duration or the vertical development of the upslope flow. Apparently, no other published report attempts to evaluate daytime upslope suppression caused by snow cover. In this section some recent observations concerned with this effect are presented.

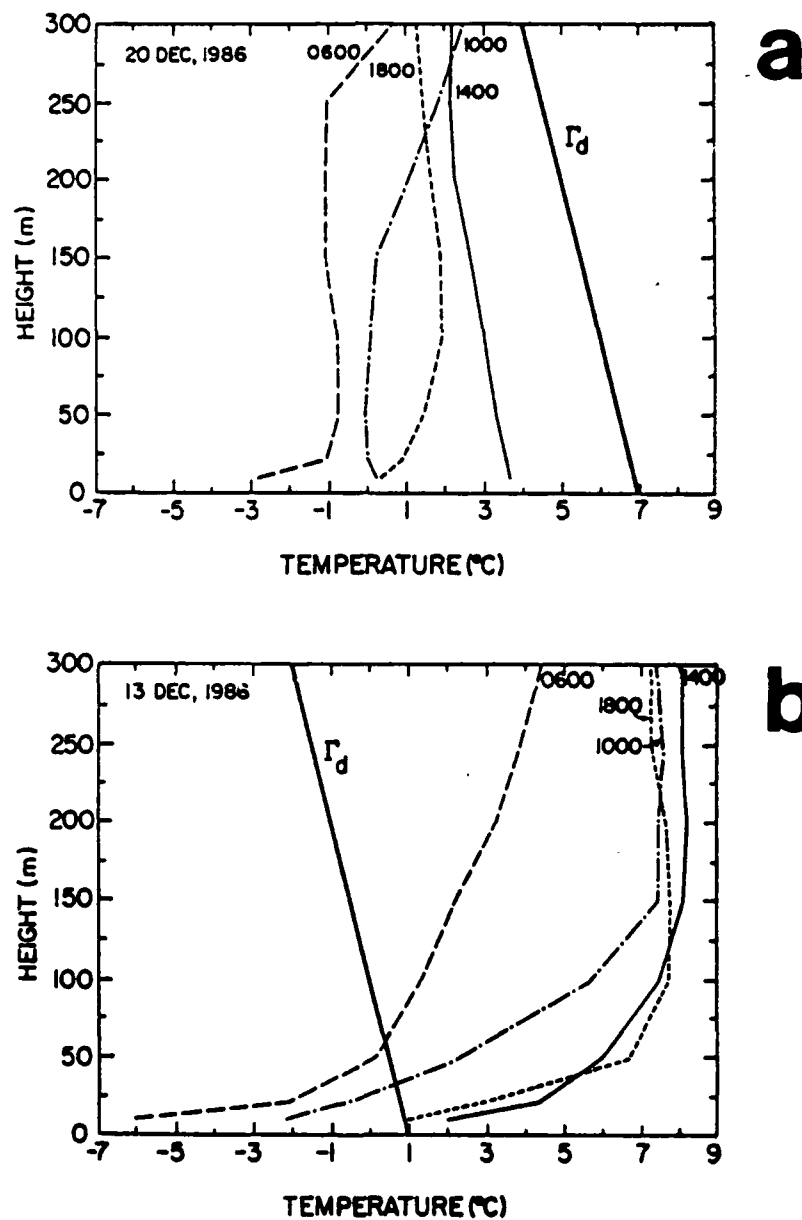


Figure 3.3: Air temperature profiles from the BAO 300 m meteorological tower located near Erie, Colorado. a) over bare ground; b) over snow cover. Γ_d represents the dry adiabatic lapse rate. The plotted temperatures are 20-min-averaged values. Profiles are labeled in Mountain Standard Time (MST).

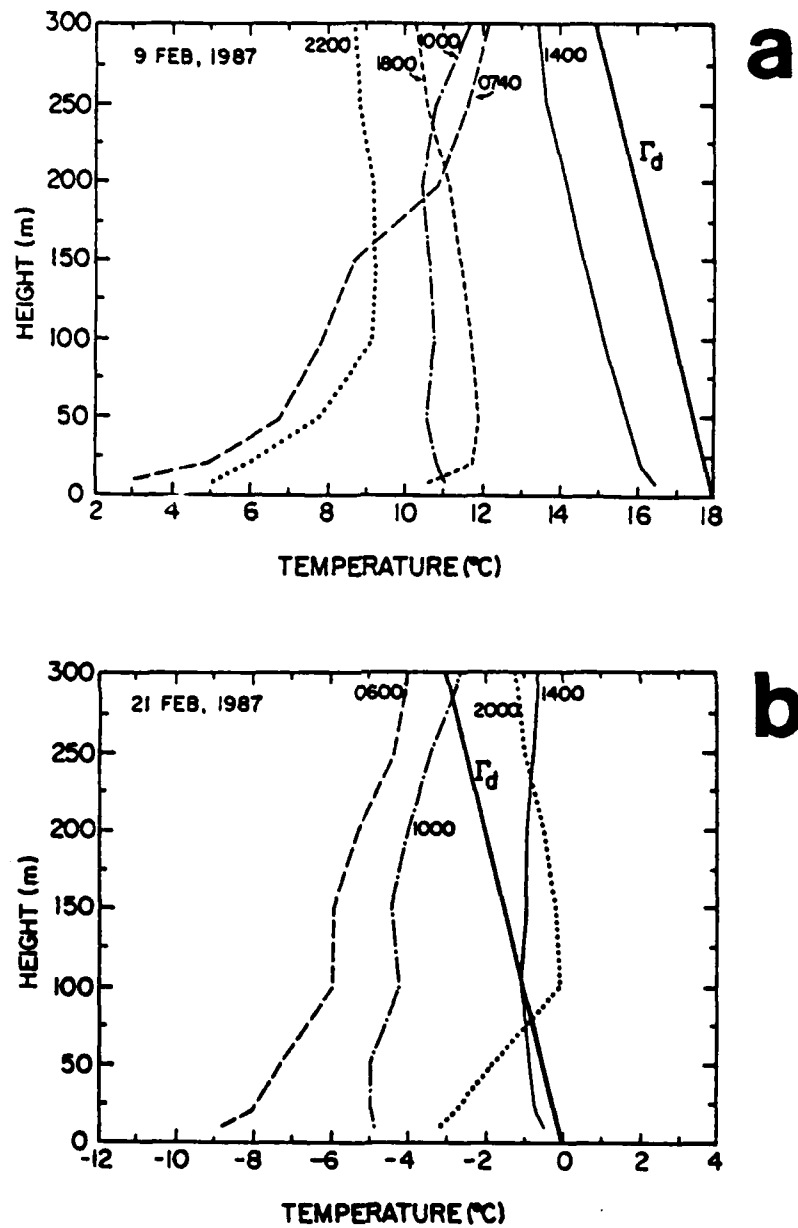


Figure 3.4: Same as in Fig. 3.3.

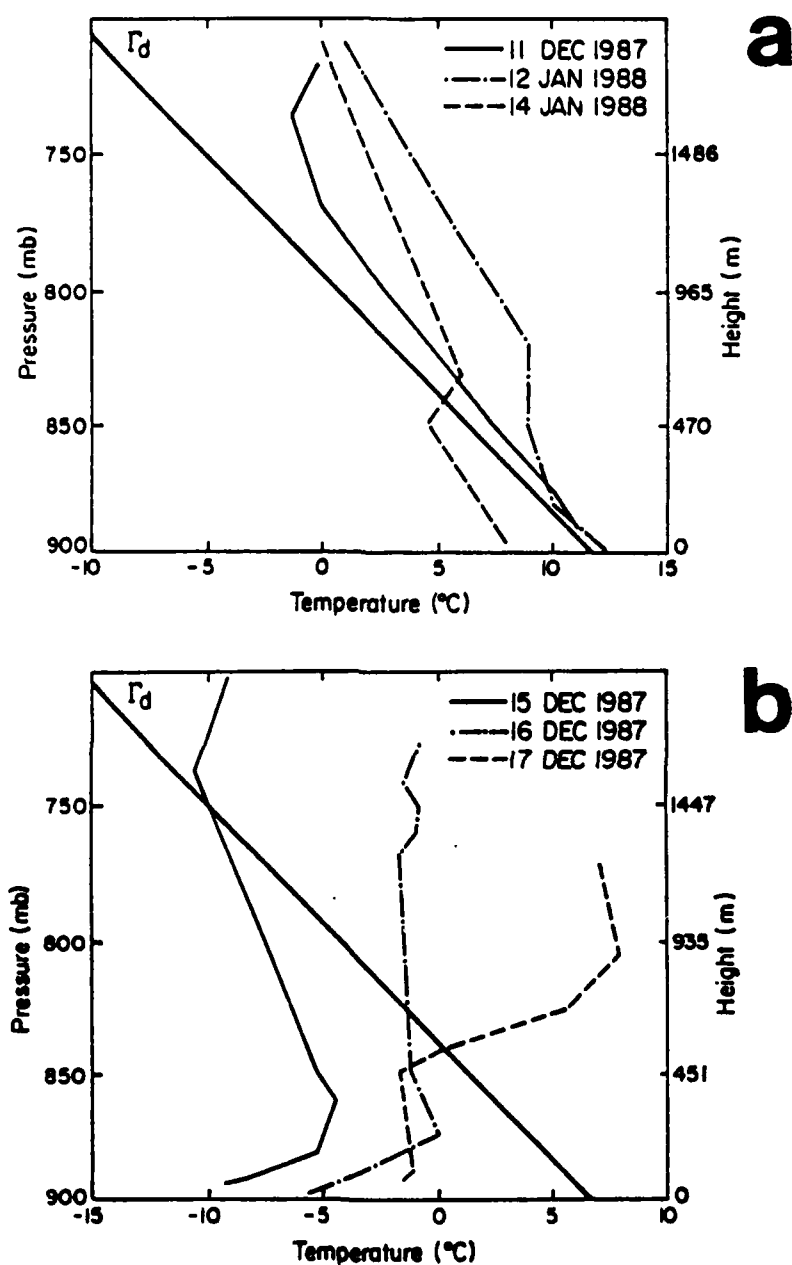


Figure 3.5: National Weather Service (NWS) radiosonde temperature soundings for Amarillo, Texas. a) over bare ground; b) over snow cover. Snow cover determination was based upon NMC depth of snow cover maps valid at 0600 CST for the given dates. The sounding time for all profiles is 1800 Central Standard Time (CST). Γ_d represents the dry-adiabatic lapse rate. (The height axis is approximated hydrostatically).

3.2.1 Location of observations

The upper South Platte River Valley in northeast Colorado (Fig. 3.6) provides an excellent location in which to observe snow cover's effect on upslope winds. There are several reasons why.

First, the natural setting is good. The slopes in this region are commonly snow-covered at times and snow free at times during the cold season. In a situation such as this it is possible to compare the upslope flows associated with bare ground and snow cover forced by similar insolation.

Second, excellent data for this region are available. The Program for Regional Observing and Forecasting Services (PROFS) (Beran and Little, 1979; Reynolds, 1983) mesonet-work of 22 automated surface observation stations measures several variables, including incoming solar radiation, air temperatures, wind speeds and wind directions. PROFS reports these variables once every five minutes as 5-minute-averaged values. Several NWS conventional observation sites are also located in the region. Furthermore, the lower boundary layer is measured by the BAO 300 m meteorological tower near Erie, CO (ERI) (Kaimal and Gaynor, 1983) (See Fig. 3.6 for locations of PROFS stations, NWS stations, and the BAO tower). The BAO tower takes measurements through the first 300 m of the atmosphere and reports 20-minute-averaged values of several variables, including temperature, wind speed, and wind direction.

Third, the typical mesoscale upslope flow pattern for this region is known in some detail. Johnson and Toth (1982) prepared composite streamline analyses of surface winds on an hourly bases through the diurnal cycle for July 1981. They observed that the flow on many individual days was similar to the composite analyses. Although the radiative forcing in July is substantially stronger than that during the winter, expected flow comparisons can still be drawn.

Consider that the magnitude of the total insolation received in the PROFS region by 1400 LST in February is about equal to the radiation received in July by 1130 LST. Ignoring the differences in cold and warm season atmospheric responses to radiative forcing, we may assume, as a first approximation, that the typical mid-afternoon upslope

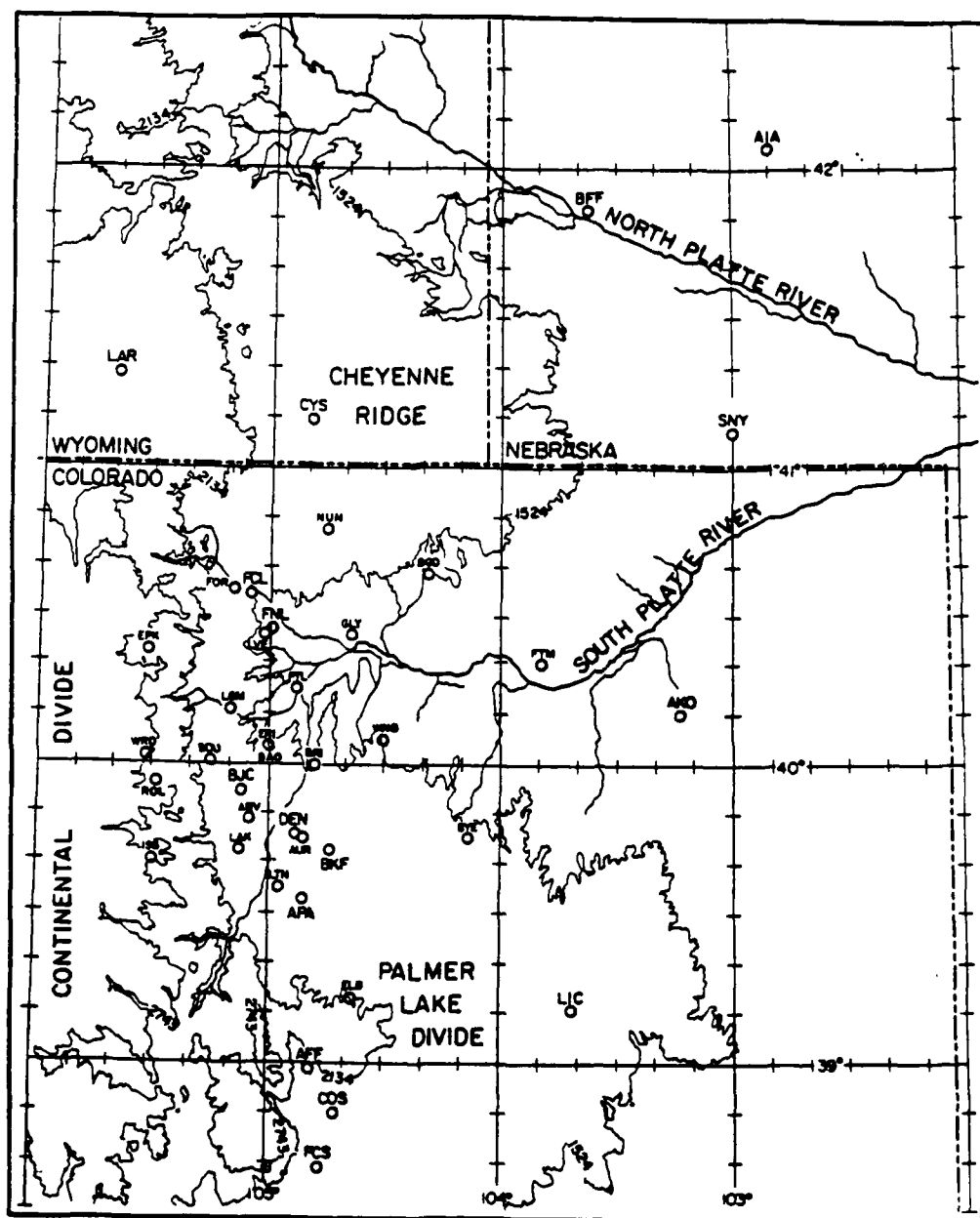


Figure 3.6: PROFS mesonetwork stations (small letters) and surrounding conventional stations (large letters). Major geographical features are identified. Elevation contours are in meters (1524 m = 5000 ft, 2134 m = 7000 ft, 2734 m = 9000 ft).

flow associated with bare ground in the winter is similar to the July 1200 LST composite analysis (Fig. 3.7).

Indeed, similar flow patterns were observed for individual synoptically unperturbed winter days in the course of this evaluation. In the absence of winter composite analyses the claim that such flows are typical is strengthened by the analyses of Johnson and Toth (1982).

3.2.2 Surface flow suppression

Fig. 3.8 suggests how the daytime surface winds are affected by the presence of snow cover. Both days were synoptically unperturbed and it appears that, at least for the BRG PROFS site, the winds were dominated by local thermal forcing. Note the drainage flow preceeding and following the daylight hours. Notice in Fig. 3.7 that the typical upslope flow would be expected to be southeasterly, but, based on the terrain, any flow from the east-northeast through the southwest may be considered upslope. The comparison in Fig. 3.8 shows that, in these cases, the upslope flow associated with the snow cover is substantially shorter in duration, with significantly reduced wind speeds (see Appendix B, Figs. B-1, 2, 5, and 6, and Appendix C, Figs. C-1 and 2 for synoptic analyses and snow cover maps for this comparison).

3.2.3 Upslope suppression above the surface

Fig. 3.9 compares the vertical structure of diurnal flow over bare ground and snow covered slopes. For the BAO tower, located near ERI, the typical upslope wind is northeasterly, but any northerly through southeasterly flow may be considered upslope. (See Fig. 3.7) Note the development of deep upslope flow by afternoon over the bare ground (Fig. 3.9a). The morning upslope and the evening drainage flows appear to begin near the surface and then propagate upward over time. Contrast the bare soil plot with the snow covered situation (Fig. 3.9b), in which the entire depth of the flow does not appear to be thermally forced by slope heating when the surface is snow covered. Upslope flow is not observed on this day (see Appendix B, Figs. B-3, 4, 7, 8, and 9, and Appendix C, Figs. C-3 and 4 for synoptic analyses and snow cover maps for this comparison).

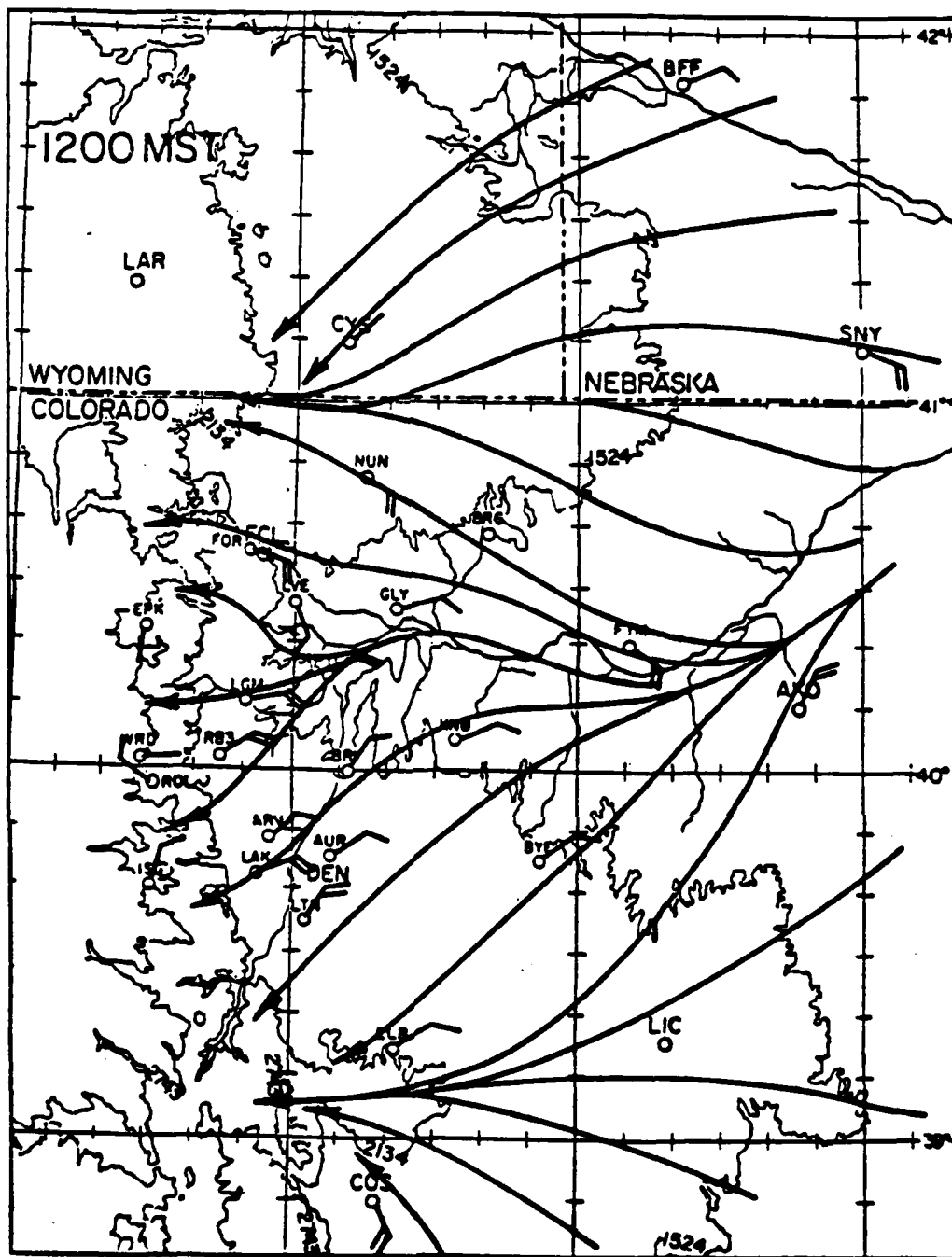


Figure 3.7: Surface streamline composite analysis from July, 1981 data. Plotted winds are in m s^{-1} (one full barb = 1 m s^{-1}). (From Johnson and Toth, 1982).

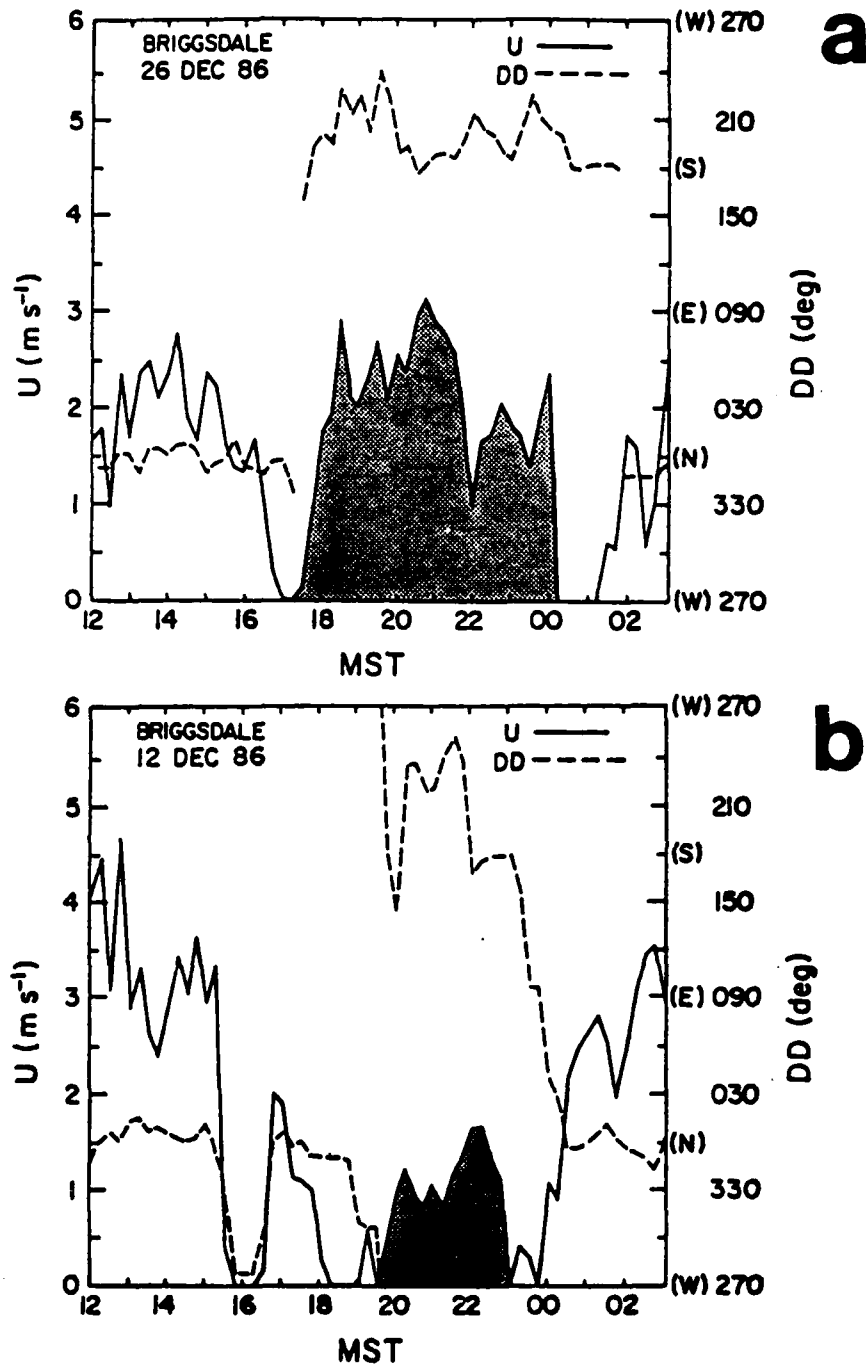


Figure 3.8: Plots of surface wind speeds (V) and direction (DD) for the PROFS station near Briggsdale (BRG), Colorado, for a) bare ground; b) general snow cover. Five-minute-averaged reports are plotted every 15 minutes. The stippled region highlights wind speeds associated with an upslope wind direction.

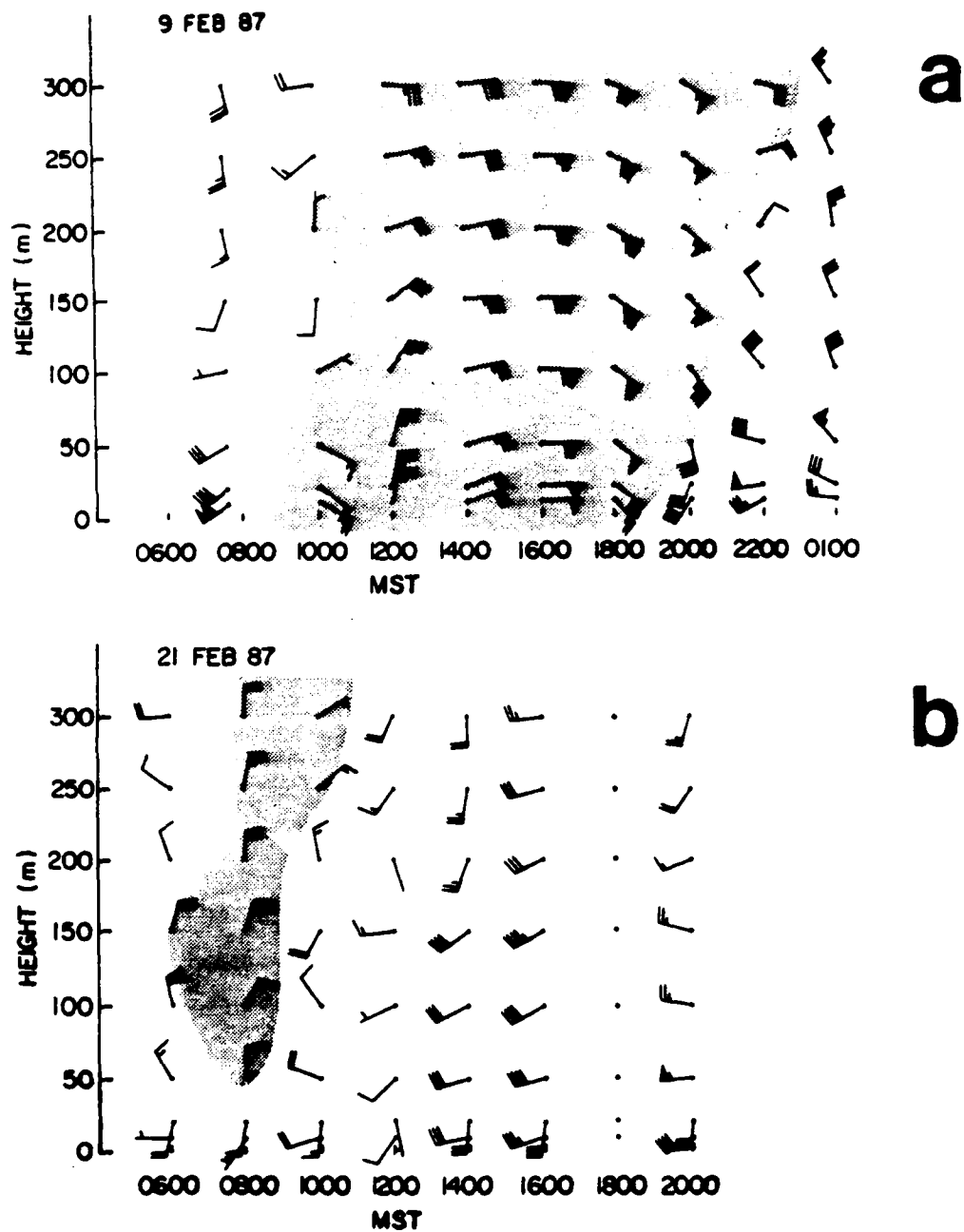


Figure 3.9: Wind plots (m s^{-1}) from the BAO tower data associated with a) bare ground; b) snow cover. (Flag = 5 m s^{-1} ; one full barb = 1 m s^{-1} ; one-half barb = 0.5 m s^{-1}). The stipled region highlights upslope flow.

3.3 Generation of the Snow Breeze

Previous studies have presented observations that are suggestive of possible snow breeze development. Johnson *et al.*, (1984) observed differences in mesoscale weather caused by variable snow cover. They discussed the possibility that a snow breeze played a role in forcing the mesoscale weather observed, but they did not directly observe the snow breeze. The situation was complicated by the interaction of topography and synoptic flow. The case did clearly demonstrate that the presence of snow cover can inhibit boundary layer development.

Wash *et al.* (1981) contrasted surface weather conditions near the boundary of a rapidly - melting snowband. They observed that on the morning of 15 April, 1980, Cedar Rapids, Iowa (CID), was located near the western edge of a mesoscale snowband. CID reported 10 cm of snow depth that morning, while Waterloo, Iowa (ALO), located about 90 km to the northwest in the snow free region, reported no snow cover. By the end of the day the snow cover completely melted in CID. Surface weather for the two sections are compared in Fig. 3.10.

Wash *et al.* attributed the daytime reduction in wind speed at CID to the reduced mixing layer depth over snow. An alternative explanation is that snow breeze effects are acting to oppose the synoptic flow near the snow boundary, resulting in reduced wind speeds. If this explanation is correct, then it appears that a synoptic flow larger than 10 m s^{-1} is strong enough to prevent the development of an opposing snow breeze, although this synoptic speed is not strong enough to mask the snow cover effect on clearly perturbing the large-scale flow.

In the situation just described, at least one observation site (CID) observed the flow effects of snow cover. Since a snow-breeze would be a mesoscale feature, it should generally be difficult to observe with the synoptic network of conventional NWS stations. The finer grid - spacing of the PROFS network is more appropriate for resolving such features. Even so, the relatively small coverage of this network renders the occurrence of a good snow boundary, clear skies, and light synoptic flow within the bounds of the region infrequent. Moreover, the PROFS network is in an area of irregular terrain. In the course of this

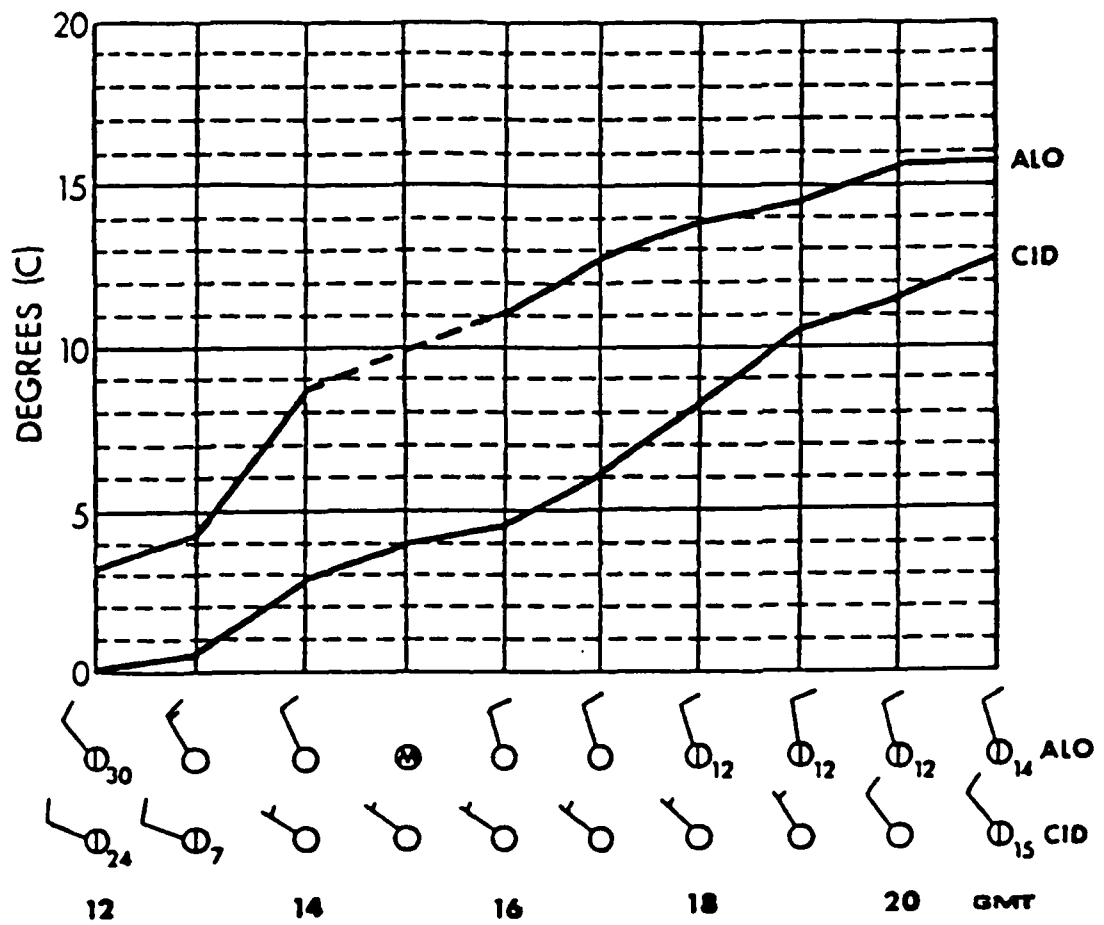


Figure 3.10: Daytime profiles of temperature ($^{\circ}\text{C}$) and plot of cloud cover and surface wind (m s^{-1}) for Cedar Rapids (CID) and Waterloo, Iowa (ALO) for 15 April, 1980. (Reproduced from Wash *et al.*, 1981.)

evaluation clear evidence of a snow breeze was not noticed in the PROFS data through two winters (1986/1987 and 87/88) of evaluation. In the absence of any clear preliminary observational evidence, initial insight concerning the snow breeze can be gained through the use of a mesoscale model.

Segal and Pielke (1988) are currently investigating the mesoscale flow impacts of snow cover with a numerical mesoscale model. The basic formulation of the model is given by Pielke (1974), Mahrer and Pielke (1977), Mahrer and Pielke (1978) and McNider and Pielke (1981). Several validation studies have shown that this model had reasonable skill in resolving mesoscale airflow patterns (e.g., Pielke and Mahrer, 1978; Segal and Pielke, 1981; and Segal *et al.*, 1982).

The current effort is focused upon the introduction of a snow layer into the model in order to simulate the surface energy balance of snow cover. Although the snow formulations are presently in bulk form, preliminary 2-D snow breeze simulations were performed in order to gain initial insight into the expected magnitude of the circulation.

Fig. 3.11 presents several mid-afternoon fields from a winter (12 February) simulation at 39°N latitude involved with a snow/bare contrast and no significant background flow.

The simulation suggests that in favorable situations a significant snow breeze is generated that is similar in intensity to the sea breeze (Fig. 3.11b). Note that the peak wind speed is over 7 m s^{-1} and the transition to a return circulation occurs at a height of about 1 km. The peak upward vertical motion is nearly 50 cm s^{-1} (Fig. 3.11c). Also note the strong inversion over the snow surface as opposed to the deep neutral layer over the bare soil (Fig. 3.11a).

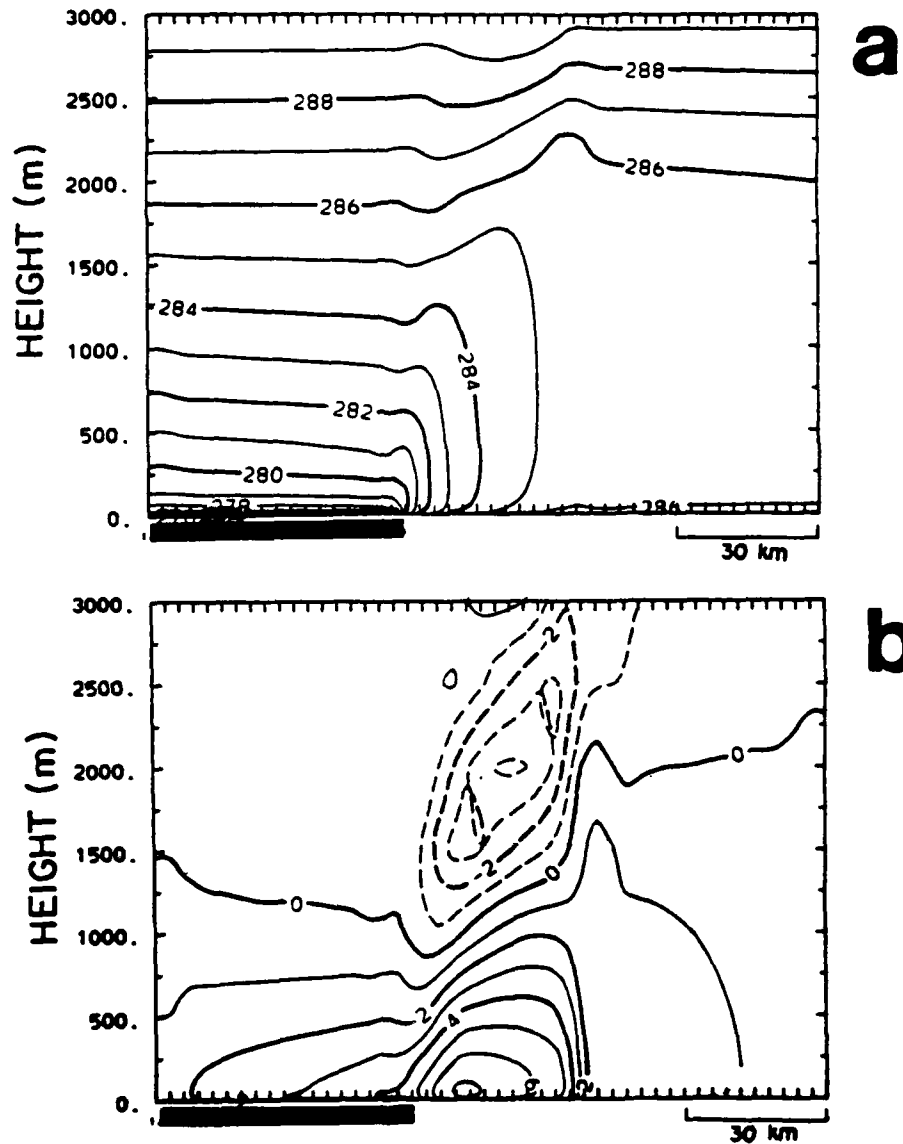


Figure 3.11: Vertical cross sections of a simulated snow breeze. a) potential temperature; b) u- component of horizontal wind; c) w- component of wind. Solid lines indicate positive values, dashed lines indicate negative values, dark line at base of figures indicates snow covered surface. (Simulation performed by Moti Segal, 1988).

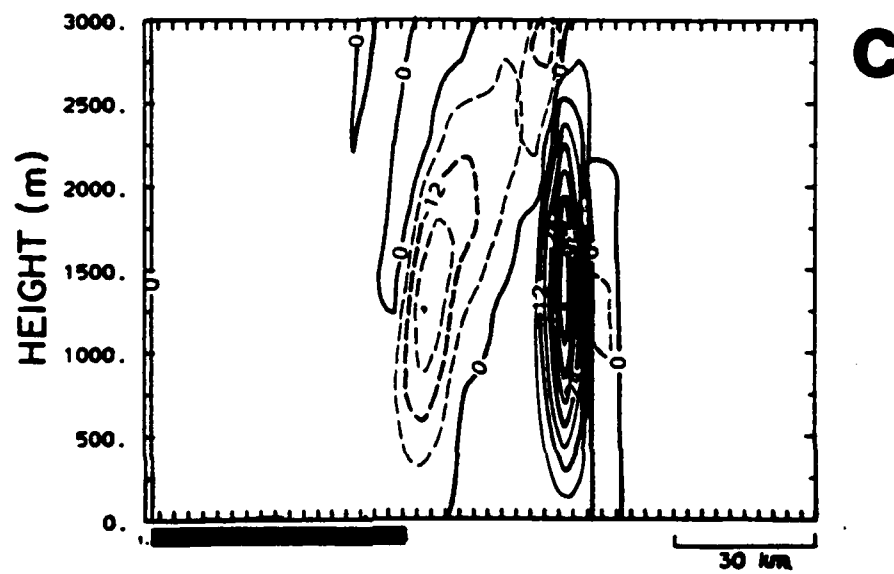


Figure 3.11: Continued.

Chapter 4

AIRCRAFT FIELD EXPERIMENT

4.1 Introduction

Gaining initial observational insight into boundary layer modification near a snow - no snow boundary requires a special approach. Using aircraft as the observational platform offers unique advantages. Because of its flexibility and range, aircraft can sample the boundary layer near the snow boundaries that exist within a relatively large region. The short time response of aircraft allows for efficient operations such that observations can focus on those days with more favorable synoptic weather patterns. Furthermore, aircraft can observe the horizontal and vertical structures of the boundary in great detail.

The National Center for Atmospheric Research¹ (NCAR) approved 40 hours for such flights to take place from 1 February - 25 March, 1988. The project was entitled the Snow Shading Boundary Layer Interaction Measurements (SSBLIM) project. (Originally, the effects of cloud shading were proposed as part of the project. Observations of such effects, however, were not pursued.) The project design is presented in Section 4.2. The remainder of Chapter 4 is devoted to case study data presentation and discussion from the results of four of the nine SSBLIM flights.

4.2 Experiment Design

4.2.1 Aircraft and instrumentation

The aircraft used in the SSBLIM project was the NCAR King Air N312D. It was instrumented such that aircraft position and height, wind velocity, temperature, moisture,

¹NCAR is sponsored by the National Science Foundation.

turbulence fluxes, aerosol concentration, IR surface temperature, and surface albedo were either measured or could be derived from measured quantities. Some instruments sampled the atmosphere at a rate of 50 samples per second (sps), while other measurements were made at 5 sps frequency. The raw data were digitally recorded on magnetic tape which were later processed on the NCAR CRAY computer at the NCAR Mesa Lab site. During the processing 50 sps data were filtered at 10 SPS and interpolated to 20 sps, and 5 sps data were finally output to tape as 1 s averages. This calibrated and edited final product forms the data set for the present evaluation.

After post-flight evaluation, NCAR found the data set of excellent overall quality (NCAR SSBLIM project documentation summary, 1988). Through the use of calibration procedures and redundant sensor comparisons the data quality from each instrument was evaluated. Based on these evaluations, the data presented in this study are generally considered to be within NCAR RAF specifications (Table 4.1). Sensible and latent heat fluxes were calculated through the use of an NCAR RAF flux program. The fluxes were calculated from 20 sps data using eddy correlation techniques (see Appendix D). More detailed discussions and references concerning the aircraft instrument systems and the data processing can be found in Miller and Friesen (1987), Lenschow and Spyers-Duran (1987), and the NCAR Research Aviation Facility Bulletin 2.

In addition, to the instruments mentioned above, forward- and downward- looking video cameras with recorders and date/time recordings were mounted on the aircraft. Also, an onboard FM radio enabled the airborne scientists to maintain contact with ground-based scientists at the CSU Weather Laboratory.

4.2.2 Flight plan

The basic flight plan for SSBLIM is shown in Fig. 4.1. The wavy vertical segments indicate the vertical profile measurements. In order to remain roughly over the same region during the profile descent, the pilots reversed the aircraft heading frequently. Since sudden changes in the aircraft's attitude can adversely affect the wind data, the turns made during the profile measurements were flown at constant altitude. This ensured that there would be no vertical gaps in reliable profile data.

Table 4.1: NCAR RAF Instrument Performance Specifications

variable	accuracy
Aircraft latitude	≤ 1.0 n mi per flight hour
Aircraft longitude	≤ 1.0 n mi per flight hour
Static pressure (fuselage)	± 1 mb
Total air temperature	$\pm 0.05^\circ\text{C}$
Absolute humidity	$\pm 5\%$ (with periodic baselining)
Radiometric surface temperature	$\pm 1.0^\circ\text{C}$
Visible radiation	not available
Geometric altitude	± 0.6 m or 2% (0 to 152 m); $\pm 3\%$ (152 to 762 m)
Aerosol concentration	not available
Horizontal wind vector component	$\pm 0.1 \text{ m s}^{-1}$ (< 10 min); $\pm (1.0 + 0.5 t)(t$ in hours)
Vertical wind	$\pm 0.1 \text{ m s}^{-1}$ (< 10 min)
Vector component	long-term accuracy not available
Horizontal direction	$\pm \text{COT}^{-1}(u/v)$

(From NCAR RAF Bulletin 2, 1988. Accuracy states combined performance of transducer, signal conditioning, and recorder. RAF-computed winds are actually a combination of the mean and fluctuating component, i.e., $u = \bar{u} + u'$, when gust probe is present).

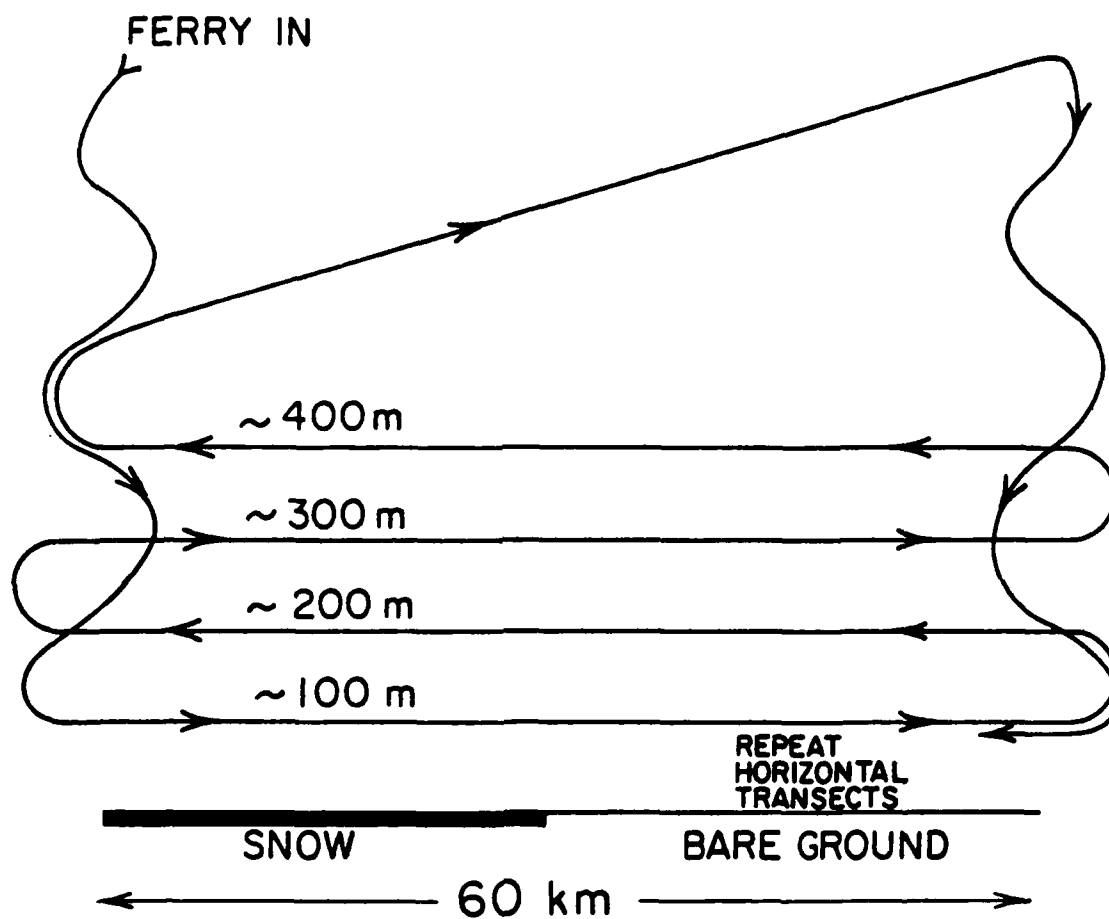


Figure 4.1: Schematic diagram illustrating the basic flight plan for the SSBLIM project.

The horizontal lines in Fig. 4.1 indicate the transects, or legs, flown at constant height above the ground. The four transects are flown after the first vertical "sounding," and then repeated about an hour later after the second sounding. This repetition provides data concerning atmospheric changes in time. Research airspeed was roughly 80 m s^{-1} , and the entire pattern shown in Fig. 4.1 would take about 150 min to complete.

This basic plan was considered to be a simple model to be applied with flexibility in practice. Indeed, the pattern proved useful for initial planning, but was not rigidly adhered to during any given flight.

4.2.3 Operations decisions

Operations were based at the NCAR RAF at Jefferson County Airport (JEFFCO) ($39^{\circ} 54.8' \text{ N}$, $105^{\circ} 7.1' \text{ W}$) near Broomfield, Colorado. The maximum flight time for planning purposes was considered to be 270 min.

Considering the 150 min of research time required to fly the planned patterns in Fig. 4.1, about 120 min, or 600 km round trip, were available for ferrying. Thus the range of the SSBLIM project was considered to be about 300 km. Flights outside this range were not ruled out, but the research portions of such flights would necessarily be curtailed.

Forecasting and go - no go decisions were made at CSU based on information provided by the CSU Weather Laboratory and the NOAA SERS Workstation. Optimum project weather conditions included a good snow - no snow boundary that was within range, clear skies, and light synoptic wind flow. Generally the goal was to begin research measurements shortly after noon MST. Thanks to the quick response times of the NCAR RAF team, final go - no go decisions could be made as late as one hour before takeoff. For SSBLIM, the final decision was usually made about two hours prior to takeoff.

Although the GOES satellite imagery on the SERS and VDUC workstations at CSU enabled the scientists to quite accurately appraise and locate good snow - no snow boundaries, the final locations and orientations of the research were decided upon in the air. Even after takeoff, however, the airborne scientists received information and guidance from the scientists at CSU through the air-to-ground FM radio link.

The number of flight hours available was important in all phases of the decision process. As mentioned previously, NCAR initially approved 40 hours for SSBLIM. Several of these hours were used prior to the start of the project for test flights. Approximately 36.5 hours were available for the 54-day project. During those 54 days nine flights were made and all of the allotted flight hours were used.

4.3 Flight #1

4.3.1 Situation

During the period 10-11 February, 1988, an arctic airmass surged southeastward down the eastern side of the Rocky Mountains and into the plains. The system forced upslope snow along the eastern Rockies as far south as the Arkansas River Valley in southeast Colorado. As is commonly the case, the storm did not distribute snow evenly upon the differently-oriented slopes. In this case, the south-facing slope north of the Arkansas River was left largely snow-covered; the north-facing slope south of the river was left bare. The event left a fairly pronounced east - west snow - no snow boundary just north of the Arkansas River near La Junta (LHX) (Fig. 4.2a). (Note that the locations and station names on all satellite photos are part of the NWS synoptic network).

By the morning of 12 February the high pressure system had moved all the way to the Gulf Coast regions of Texas and Louisiana. The arctic air mass had moved eastward and Colorado was now under the influence of a second high pressure system centered in Utah (Fig. 4.3). The weak troughing between these highs lay generally north - south near the Colorado - Kansas border. The surface geostrophic wind was northwesterly over southeast Colorado.

Since the skies were clear, the pressure gradient was not overwhelmingly strong, and the arctic airmass had moved eastward, the CSU researchers decided to proceed with the first SSBLIM flight. The planned transects were positioned over the snow boundary near LHX as shown in Fig. 4.2.

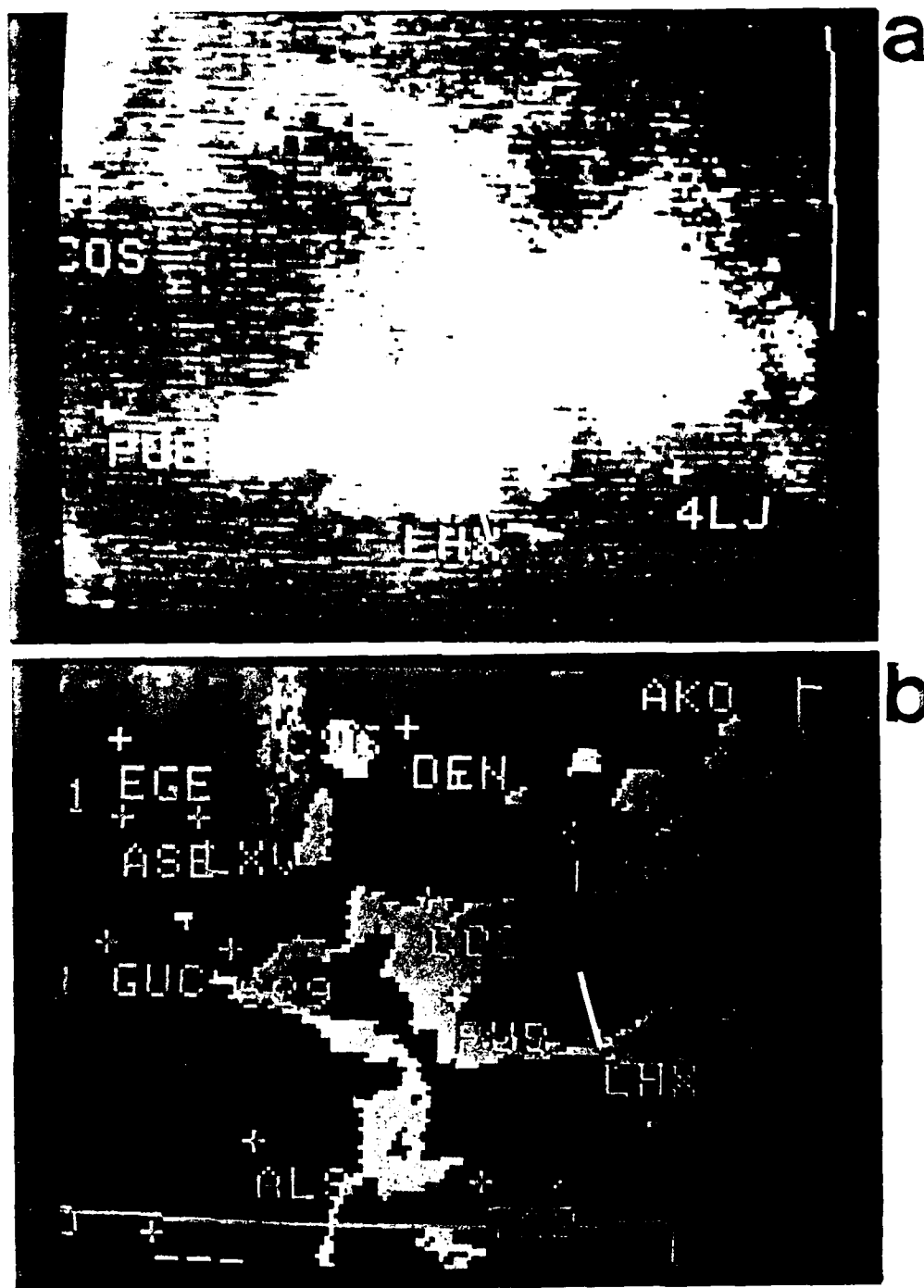


Figure 4.2: GOES satellite imagery from 12 February, 1988, photographed from NOAA SERS workstations. (a) Visible image, 1132 MST; (b) Infrared (IR) image, 1315 MST. Contour interval is 5°C . The brightened area (yellow-orange) in (b) is bounded by the -10°C and -15°C isotherms, with cooler temperatures closer to the snow cover. Superimposed lines indicate flight transects. Note the navigational shift in the station location between the figures. According to flight logs, figure (a) is more accurate).

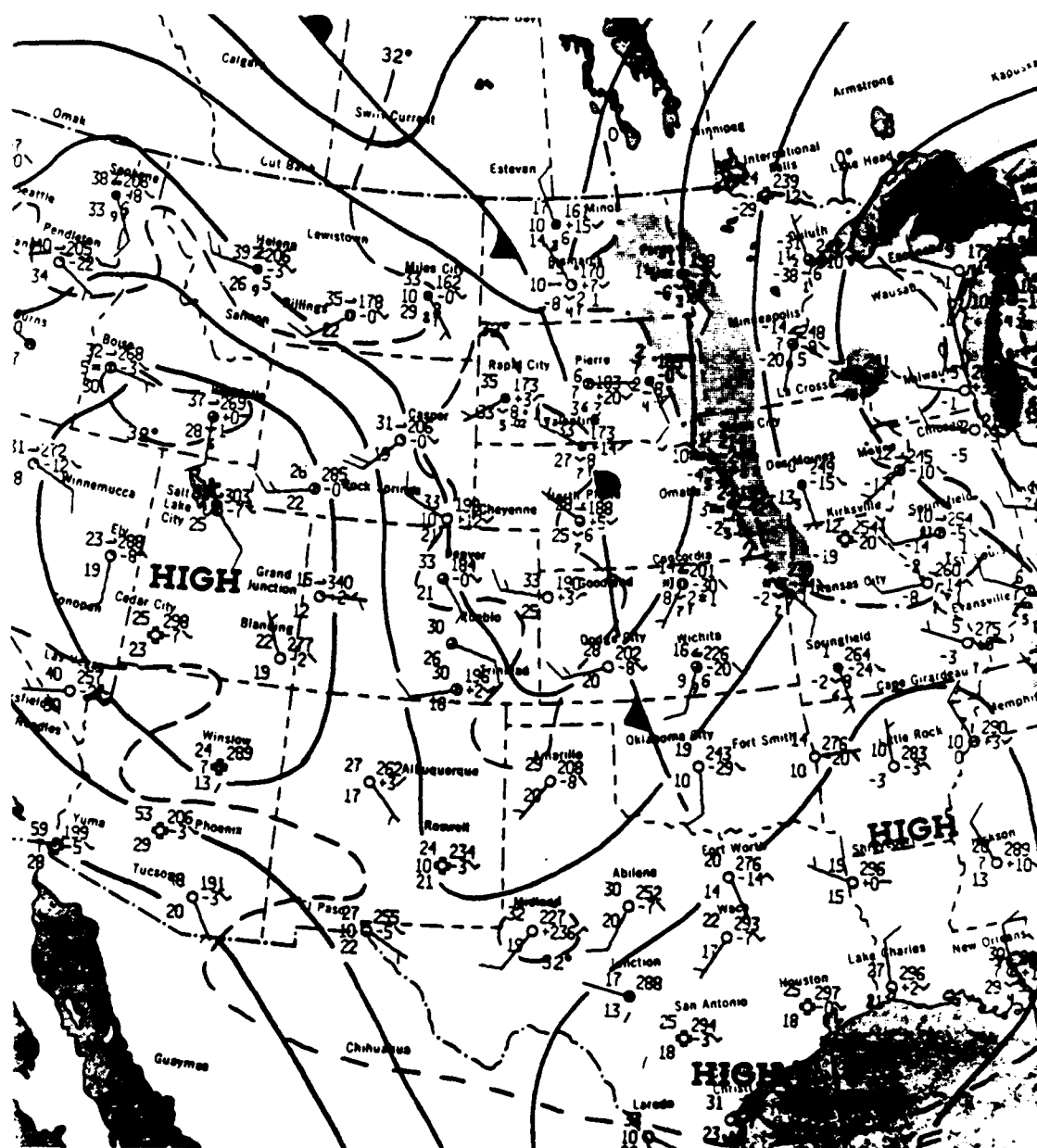


Figure 4.3: Surface synoptic weather analysis for 12 February, 1988, 0500 MST. (Reproduced from "Daily Weather Maps", Climate Analysis Center.)

4.3.2 Measurements

By early afternoon a distinct surface temperature gradient had developed across the boundary as seen in GOES satellite imagery (Fig. 4.2b and 4.4). Fig. 4.4 presents a refined view of the afternoon satellite-observed surface temperature. The relatively sharp transition from bare ground to snow cover is evidenced by a drop of 7°C over a 10 km distance ($0.7^{\circ}\text{C km}^{-1}$). An even sharper gradient exists about 20 km east of the chosen transect ($\sim 1.0^{\circ}\text{C km}^{-1}$). As will be seen later, the actual temperature change over a 10 km distance near the snow boundary (as measured by the aircraft) is about twice that observed by the satellite. The satellite-observed temperatures are involved with much larger-scale averaging than the aircraft values. Furthermore, the aircraft measured warmer temperatures over the bare soil ($\sim 2\text{--}3^{\circ}\text{C}$) than did the satellite, presumably due to a greatly reduced optical depth. (See Fig. 4.6a for aircraft-observed surface temperatures.) Plotted measurements from the aircraft are shown in Figs. 4.5 and 4.6.

Although measured at sites located only about 50 km apart, the vertical profiles show how different the boundary layer is over the snow and the bare soil. The vertical profiles (Fig. 4.5) show that a mixed layer had developed over the bare soil region to a height of over 1100 m. The lower atmosphere over the snow, on the other hand, was strongly stable. The lowest 200 m of air over the snow was relatively stagnant, with a strong inversion apparently trapping the air below. Note the high humidity and aerosol concentration (Fig. 4.5b and c) just above the snow surface. In the lowest portions of the profiles the potential temperature is about 5 K cooler over the snow than that over the bare soil region (Fig. 4.5a). Differences in the wind over the two regions are also illustrated by the profiles (Fig. 4.5d and e).

The background synoptic flow for this case is apparently complicated. It probably involves interaction of the geostrophic flow, irregular terrain, friction, and thermal upslope forcing. The resultant flow, as is seen above 100 m in the vertical profiles, is generally southerly at $5\text{--}9\text{ m s}^{-1}$. The flow over the snow (above 100 m) is slightly more westerly in direction and is significantly stronger in speed. This flow is expected to be closer to the geostrophic flow than the flow observed over the bare soil region since there is less friction

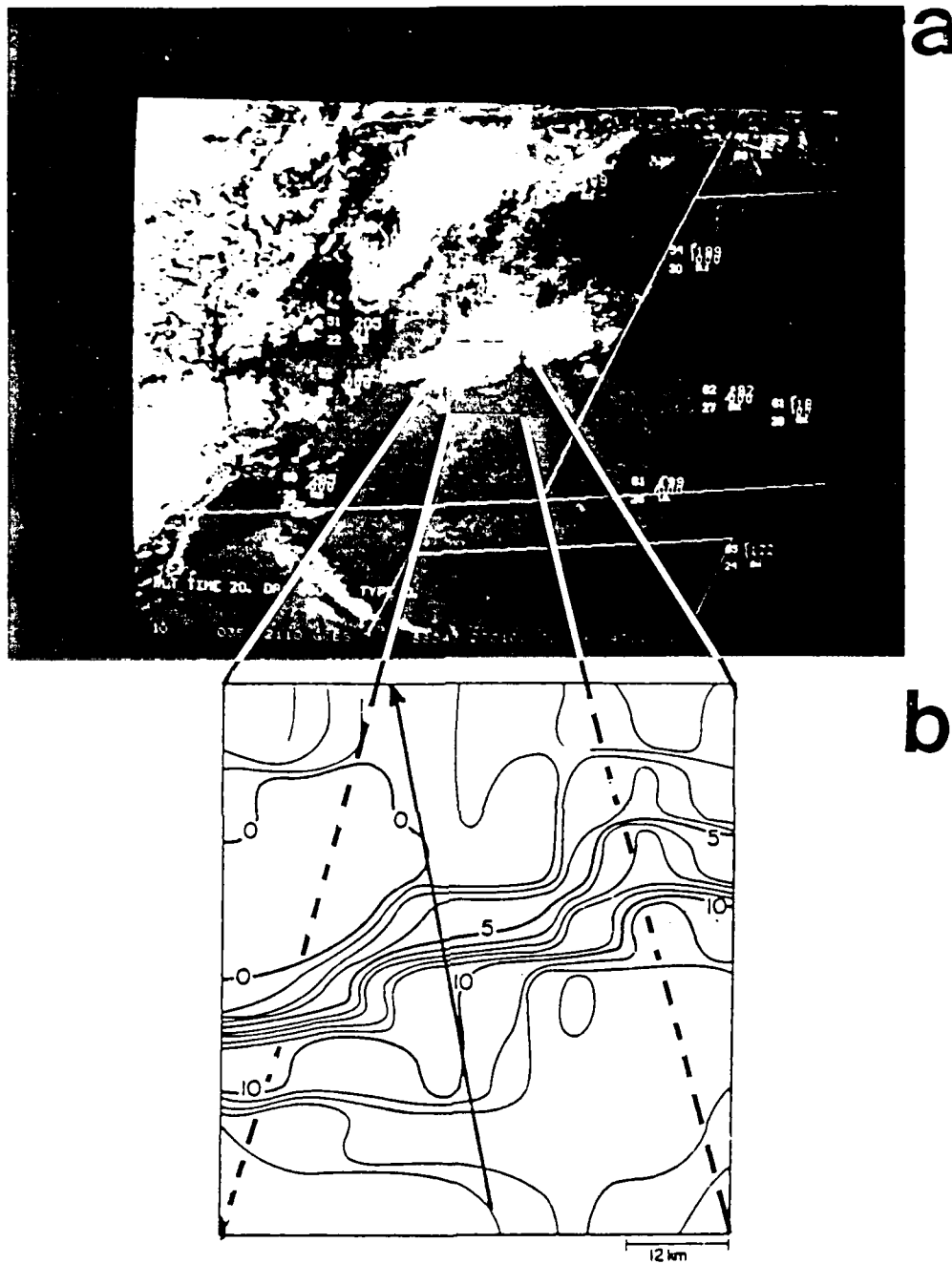


Figure 4.4: (a) Goes IR satellite image for 12 February, 1988, 1301 MST and, (b) isotherm analysis for area outlined by small square in (a) (based upon VDOC image processing). Isotherm analysis is hand-smoothed and the contour interval is 1°C . The heaviest line indicates portion of flight transect.

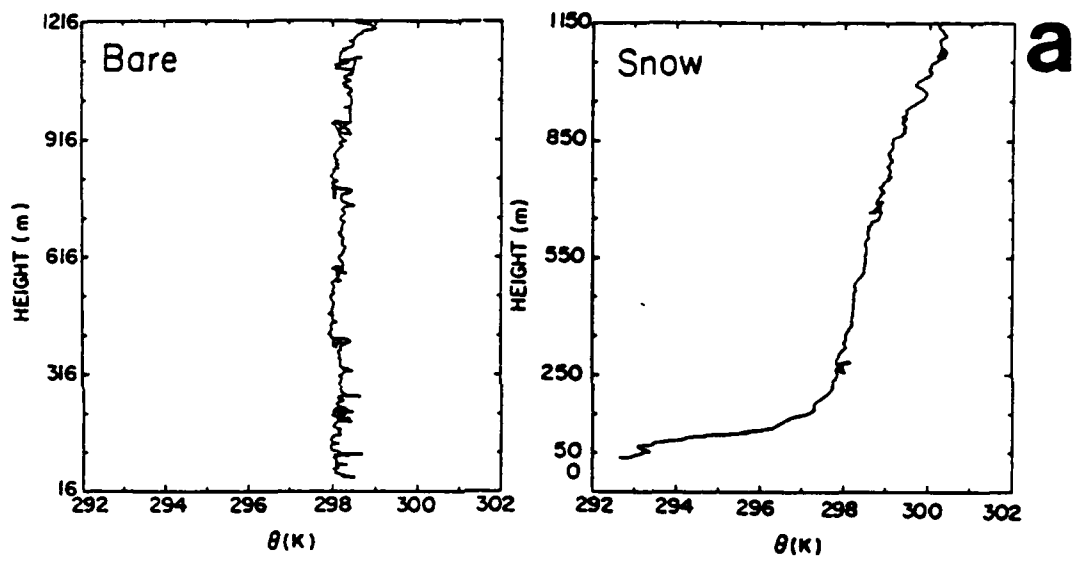


Figure 4.5: (a-e). Vertical profile measurements from flight #1. Bare measurements were made from 12:30:00 - 12:57:10 MST. Snow measurements were made from 14:16:55 - 14:35:00 MST.

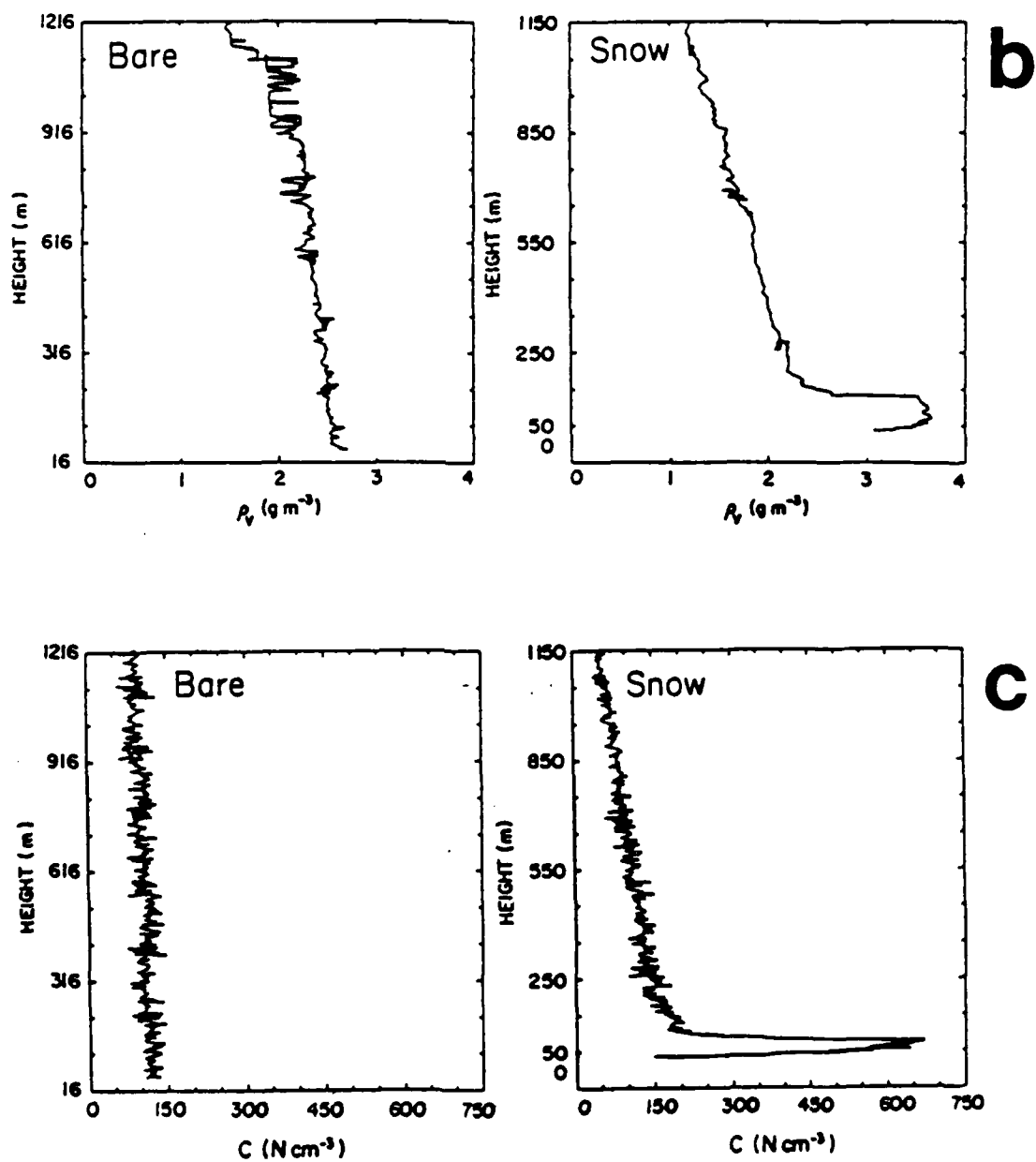


Figure 4.5: Continued.

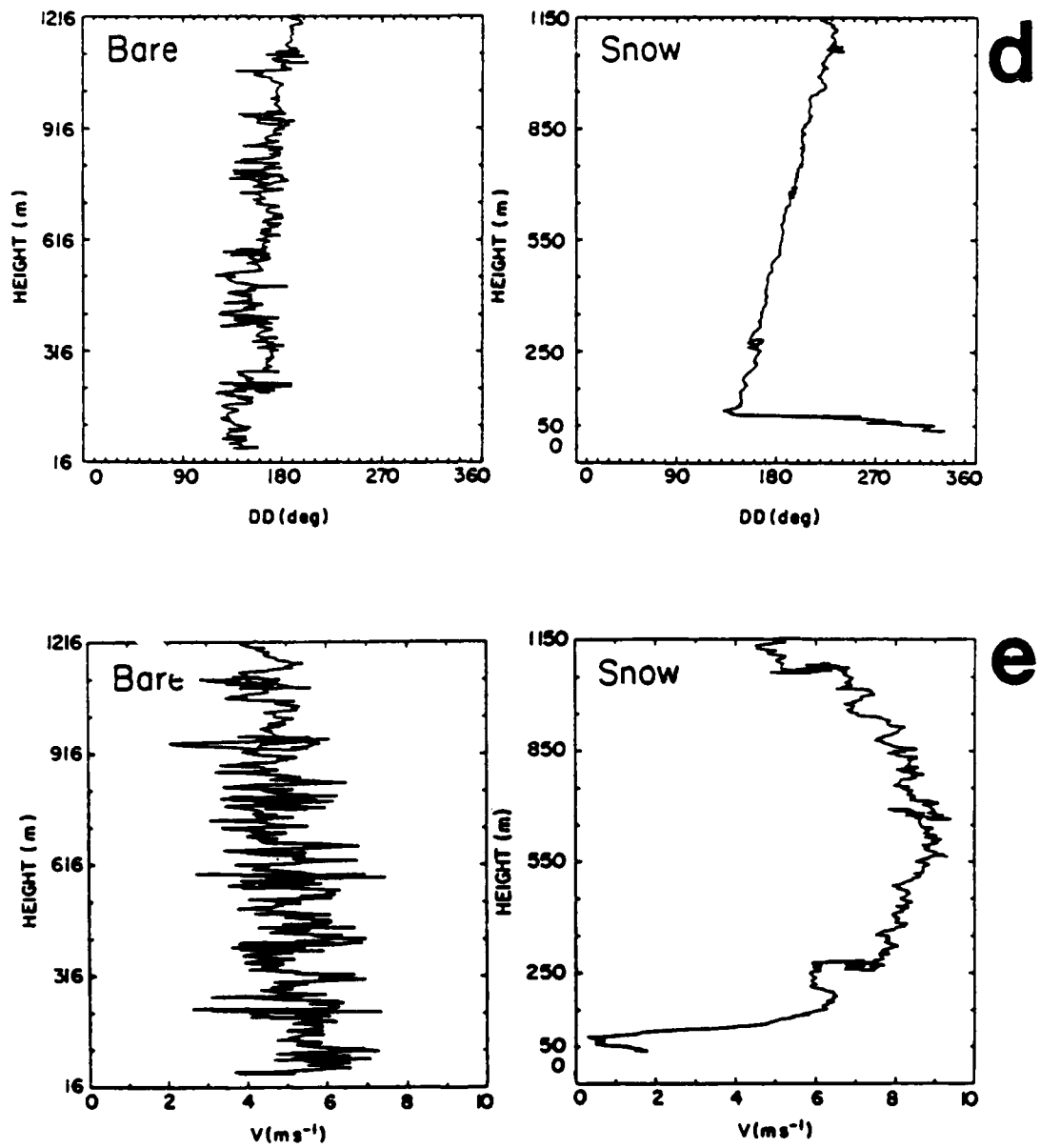


Figure 4.5: Continued.

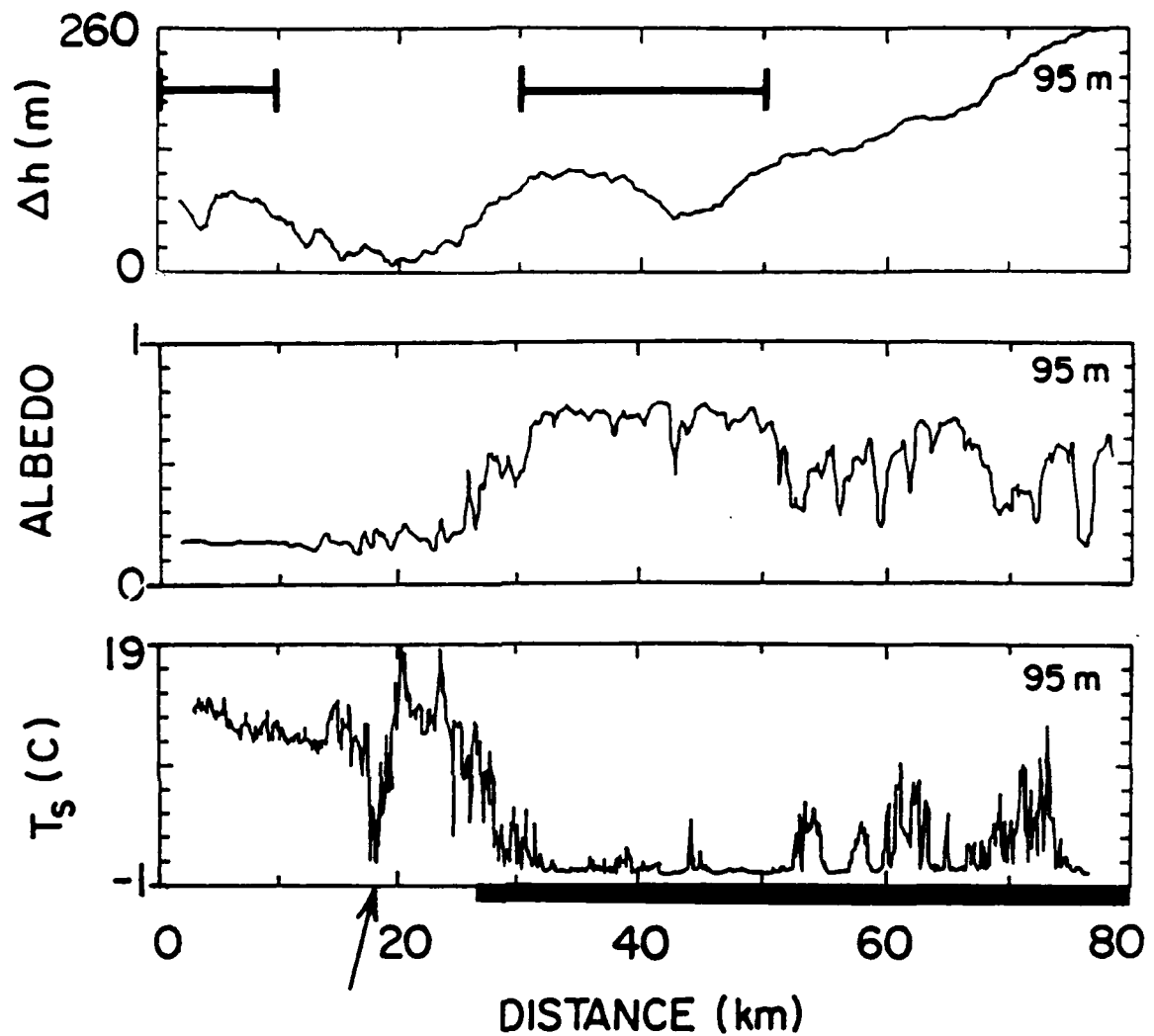


Figure 4.6: (a). Plotted aircraft measurements from flight #1 horizontal transects are shown in Figs. 4.6 (a-i). 95 m data measured from 12:48:48 - 13:13:24 MST. 170 m data were measured from 13:16:20 - 13:32:00 MST. 340 m data were measured from 13:34:18 - 13:48:30 MST. 710 m data were measured from 13:52:10 - 14:08:00 MST. Dark line indicates snow-covered portion of transect. The Δh plot was derived from measured air pressure. The arrow associated with the lowest terrain height depicts the location of the frozen Arkansas River. The bars on the Δh plot indicate the locations of the vertical profile measurements.

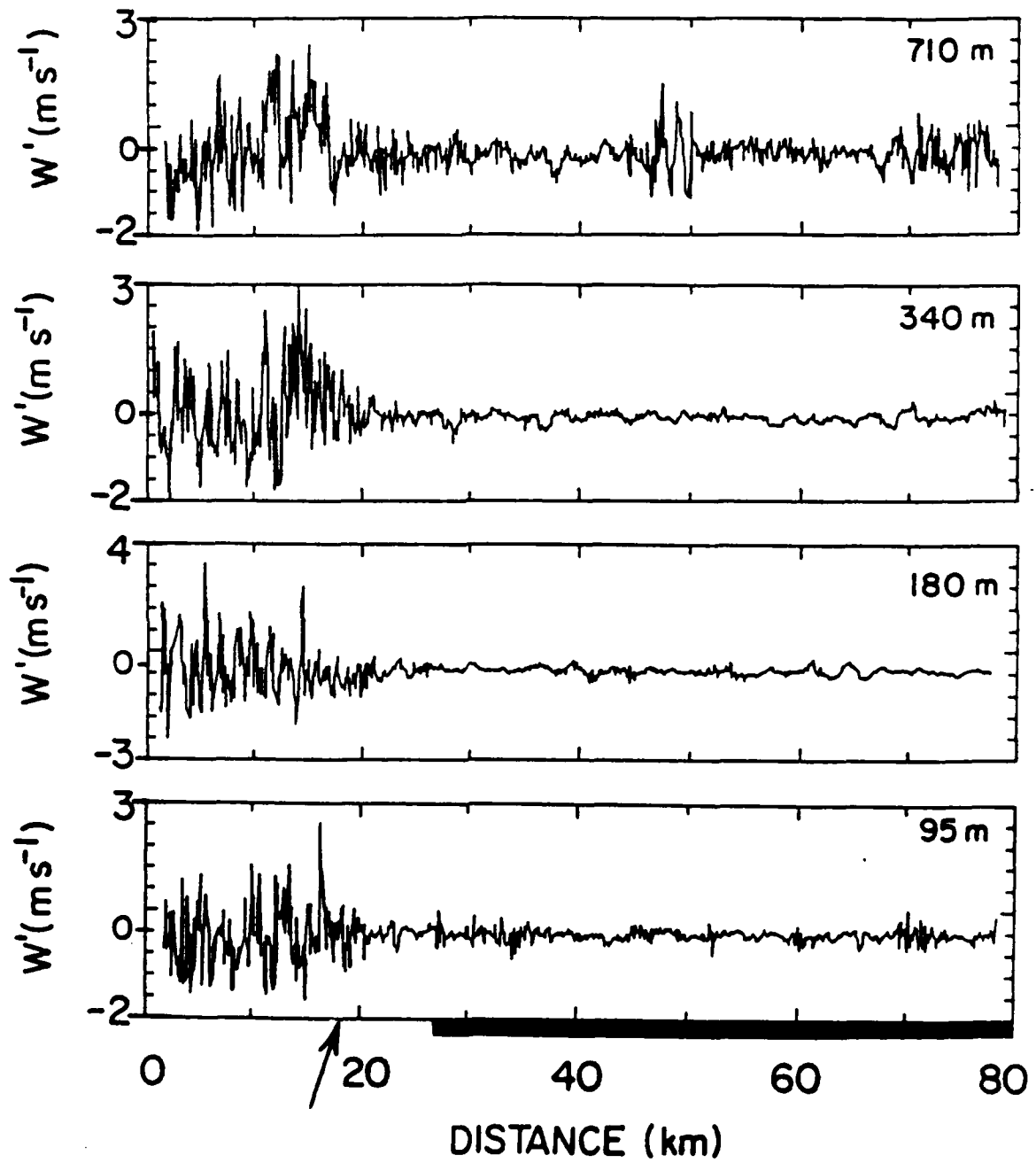


Figure 4.6: (b). Tick mark interval for w' for 95 m, 340 m, and 710 m data is 0.5 m s^{-1} ; for 180 m data it is 0.7 m s^{-1} .

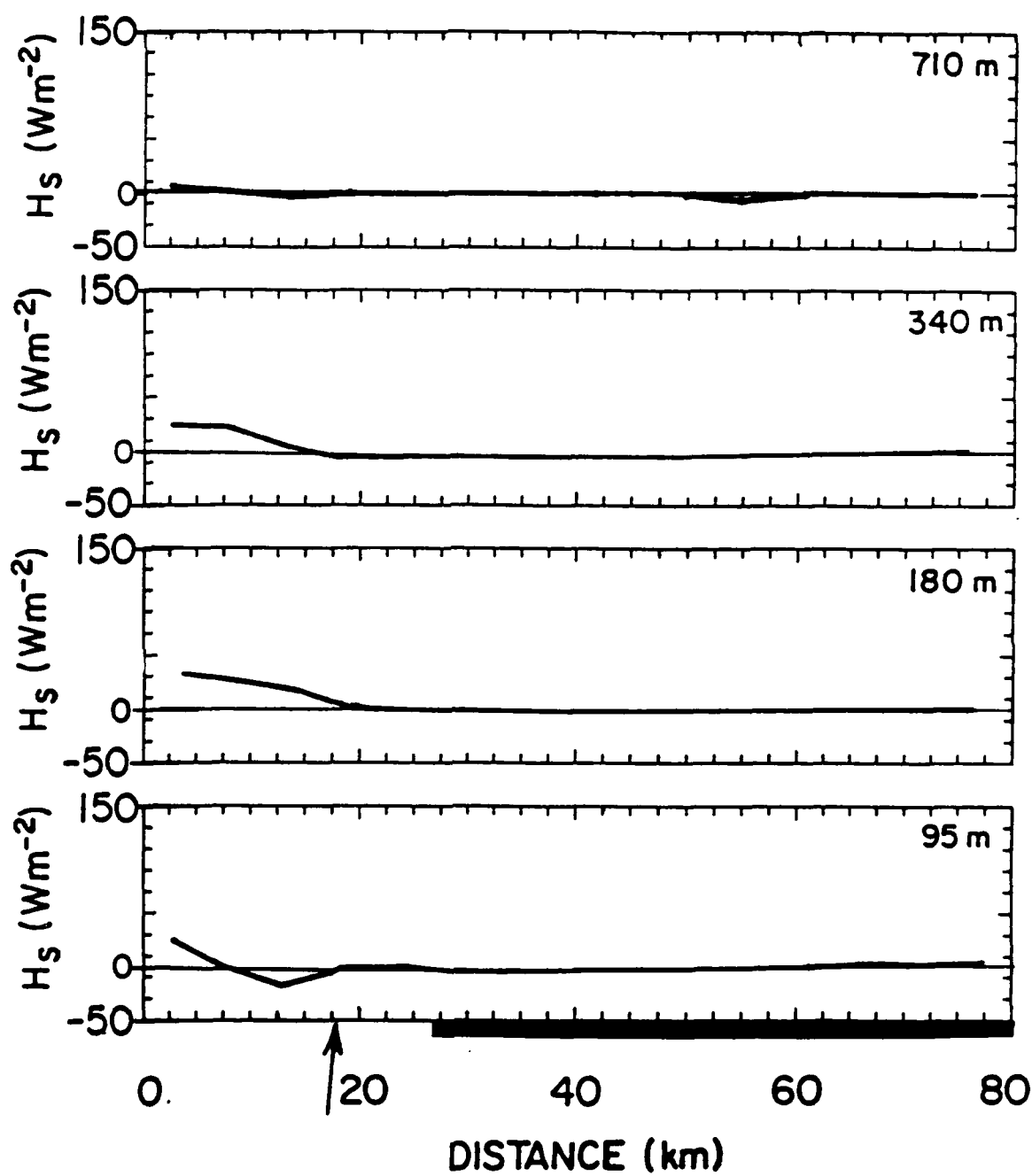


Figure 4.6: (c). Tick mark interval for H_S is 20 W m^{-2} .

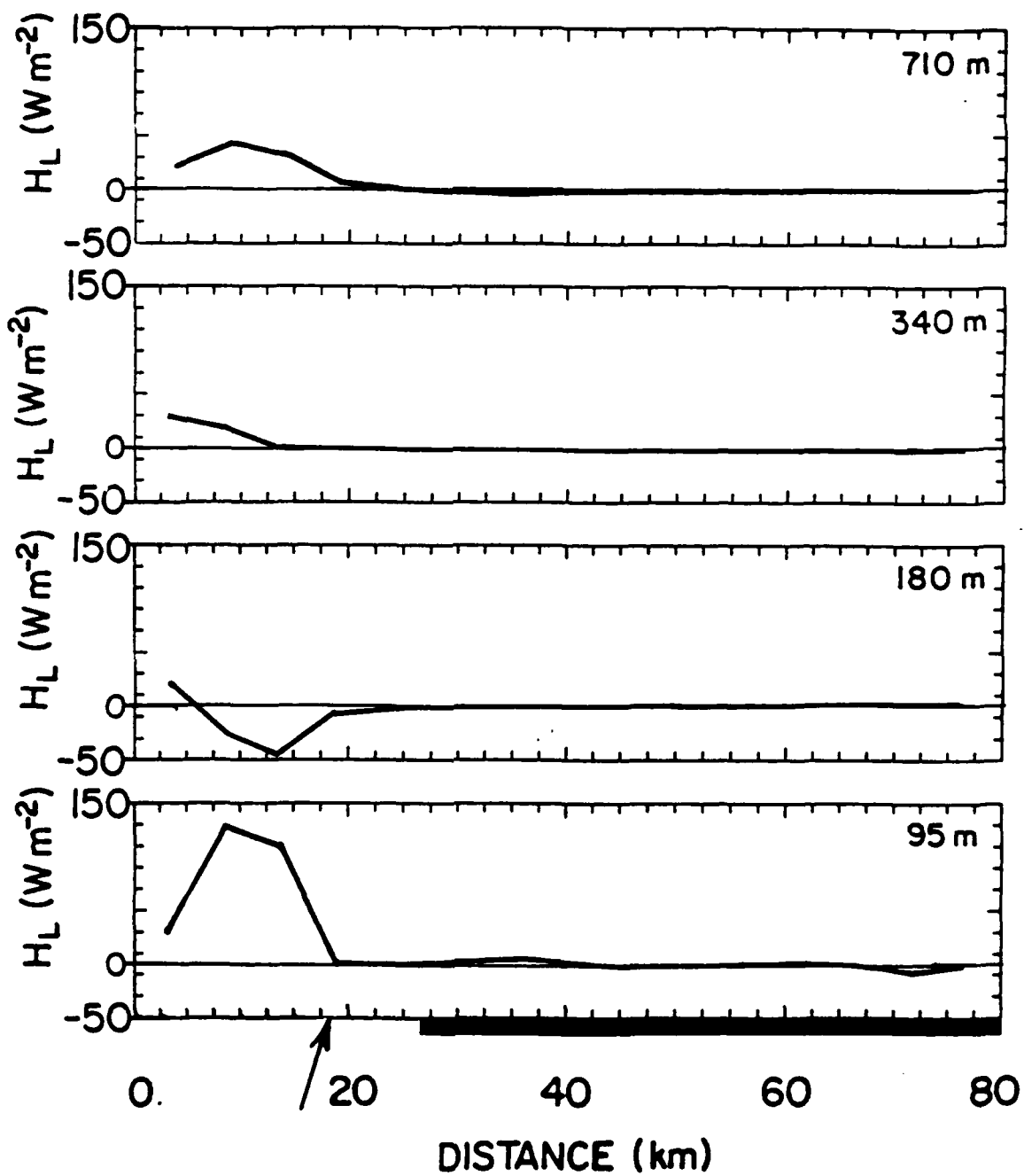


Figure 4.6: (d). Tick mark interval for H_L is 20 W m^{-2} .

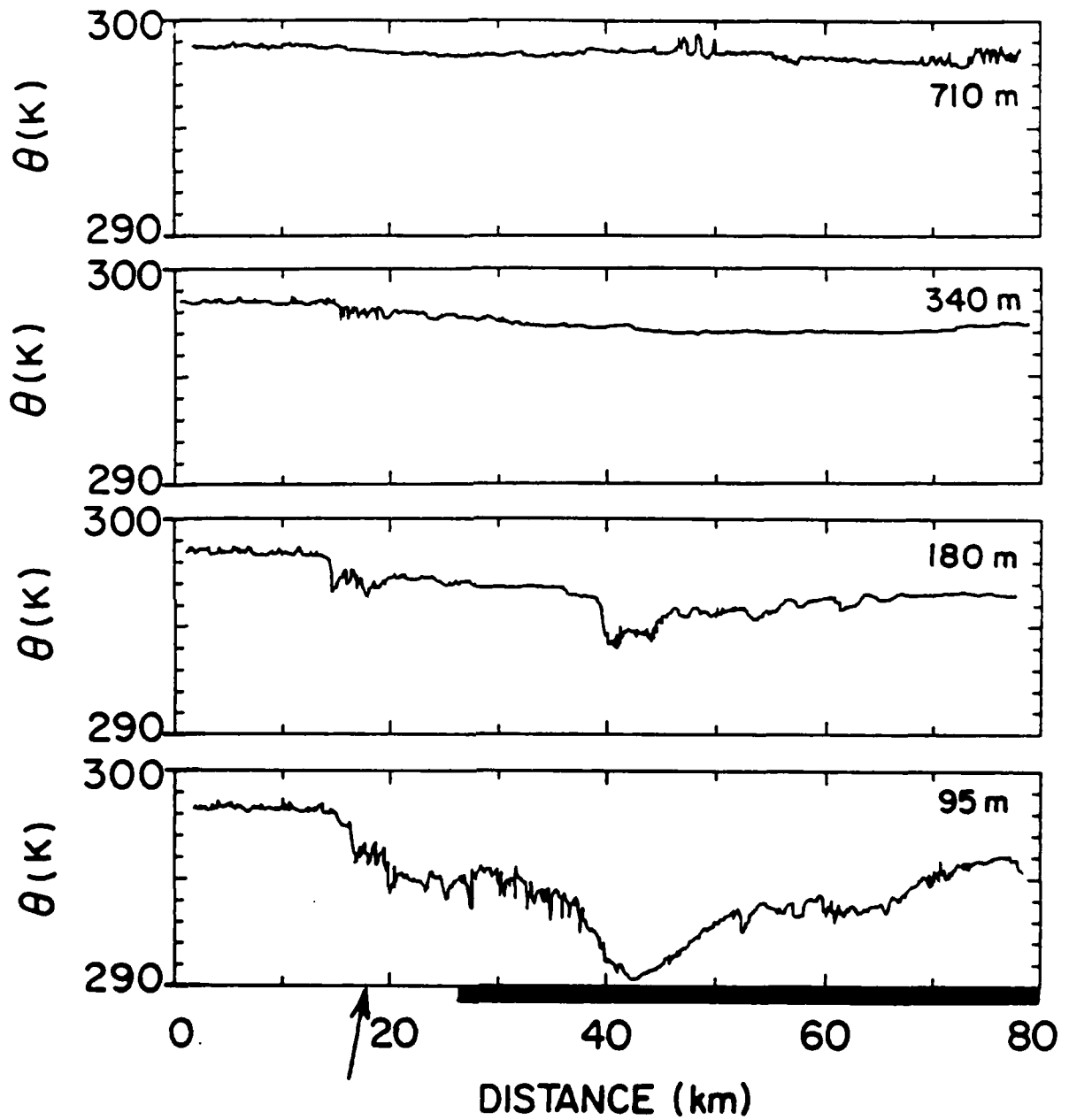


Figure 4.6: (e). Tick mark interval for θ is 1 K.

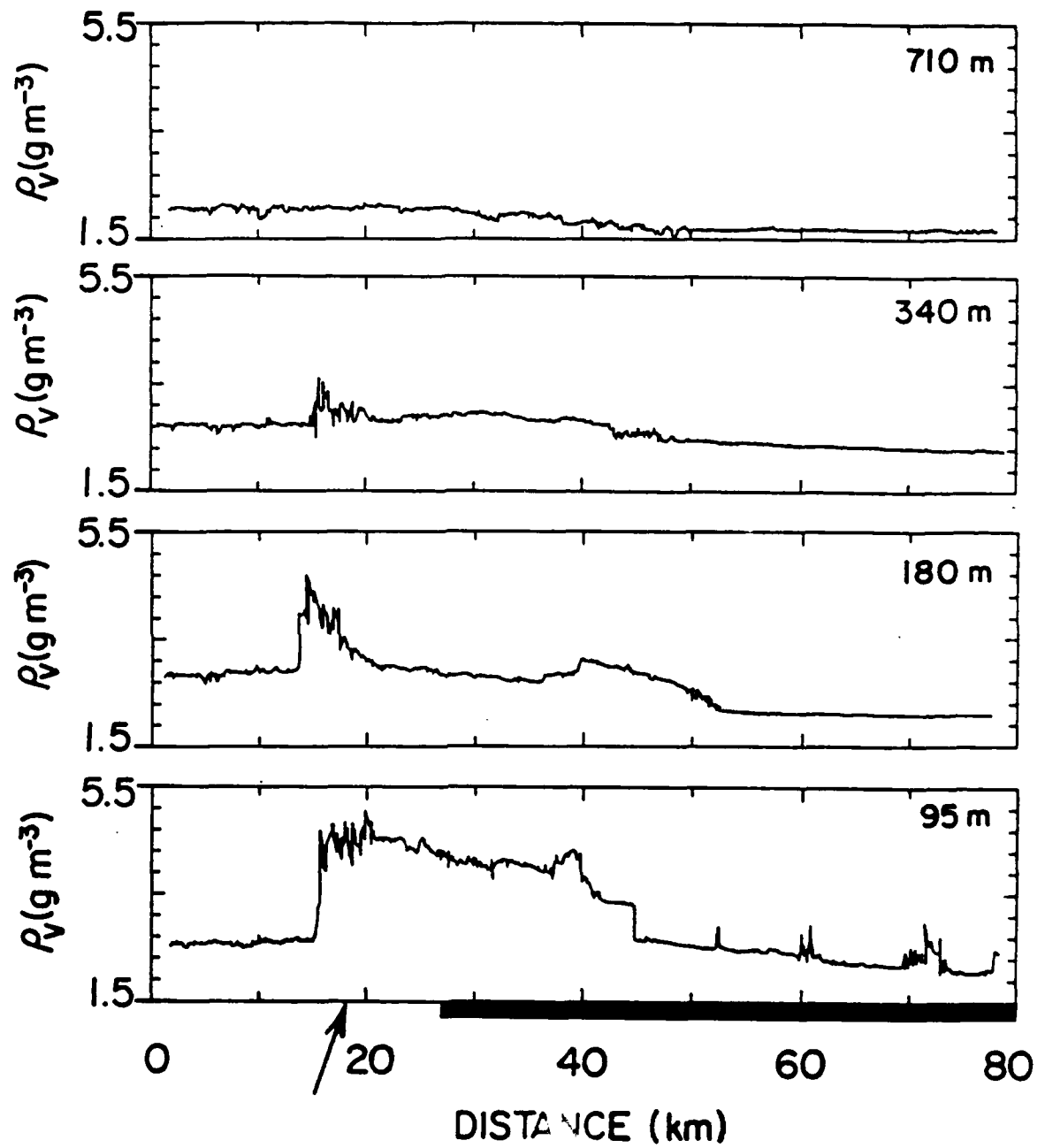


Figure 4.6: (f). Tick mark interval for ρ_v is 0.4 g m^{-3} .

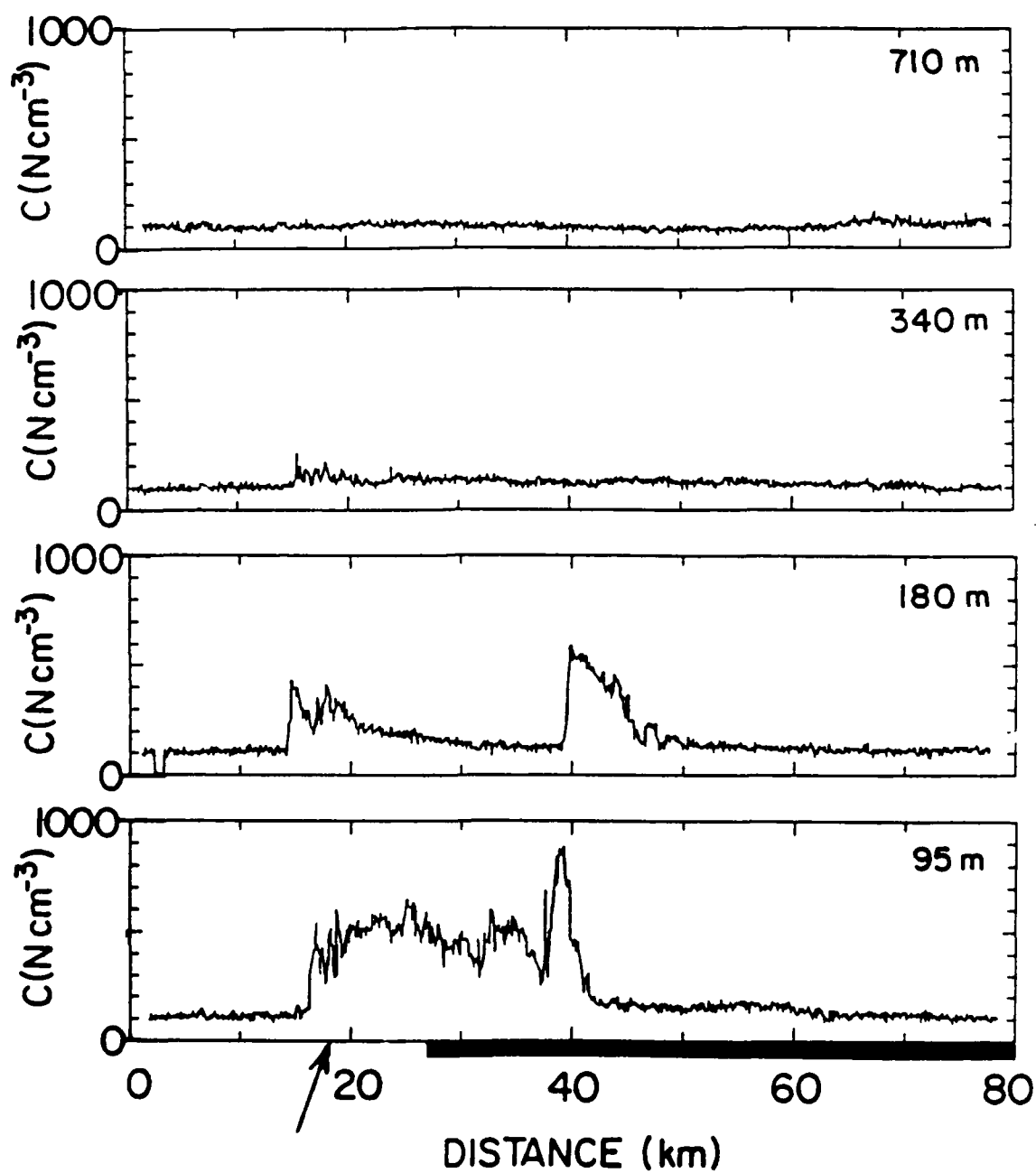


Figure 4.6: (g). Tick mark interval for C is 100 particles per cubic centimeter.

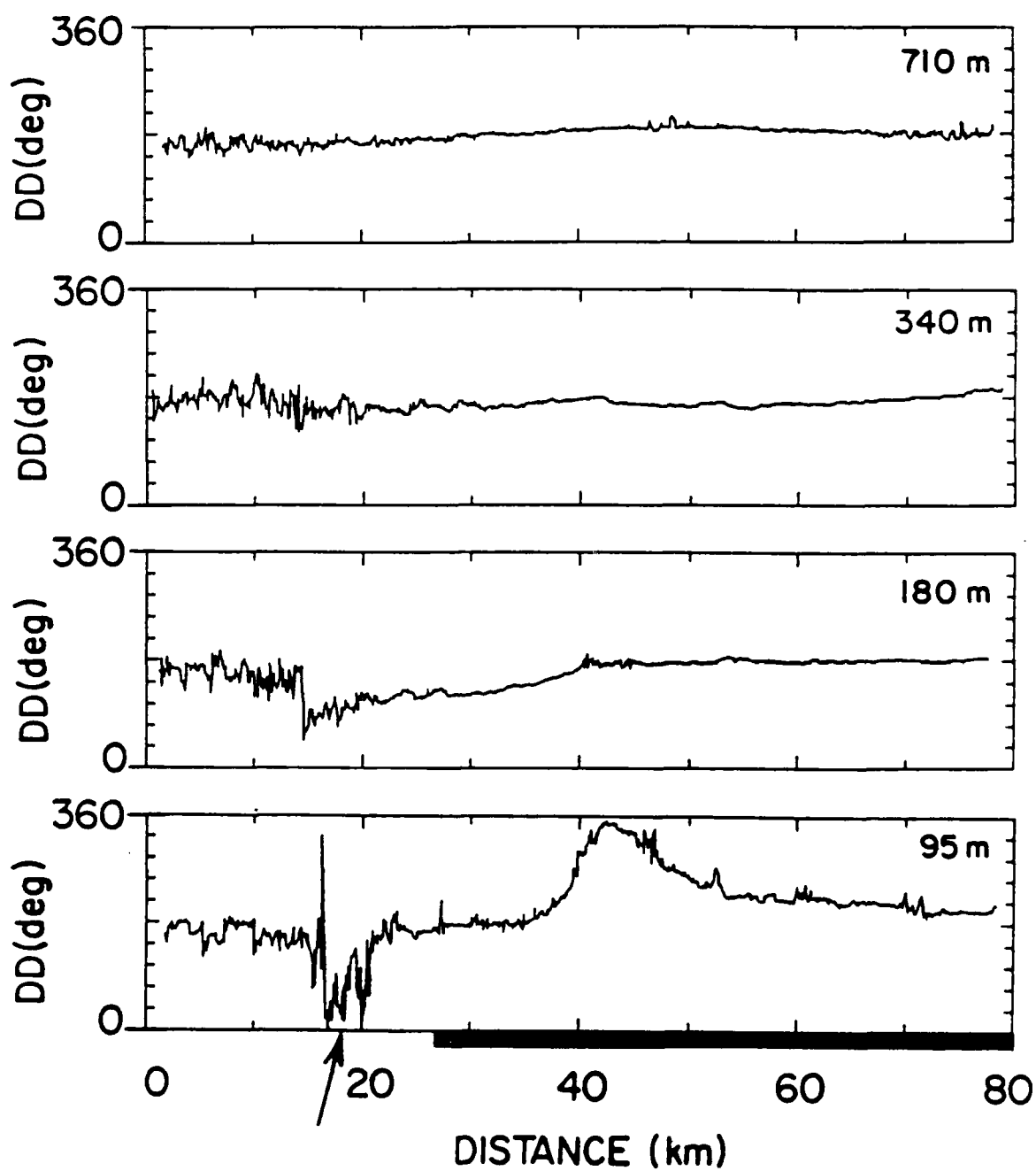


Figure 4.6: (h). Tick mark interval for DD is 36° .

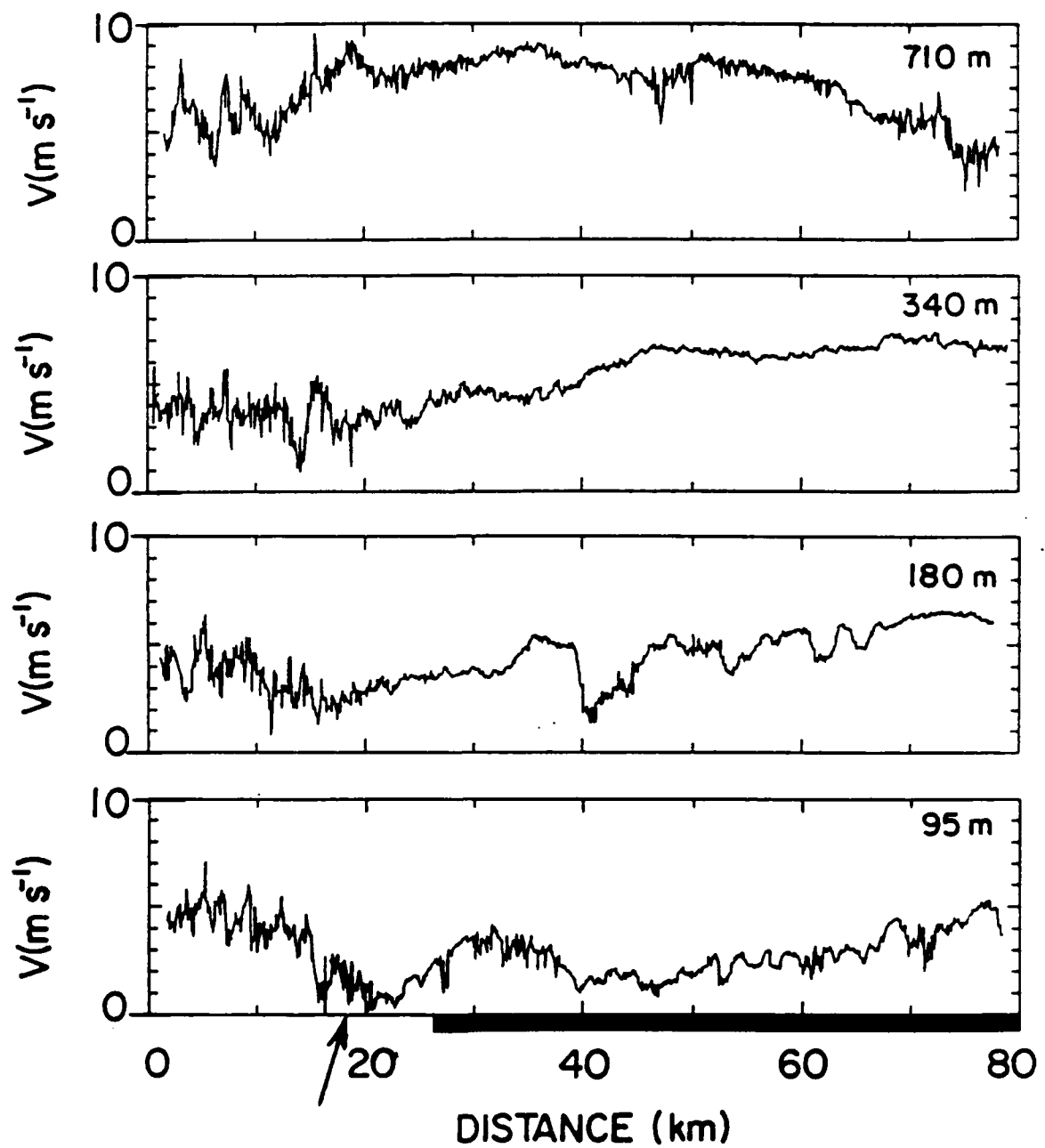


Figure 4.6: (i). Tick mark interval for V is 1 m s^{-1} .

over the snow due to the relative lack of mixing there. (Note the more turbulent nature of the wind speed profiles over the bare soil.) It is possible that the higher wind speeds observed over the snow are caused by a component of the snow breeze return circulation (see Fig. 4.6 for evidence of the snow breeze). There is also expected to be less upslope thermal forcing over the snow. More significant differences in the winds between the two regions are found below 100 m.

At the lowest sounding level the flow over the bare region is southerly at $4 - 5 \text{ m s}^{-1}$. Over the snow the flow is north - northwesterly at nearly 2 m s^{-1} . As will be seen in the data from the horizontal legs (Fig. 4.6), this north - northwesterly opposing wind appears to be a snow breeze.

Data from the horizontal transects flown across the snow boundary are presented in Fig. 4.6a-i. The varying topography (Δh in Fig. 4.6a), the presence of the relatively narrow, frozen Arkansas River (located at the lowest minimum in the Δh plot of Fig. 4.6a, at about 17 km along the transects), and the snow/bare soil contrast (indicated in the figures) are apparently responsible for several boundary layer anomalies, including wind deflections.

Fig. 4.6a shows that there is a relatively sharp gradient in surface temperature from 17°C to 0°C from the bare soil to the snow surface. Note that the surface temperature plot indicates that the snow cover is quite uniform for a distance of about 20 km. It then becomes patchy. The sharp, narrow surface temperature drop to near 0°C at about 17 km represents the aircrafts' crossing of the frozen Arkansas River. Note also the significant change in albedo that occurs from the bare soil to the snow cover. The effects of the snow cover, the undulating terrain, and the Arkansas River on the atmosphere are significant.

Figs. 4.6b-d reveal the differences in the turbulence of the atmosphere over the snow-covered and bare surfaces. Although the sensible heat fluxes (Fig. 4.6e) are not large, they are generally toward the atmosphere over the bare soil and nearly zero over the snow. The latent heat flux generally follows the same pattern (Fig. 4.6d).

Fig. 4.6e shows that the atmosphere north of the Arkansas River and also over the snow is cooler than the air over the bare soil region through a height of 340 m. The most

significant potential temperature difference is noticed at the lowest flight level (95 m). The potential temperature of the atmosphere is shown to drop as the air is advected over the frozen Arkansas River (as one looks at the figures, air is generally being advected by the background flow from left to right). A second potential temperature drop is measured well over the snow region and appears to be related to a cold pool of air in a small terrain minimum. The total drop in potential temperature from the warm bare soil region to the coolest air over the snow is about 8 K at 95 m. Less significant but noticeable decreases in potential temperature are measured at 170 and 340 m.

Fig. 4.6f-g show that in addition to being cooler, the air north of the Arkansas River and over the snow is more moist and more aerosol-laden than the bare region air. These changes are accompanied by changes in the local wind flow.

Figs. 4.6h-i show that there are two zones of wind deflection at 95 m. They are located in the same positions as the other modifications noted above. Just downwind of the Arkansas River there is a small zone (about 4 km long) where the wind is changed. Instead of experiencing the background flow of about 5 m s^{-1} out of the south, this small region has a wind flow of $1 - 2 \text{ m s}^{-1}$ out of the northeast, generally opposing the background flow. As the aircraft proceeds north of the river, the winds return to the general background flow. When the aircraft reaches the zone of cool air over the snow, another small zone of changed wind is detected. In this zone, an apparent snow breeze which very nearly directly opposes the background flow exists. The opposing flow reaches a maximum intensity of about 2 m s^{-1} . Similar but less significant wind changes occur at 170 m. Above that, only the turbulent differences in the character of the wind over the two surfaces are noticed.

4.3.3 Cross section analysis and summary

Another perspective on the data is gained by examining smoothed cross section analyses drawn from the plotted aircraft data (Fig. 4.7). The potential temperature (θ) plot shows strongly stable air over the snow. The two zones of horizontal temperature decrease are apparent, as are the associated snow breezes (note the u-plot. The u-plot represents

the component of the flow that is parallel to the flight transects). The entire region affected by the snow breeze systems are also marked by lower atmospheric trapping of water vapor and aerosols (Fig. 4.7b-c).

The snow - no snow gradient was sharp for this flight, but the good snow cover extended only for a distance of about 20 km. The average ambient temperature for the 95 m leg was about 9°C. Although the situation was complicated by background flow, variably sloping terrain, and the presence of the Arkansas River, the flight was supportive of the hypothesis.

4.4 Flight #7

4.4.1 Situation

From 16 - 18 March, 1988 a late winter storm moved southeastward from the Four Corners region into the northern Gulf of Mexico (Fig. 4.8). As it passed, it left a snowband that stretched from the central Texas panhandle through northwest Oklahoma and into southeastern Kansas (Fig. 4.9a). As is seen in the satellite imagery, fairly sharp snow - no snow boundaries existed along the northwest and southeast sides of the snow band.

Although it was out of the planned 300 km range for the project and other areas of snow cover were closer, the Texas - Oklahoma panhandle snowband forced serious flight consideration. The band was fresh, relatively deep (maximum snow depth report of 30 cm at Gage, Oklahoma (GAG)), had sharp boundaries, and existed over relatively flat terrain. Since the end of the the project was near (25 March) and sufficient flight hours were left (about 14), the CSU researchers decided to perform an abridged set of measurements over the northwest boundary of this snow band.

On the morning of 18 March, the snow band region was under the influence of high pressure centered in western Colorado. A northwesterly surface geostrophic wind prevailed across the region. The chosen transect location and orientation are shown in Fig. 4.9.

4.4.2 Measurements

The surface temperature gradients across the snow - no snow boundary were substantial by early afternoon (Fig. 4.9b and 4.10). Fig. 4.10 shows that across the snow

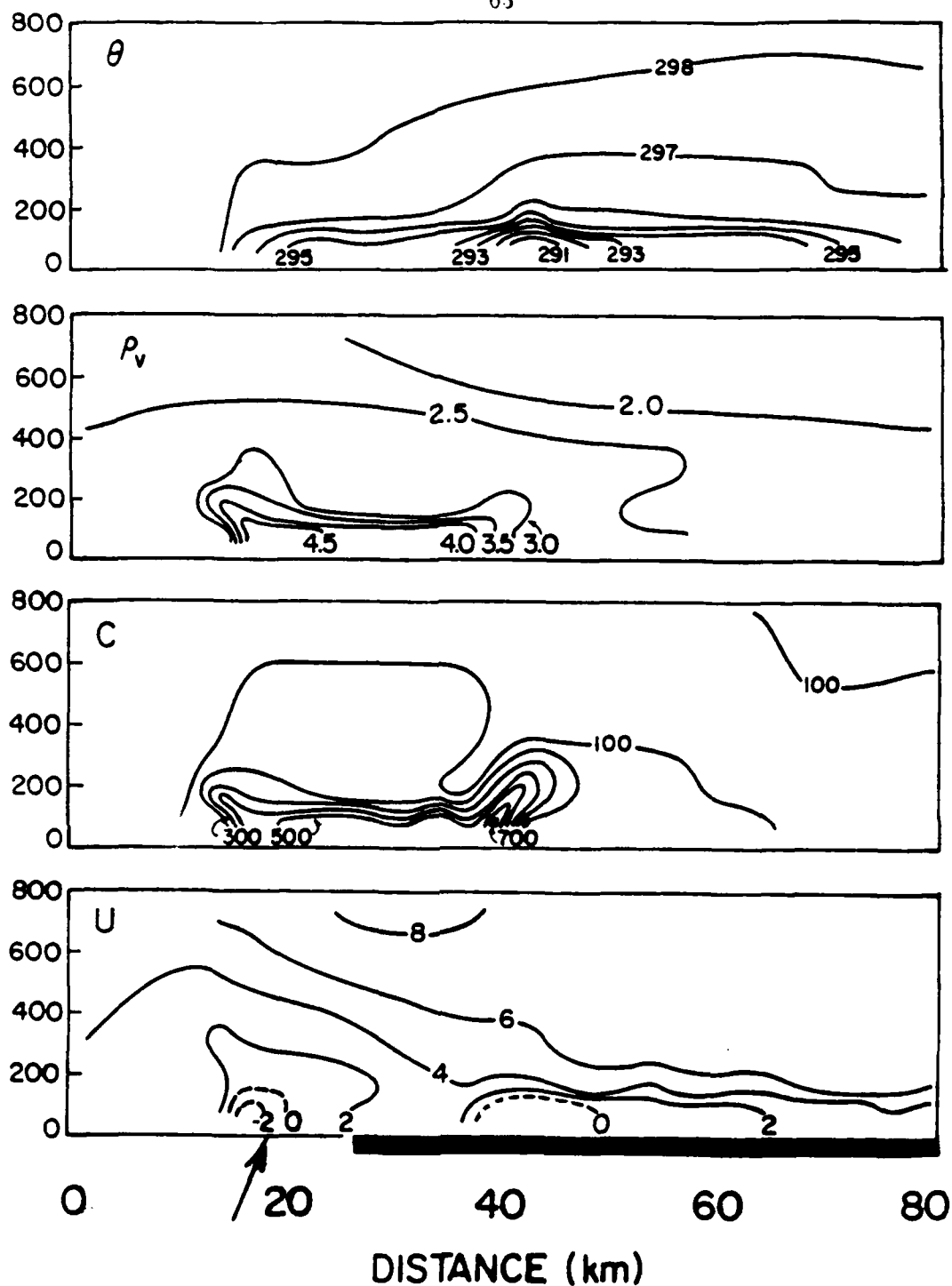


Figure 4.7: Cross section analyses for flight #1 based on the horizontal transect data presented in Fig. 4.6. For θ , the contour interval is 1 K; for ρ_v , the contour interval is 0.5 g m^{-3} ; for C , the contour interval is $100 \text{ particles cm}^{-3}$; and for u , the contour interval is 2 m s^{-1} . Dashed line indicates flow in the negative x direction and the vertical-axes indicate height (m). The dark line and arrows are as in Fig. 4.6. The distance scale and the x -axis, lies along the flight transect with the positive (x) direction pointing toward 350° as measured clockwise from the north.

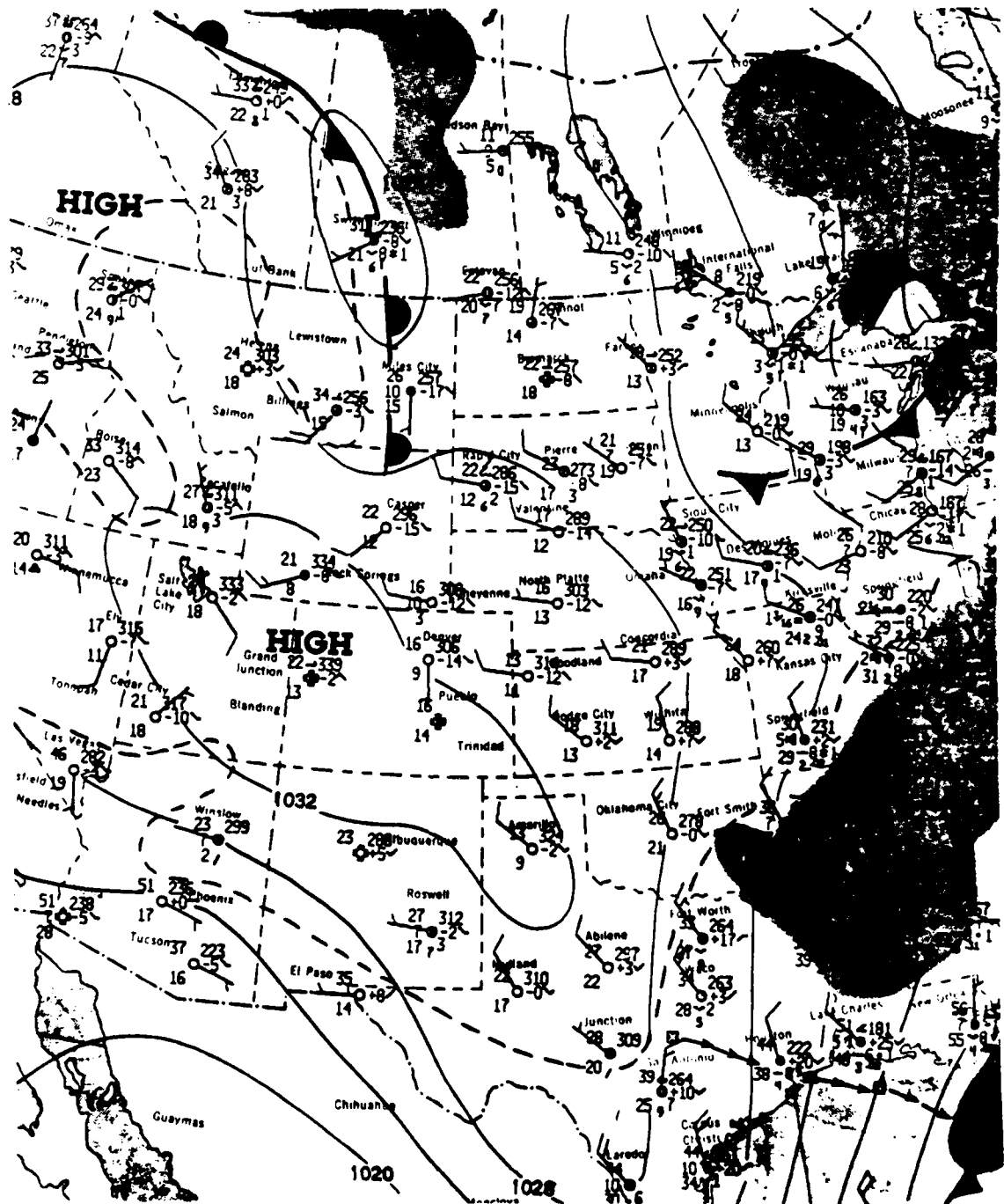


Figure 4.8: As in 4.3 except for 18 March, 1988.

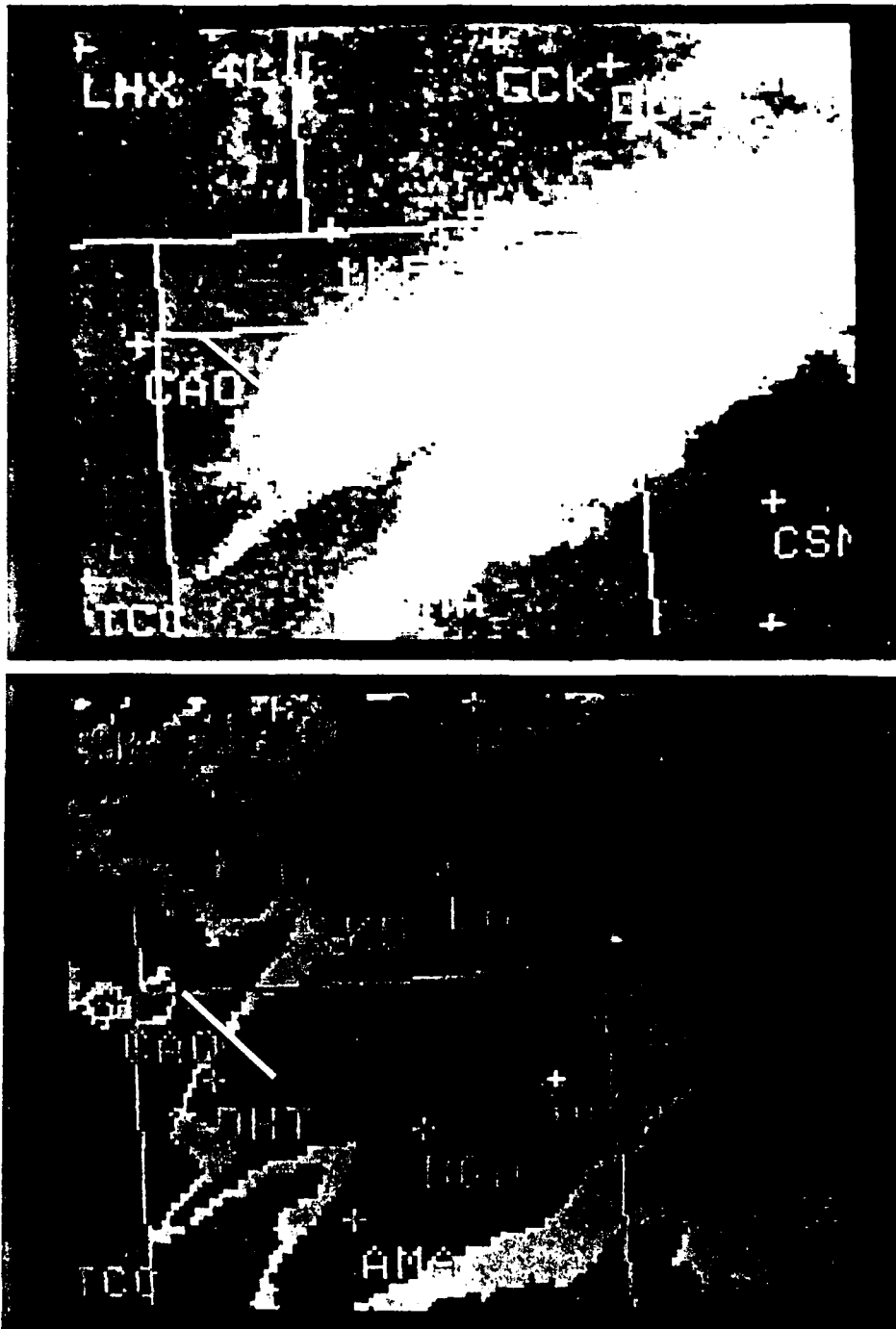


Figure 4.9: As in Fig. 4.2 except for 18 March, 1988. Also (a) visible image is for 1017 CST; and (b) IR image is for 1345 CST.

boundary near the chosen transect location, a surface temperature change of 8°C in 11 km was observed by satellite ($\sim 0.7^{\circ}\text{C km}^{-1}$). Again, stronger gradients were observed by aircraft (Fig. 4.12a). Judging from these infrared satellite photos the transect location choice was quite good. Plotted aircraft measurements are presented in Figs. 4.11 - 4.13.

The "snow-covered" region for this flight was patchy and melting. Some areas of bare soil and vegetation were clearly visible. As in flight #1, the vertical profile measurements reveal a very different boundary layer over the snow-covered and snow-free regions.

A neutral layer developed over both surfaces, but it is much deeper over the bare soil. The plots in Fig. 4.11 reveal a boundary layer depth of about 1800 m over the bare region; over the snow, the boundary layer depth is only about 400 m. The profiles show that over the snow the lowest several hundred meter layer of the atmosphere is about 7 K cooler than the low-level air over the bare region. As in flight #1, the low-level profile data hint at the existence of snow-breeze.

Over both regions the flow is generally north-northwesterly. In the lowest several hundred meters the flow is $5\text{--}8\text{ m s}^{-1}$ over the bare region while over the snow it is more westerly and only $1\text{--}3\text{ m s}^{-1}$ (Fig. 4.11d-e).

Data from the first 90 m flight transect are shown in Fig. 4.12. Note that the terrain is less undulating in this case (Fig. 4.12a). The surface temperature and albedo plots indicate a reasonably good contrast between the bare soil and the patchy snow (Fig. 4.12b-c). The surface temperature gradient is roughly 18°C across the transect (from about 24°C over the bare soil to about 6°C over the patchy snow). Again the presence of the snow cover had a major impact on the overlying atmosphere.

Fig. 4.12d-f show the changes in turbulence characteristics along the transect. Note the large change in upward sensible heat flux (Fig. 4.12e). This flux ranges from about 200 W m^{-2} at the transect beginning over bare soil to about 20 W m^{-2} deep within the snow band. On the other hand, the latent heat flux is small over the apparently dry bare soil, but increases over the snow (Fig. 4.12f). The observed atmospheric contrasts of potential temperature, absolute humidity, and wind are substantial and abrupt, as across a frontal boundary.

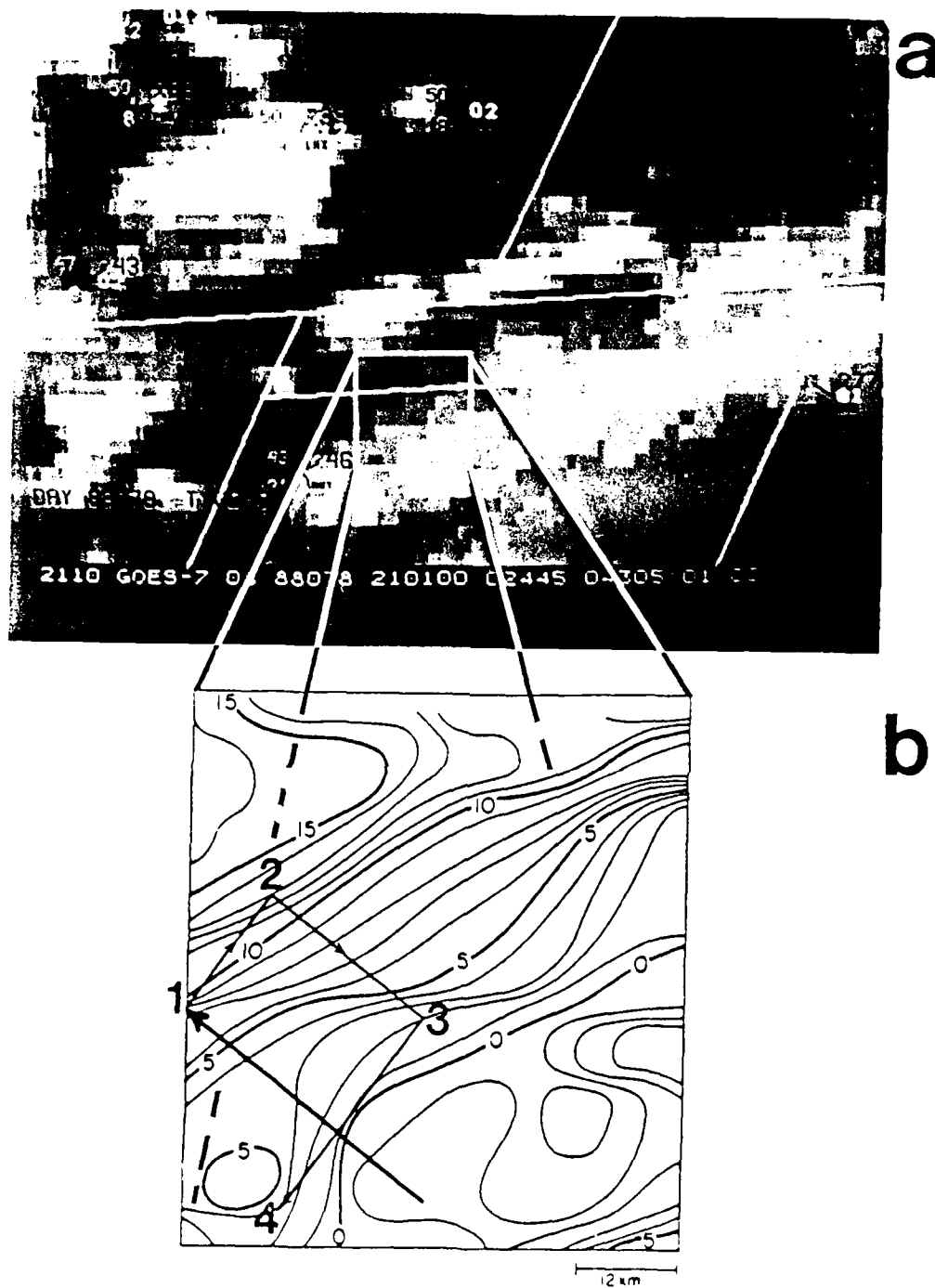


Figure 4.10: As in Fig. 4.4 except for 18 March, 1988, 1501 CST. Also, heavy line indicates portion of flight #7 transect. The rectangular pattern near the transect line (with 90° angles labeled 1, 2, 3, and 4) depicts the flight pattern on which the data presented in Fig. 4.11 were measured. 1-2 is a segment over bare soil, parallel to the snow boundary; 3-4 is also parallel to the boundary, but is over snow cover.

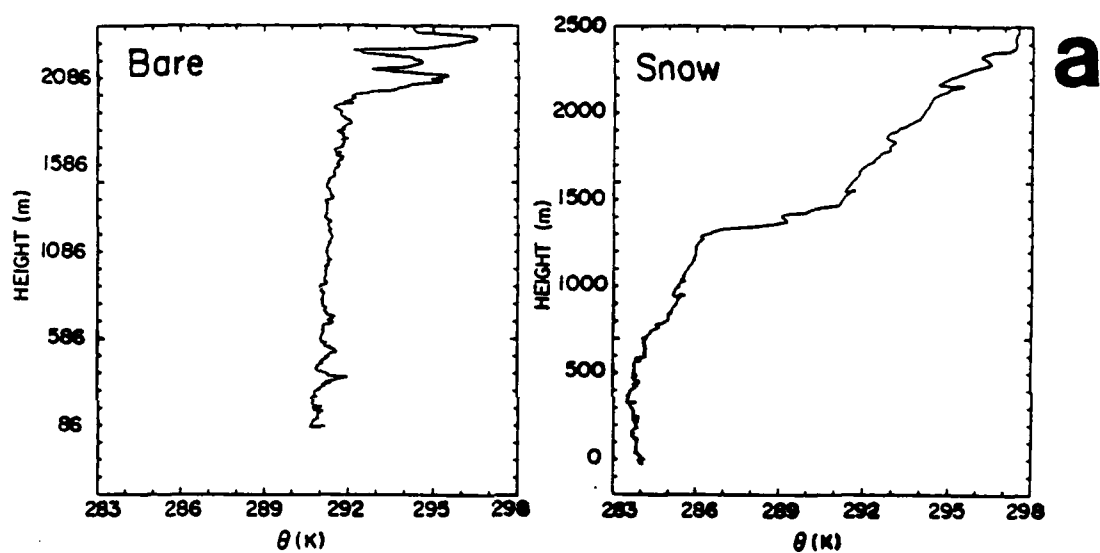


Figure 4.11: (a-e). Vertical profile measurements from flight # 7. Snow measurements were made from 13:55:40 - 14:13:17 CST. Bare measurements were made from 15:36:23 - 15:47:00 CST.

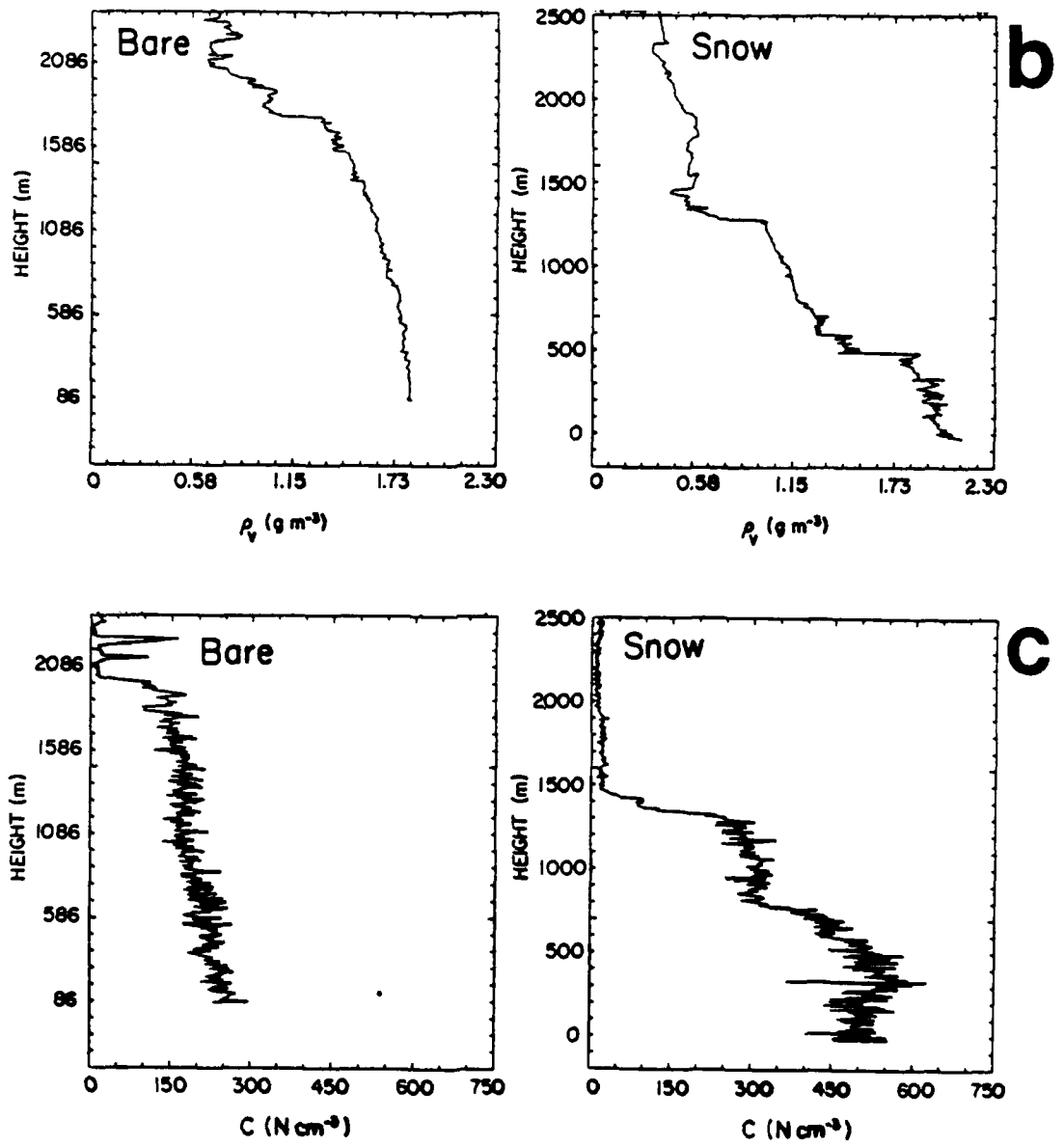


Figure 4.11: Continued.

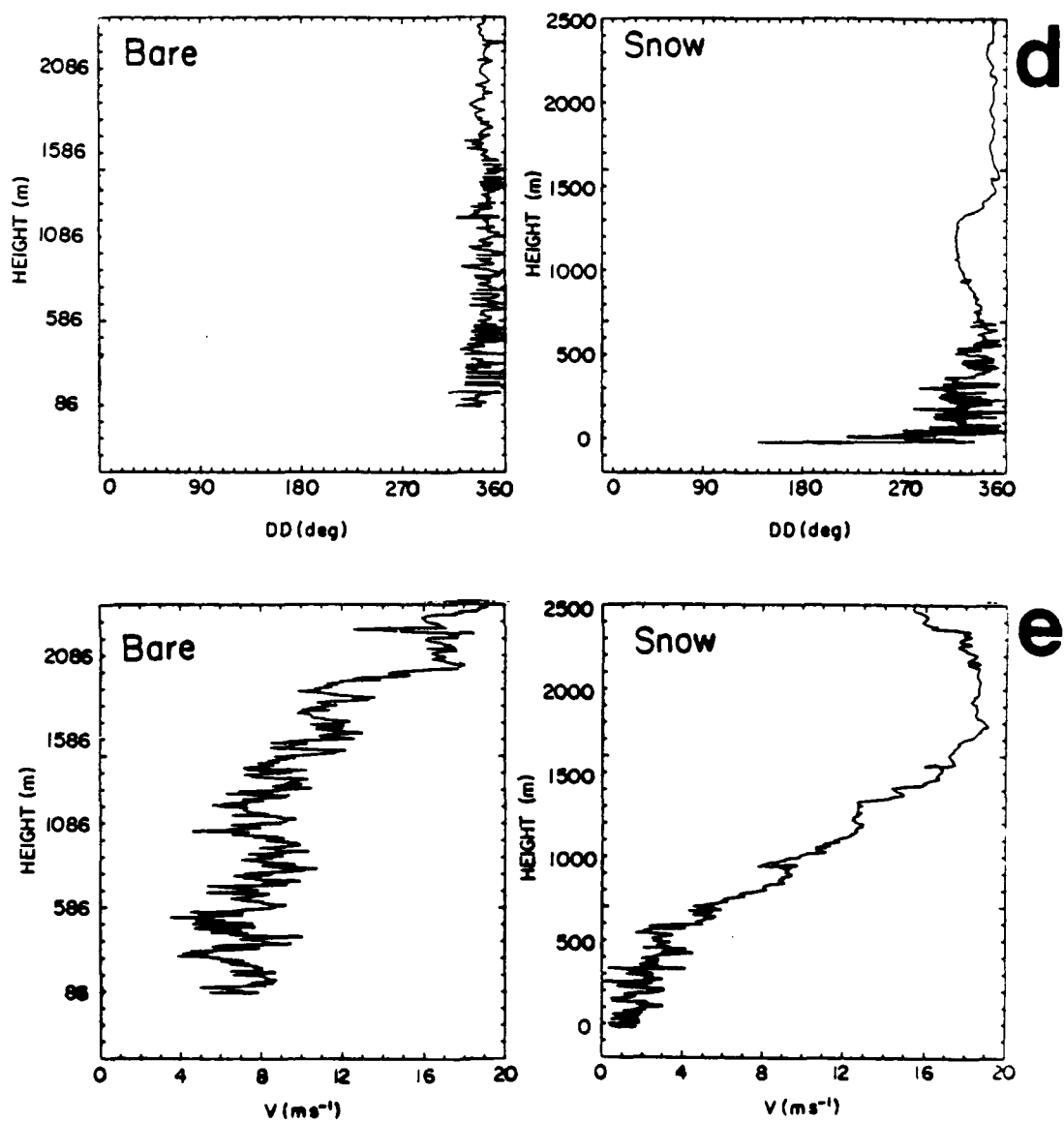


Figure 4.11: Continued.

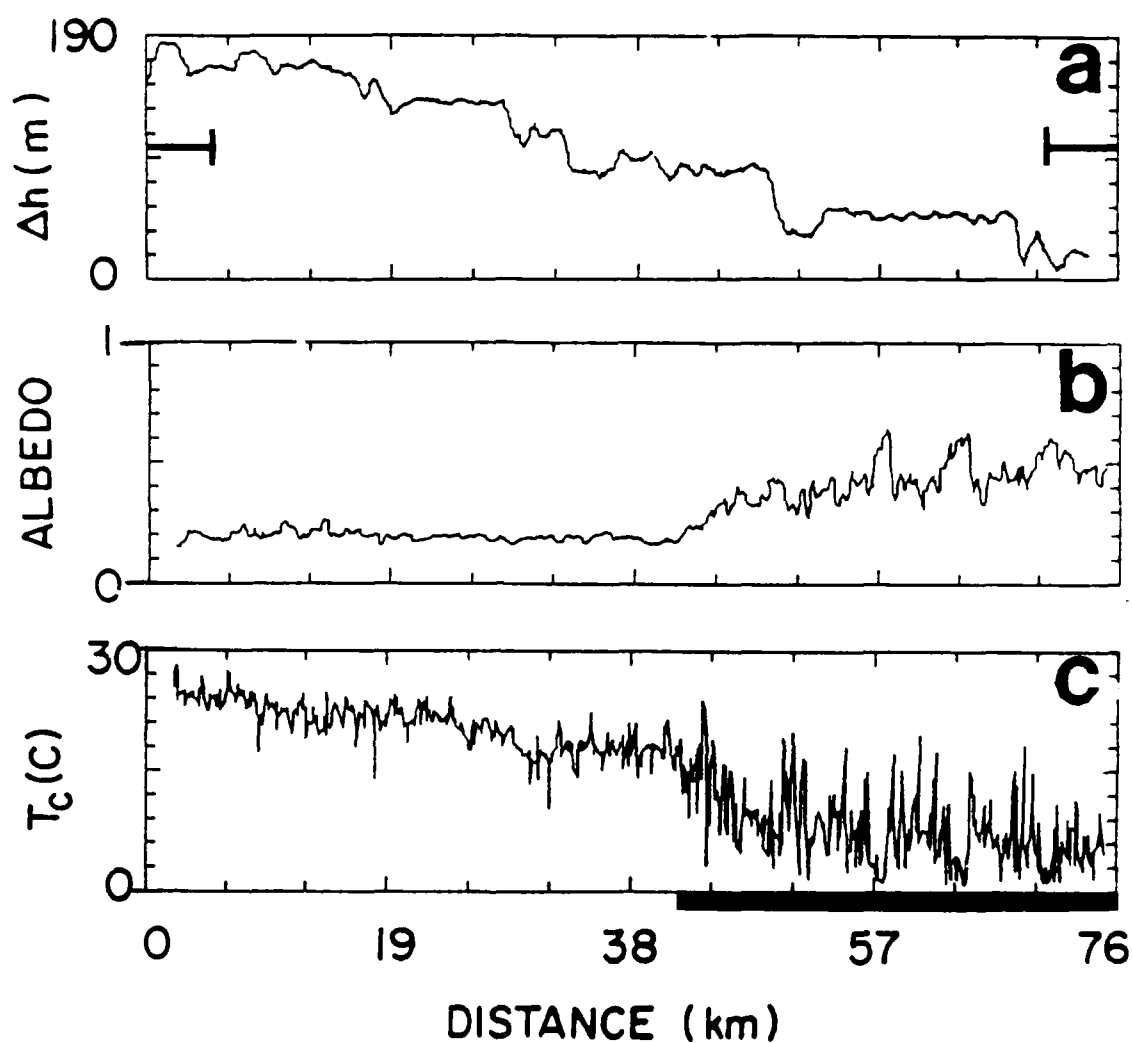


Figure 4.12: (a-j). 90 m flight transect data measured from 14:13:50 - 14:28:43. Dark line indicates snow-covered portion of transects. Fig. 12a, the relative terrain (Δh) plot, is based upon measured air pressure. The location of the vertical profile measurements over the snow (partially depicted by the bar and arrow in the Δh plot (Fig. 4.12a) extends another 10 km beyond the right-hand side of the figure. Similarly, the location of the bare vertical profile measurements extend another 21 km beyond the left-hand side of Fig. (a). The tick mark interval for Δh is 19 m; for albedo it is 0.1; for T_c is 3°C.

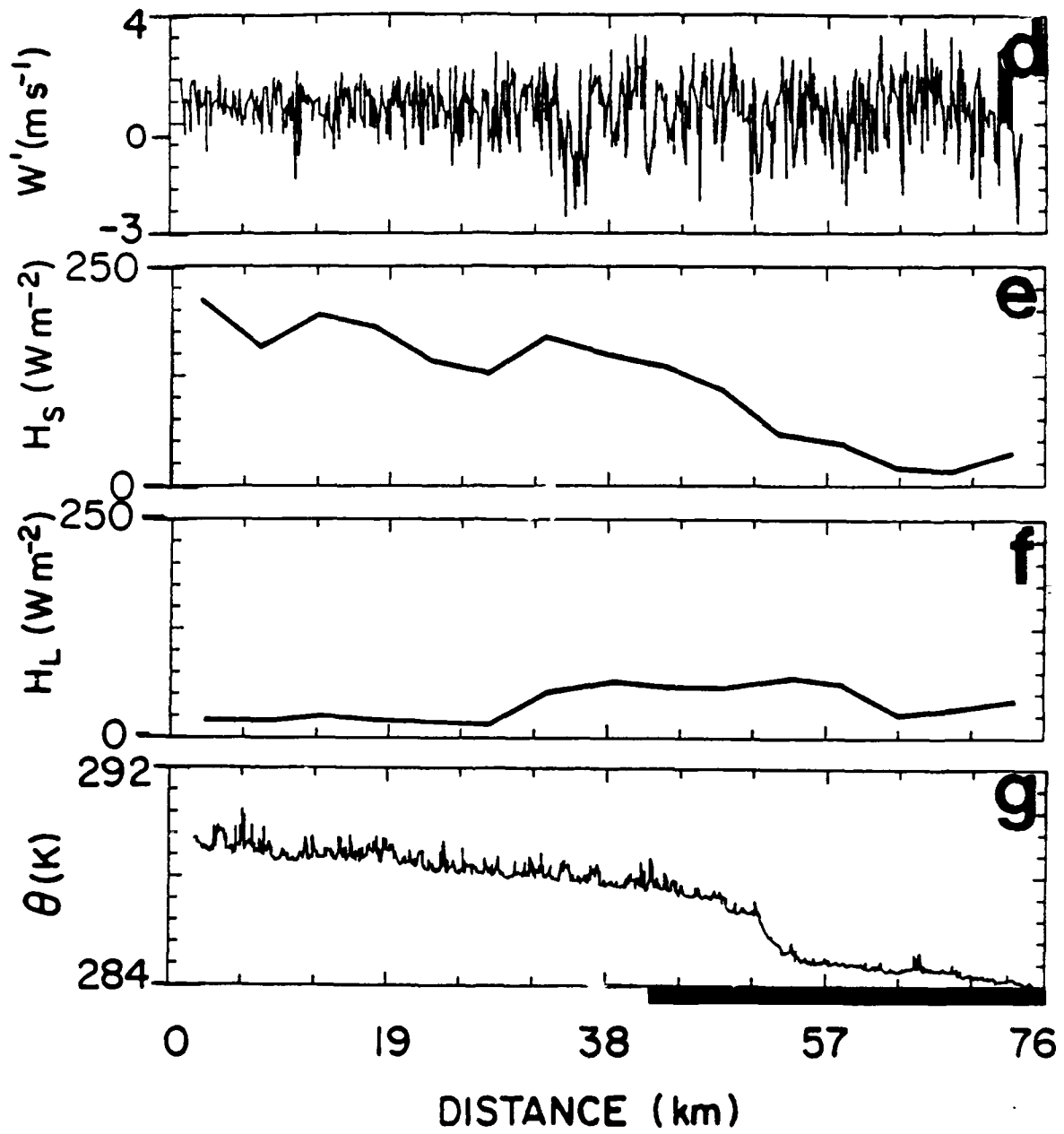


Figure 4.12: Continued. Tick mark interval for w' is 0.1 m s^{-1} ; for H_S and H_L it is 25 W m^{-2} ; and for θ is 0.8°C .

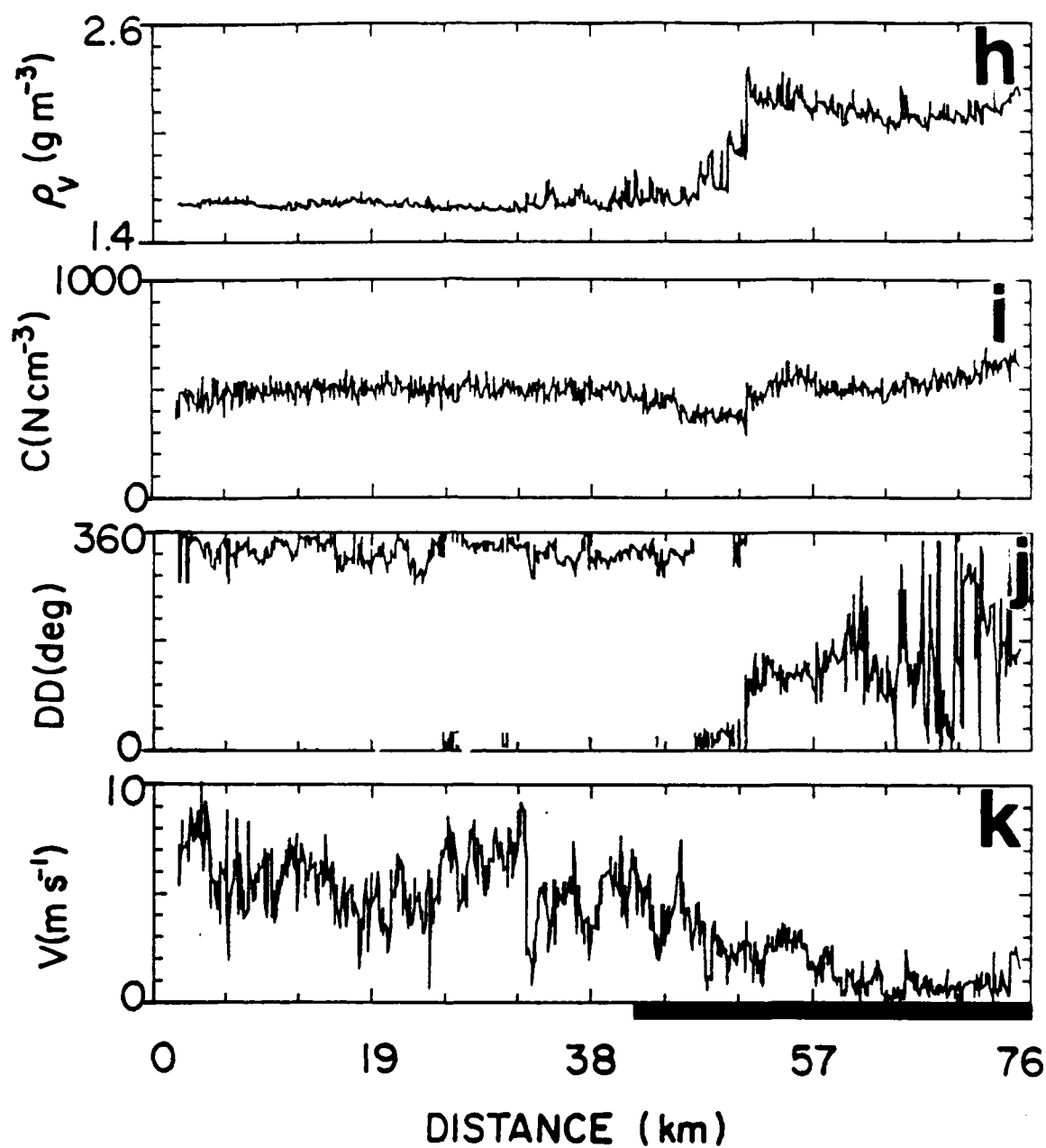


Figure 4.12: Continued. Tick mark interval for ρ_v is 0.12 g m^{-3} ; for C it is 100 N cm^{-3} ; for DD it is 36° ; and for V it is 1 m s^{-1} .

The potential temperature change is about 5 K across the transect with most of that change occurring within a 5 km zone (Fig. 4.12g). Within nearly the same zone the absolute humidity increases from about 1.6 g m^{-3} to 2.2 g m^{-3} . The wind measurements show distinct snow-breeze development (Fig. 4.12h).

The winds over the bare region reflect the background flow ($4\text{--}8 \text{ m s}^{-1}$ from the north-northwest; Fig. 4.12j-k). This flow would nearly directly oppose a mesoscale circulation induced by the surface contrast. This is, in fact, what happens as the wind flow on the snow side of the boundary is generally south-southeasterly at about 1 m s^{-1} . The fact that the background flow is moderate (less than 10 m s^{-1}) and from a direction opposing the snow-breeze is probably responsible for the frontal-like changes in the lower atmosphere near the snow boundary, (Estoque, 1962). In calm conditions it would be expected that the snow-breeze should extend to a considerable distance over the bare soil. The changes in temperature and moisture would probably then occur over a greater horizontal distance.

A second flight along the same transect about an hour later shows even stronger contrasts and a better developed snow-breeze (Fig. 4.13). Note that the snow-breeze near the boundary has reached about 4 m s^{-1} in intensity (Fig. 4.13i-j).

A 90 m transect shaped like the rectangular pattern in Fig. 4.10b was also performed. The data from this run (Fig. 4.14a-h) establish the existence of the observed atmosphere contrasts through some distance parallel to the snow - no snow boundary.

4.4.3 Cross sectional analysis and summary

The cross section analyses show noticeable gradients in potential temperature and moisture through a height of about 1200 m (Fig. 4.15a-b). The aerosols are not mixed as well vertically over the snow-covered portion of the transect (Fig 4.15c). Evidence of the snow breeze is clearly displayed in the u -field. In fact, it appears that we may even begin to see the upper return circulation at about 1200 m altitude.

The data from this flight turned out to be the most clearly supportive of the hypothesis of the 9 SSBLIM flights. Although the snow region was somewhat patchy and transferring sensible heat to the atmosphere, the moderate opposing (relative to the snow breeze)

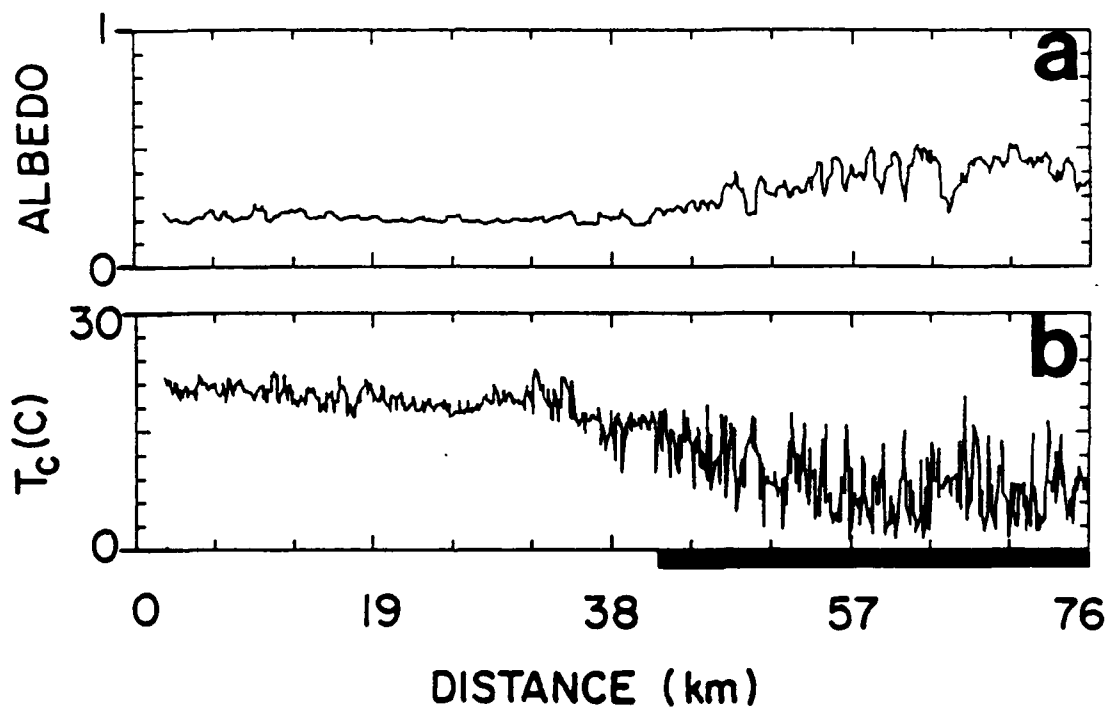


Figure 4.13: (a-j) As in Fig. 4.12 except for 14:21:30 - 14:36:23 CST. (Terrain height figure and sounding locations omitted). Tick marks are as in Fig. 4.12.

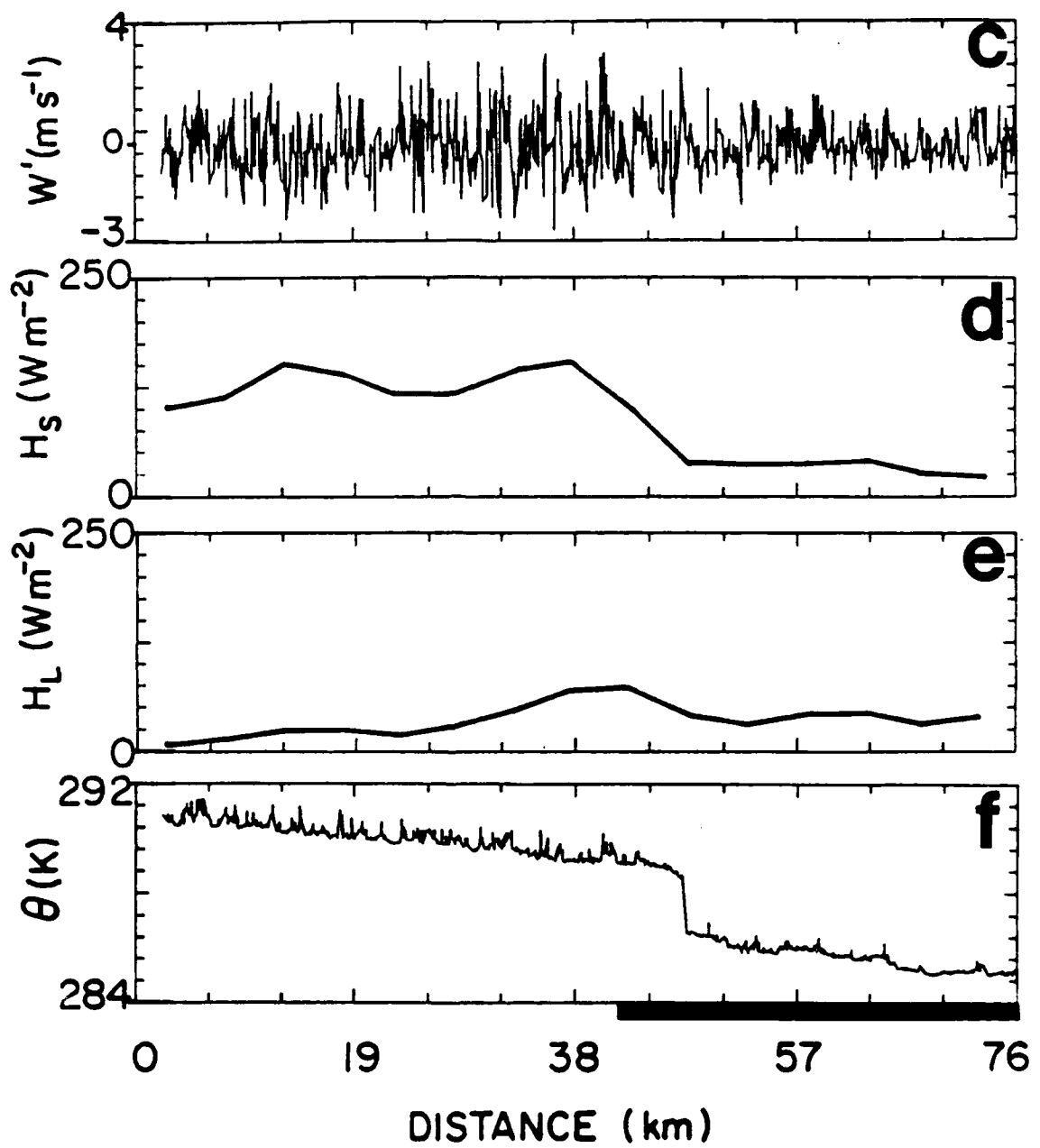


Figure 4.13: Continued.

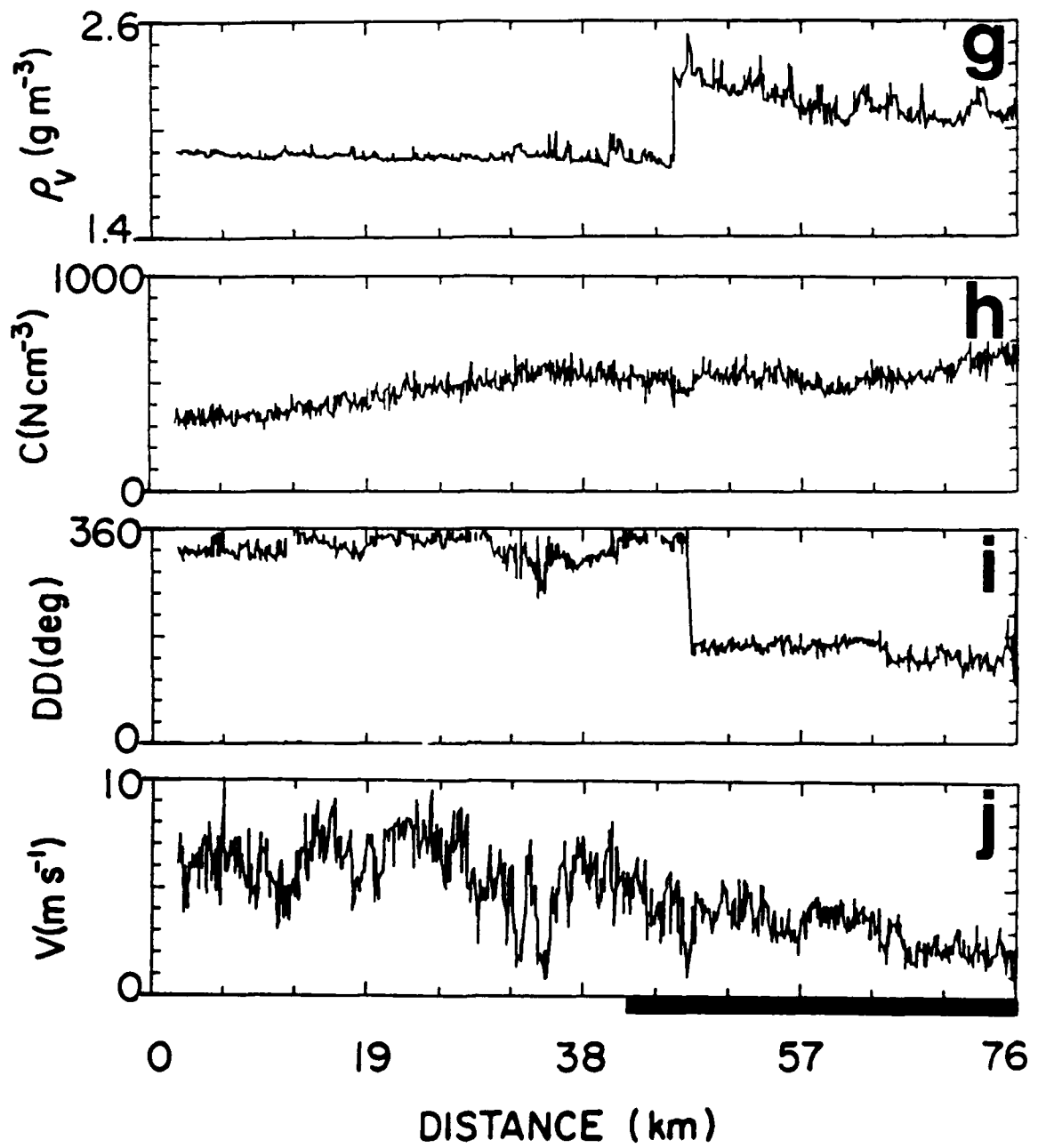


Figure 4.13: Continued.

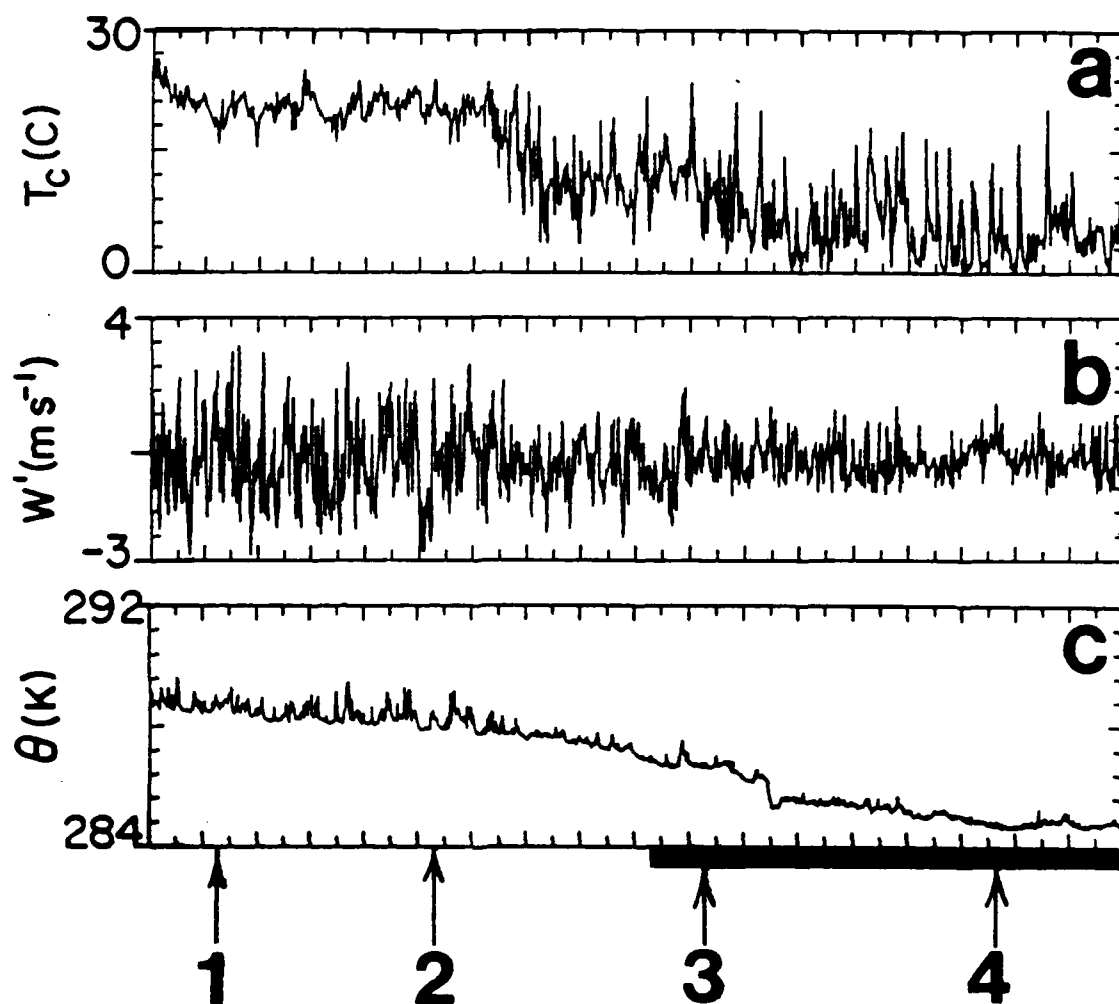


Figure 4.14: (a-h). 90 m flight data measured from 14:35:00-14:53:00 CST. The numbered arrows point out the four 90-degree turns shown in the schematic flight path superimposed on Fig. 4.10b. (After 4.10b DD): 1-2 and 3-4 are segments parallel to the snow - no snow boundary but were flown over bare soil and snow cover, respectively. Dark line indicates snow-covered portion of transect. Left to right tick mark interval is 30 s. Other tick mark intervals are as in Fig. 4.12.

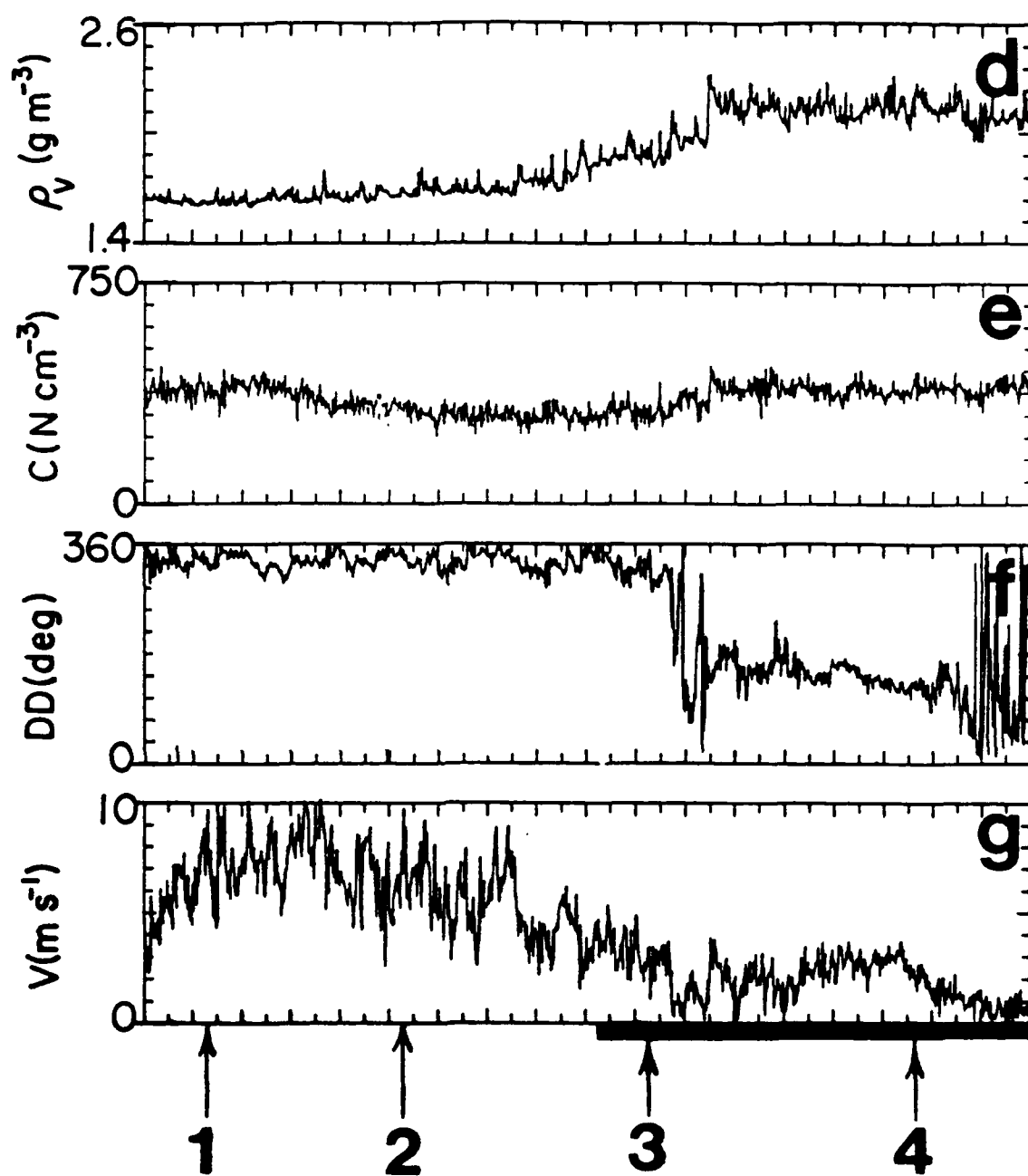


Figure 4.14: Continued.

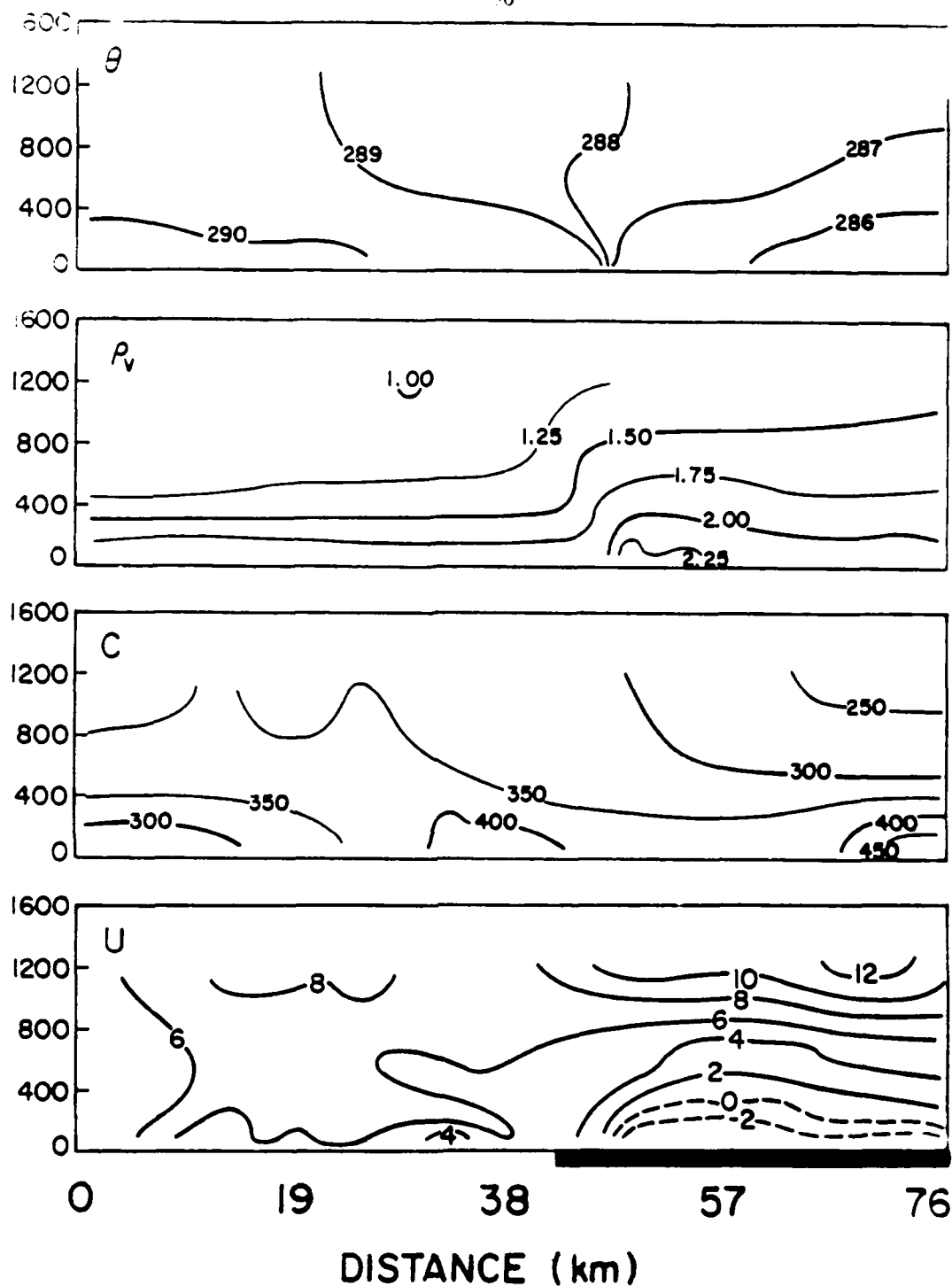


Figure 4.15: Cross section analysis for flight #7 based on horizontal transect measurements. For θ , the contour interval is 1 K; for ρ_v , the contour interval is 0.25 g m⁻³; for C , the contour interval is 50 particles cm⁻³; and for u , the contour interval is 2 m s⁻¹. Dashed lines indicate flow in the negative- x direction and the vertical-axes indicate height (m). The distance scale and the x -axis, lies along the flight transect with the positive (x) direction pointing toward 130° as measured clockwise from the north. Dark line indicates snow-covered portion of the transects.

background flow actually enhanced the observed atmospheric gradients. For comparison with the other flights, note that the average 90 m ambient temperature during this flight was about 3.5°C.

4.5 Flight #8

4.5.1 Situation

Since the results from flight #7 were clearly supportive of the hypotheses, flight #8 was made the following day (19 March, 1988) over the same snowband. The shape and extent of the snow was modified due to melting. A new transect, shown in Fig. 4.16a, was chosen. The most significant synoptic changes from the previous day were a stronger background flow (southwesterly at about 13 m s^{-1} at 100 m as seen in Fig. 4.20h-i), and a warmer day. The average 100 m ambient temperature for this flight was about 12°C (see Fig. 4.17 for the morning surface weather map).

4.5.2 Measurements

The afternoon satellite observed surface temperature gradients for this flight were, again, substantial (Fig. 5.16b and 4.18). Fig. 4.18b shows a broad transition zone across the boundary where the surface temperature change 14° in 26 km ($\sim 0.54^\circ \text{ km}^{-1}$). This is also close to the surface temperature gradient observed by the aircraft (Fig. 4.20a). Apparently, the transect location choice was a good one. Plotted aircraft measurements are presented in Figs. 4.19 and 4.20.

The vertical profile measurements (Fig. 4.19) show development of a boundary layer to a depth of about 900 m over the bare region while the air over the snow is very stable.

The lower atmosphere over the snow is as much as 5 K cooler than that over the bare ground, and apparently little moisture has been mixed upward over the snow.

Fig. 4.20a-i shows the plotted horizontal transect measurements. The surface temperature and albedo measurements indicate that the snow - no snow "boundary" is a rather broad transition zone. Satellite images showed that there was much melting during this day. The overall surface temperature change along the transect is large (from about -1°C to about 26°C).

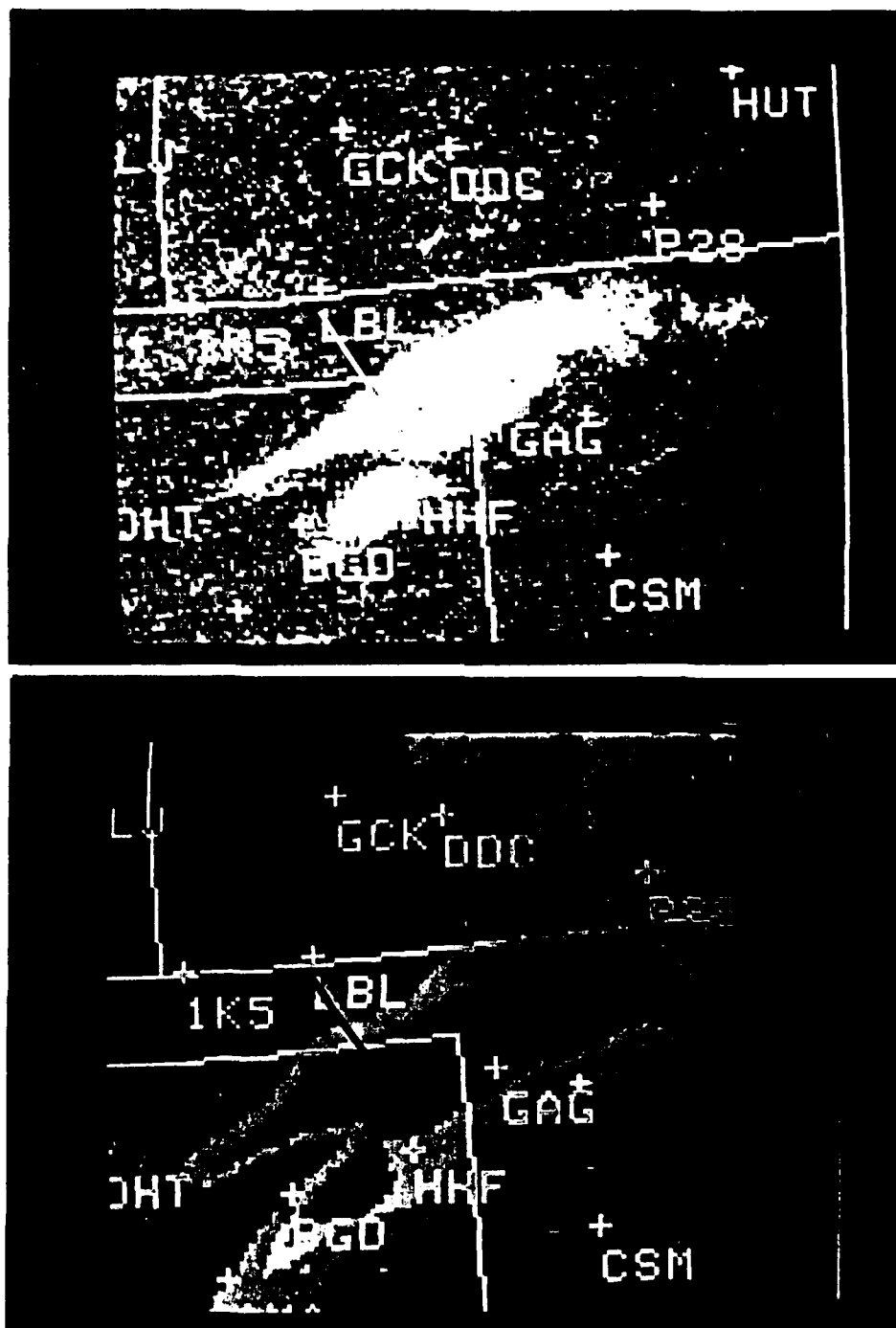


Figure 4.16: As in Fig. 4.2 except for 19 March, 1988. Also (a) visible image is for 1647 CST; and (b) IR-image is for 1345 CST.

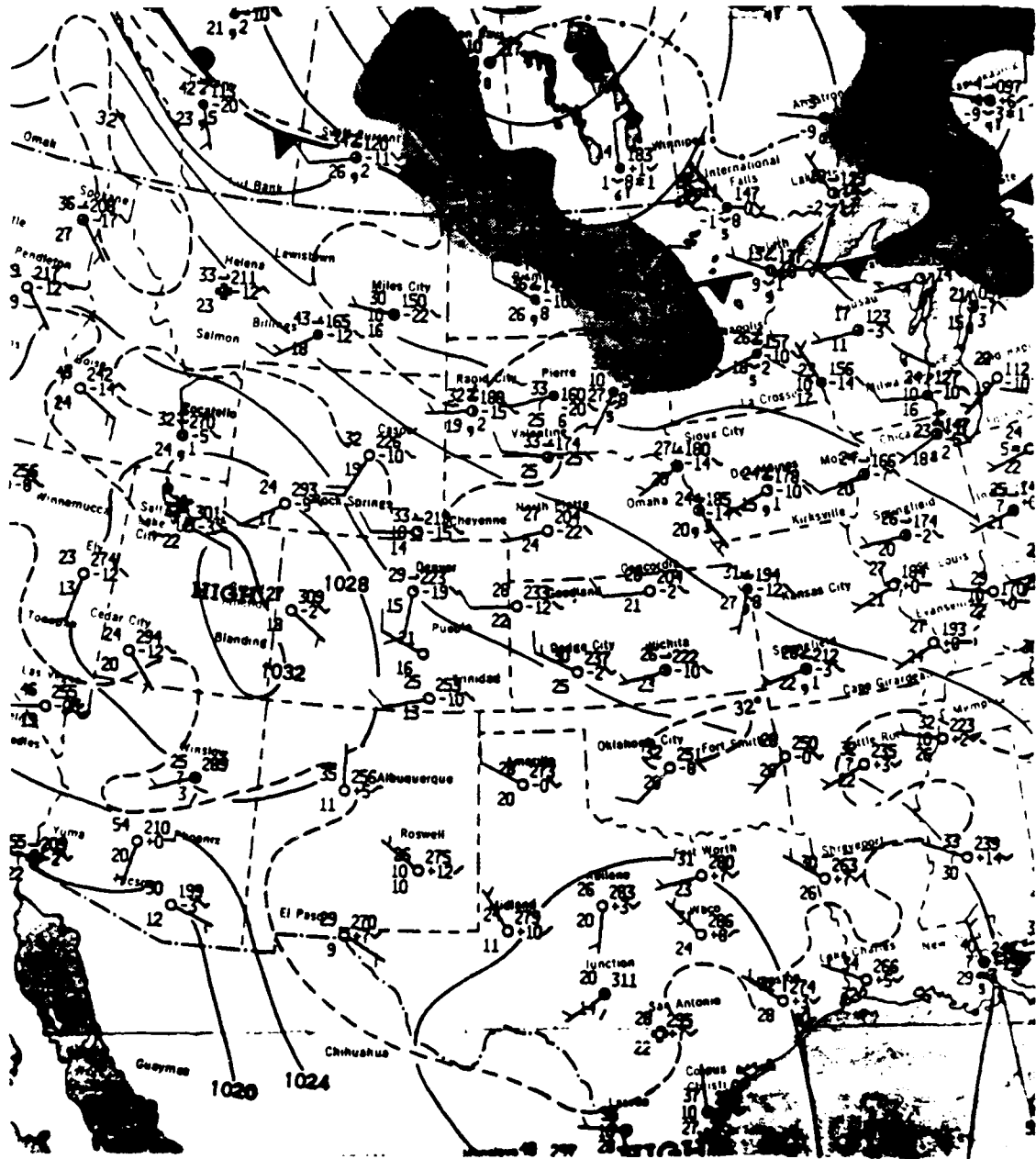


Figure 4.17: As in Fig. 4.3 except for 19 March, 1988.

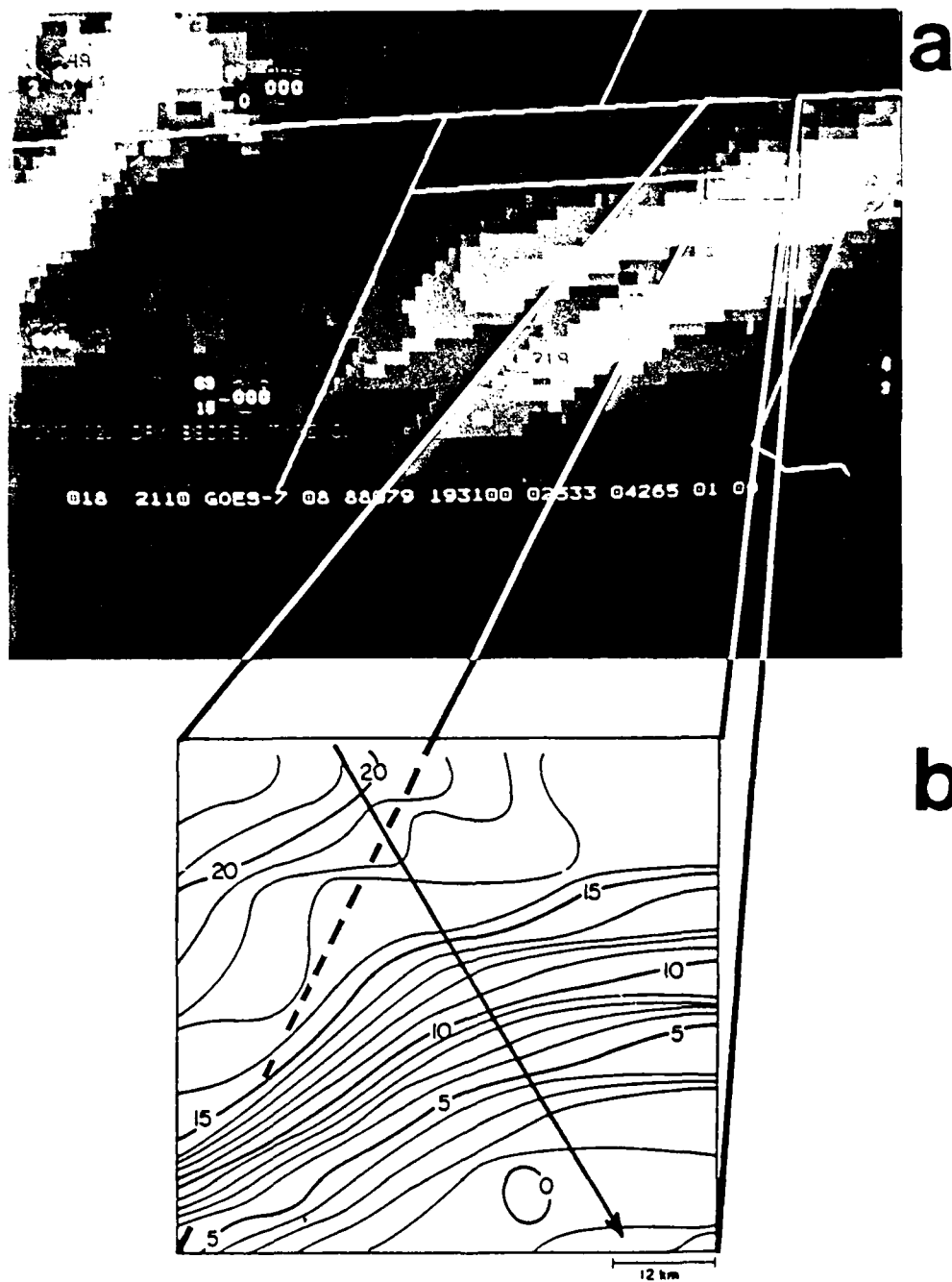


Figure 4.18: As in Fig. 4.4 except for 19 March, 1988, 1331 CST. Also, heaviest line indicates flight #8 transect.

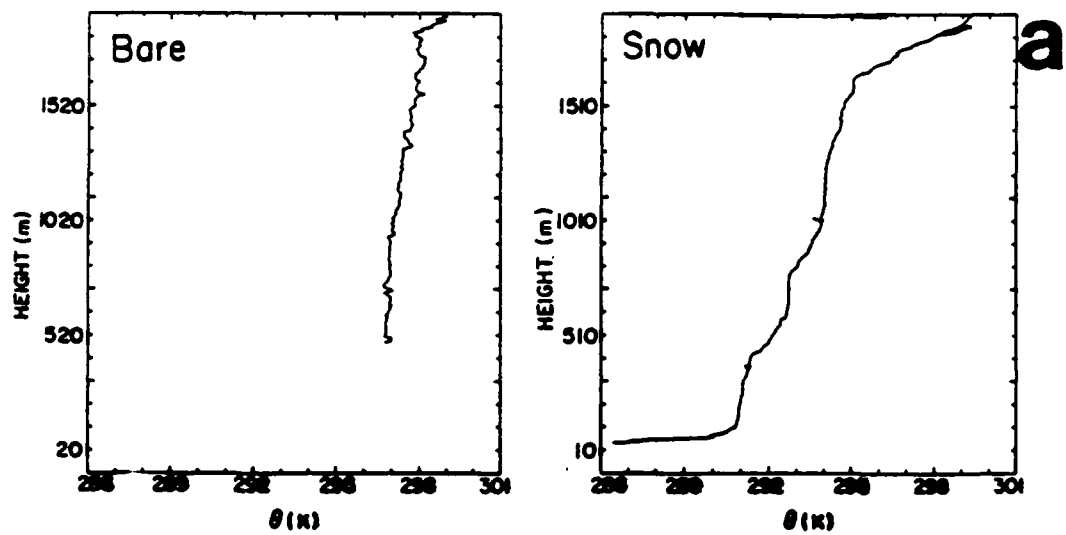


Figure 4.19: (a-e). Vertical profile measurements from flight #8. Snow measurements made from 12:54:10 - 13:14:50 CST. Bare measurements made from 14:36:38 - 14:46:00 CST.

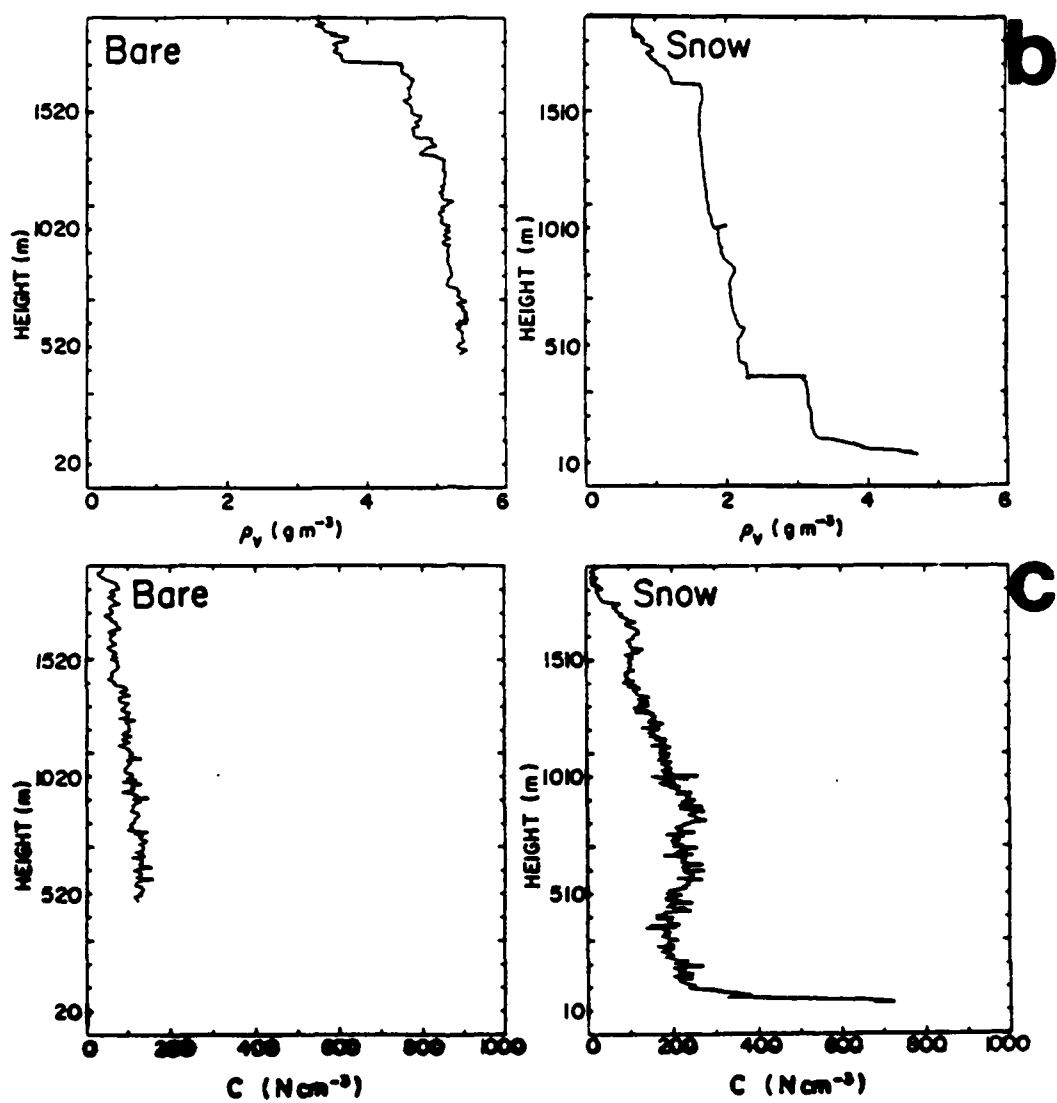


Figure 4.19: Continued.

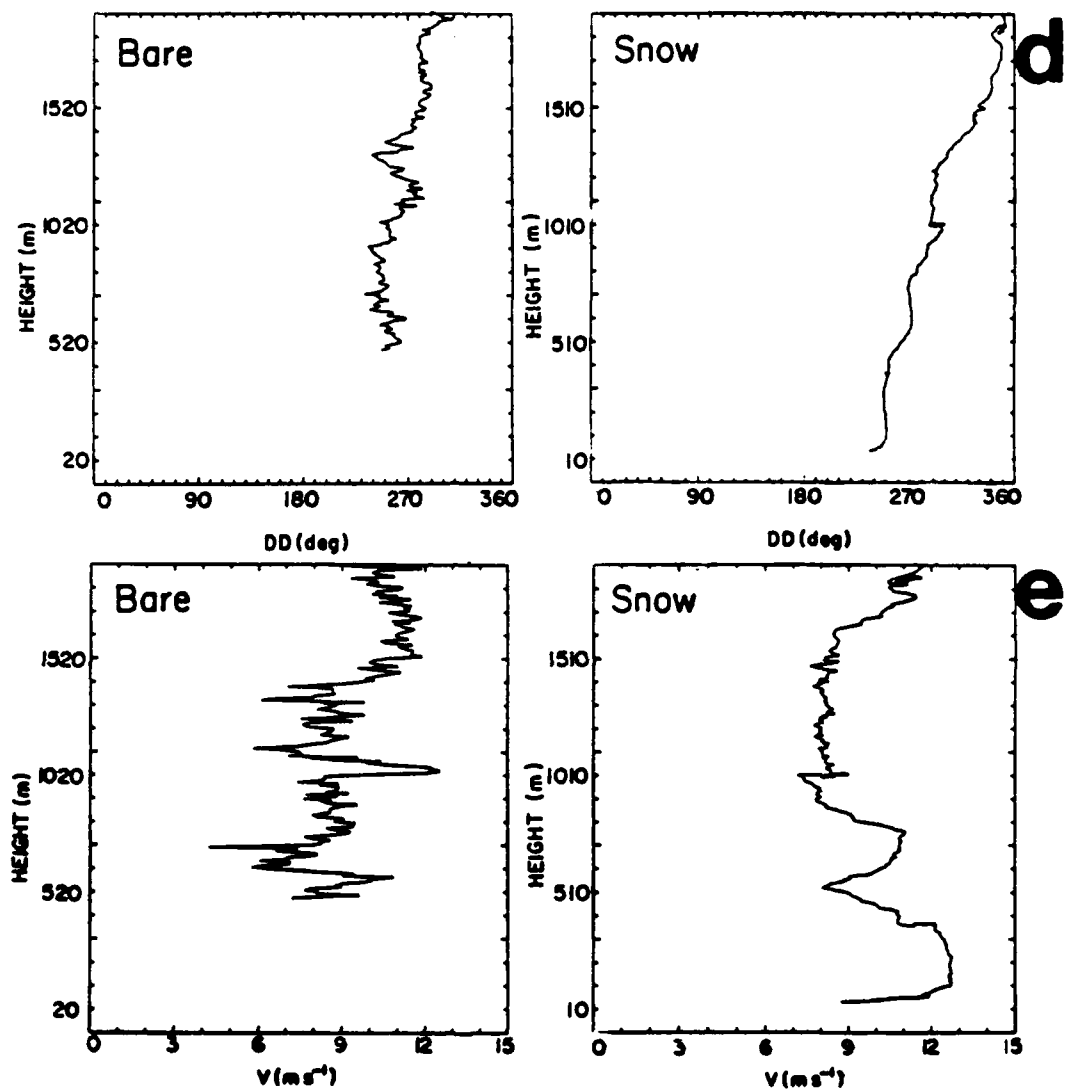


Figure 4.19: Continued.

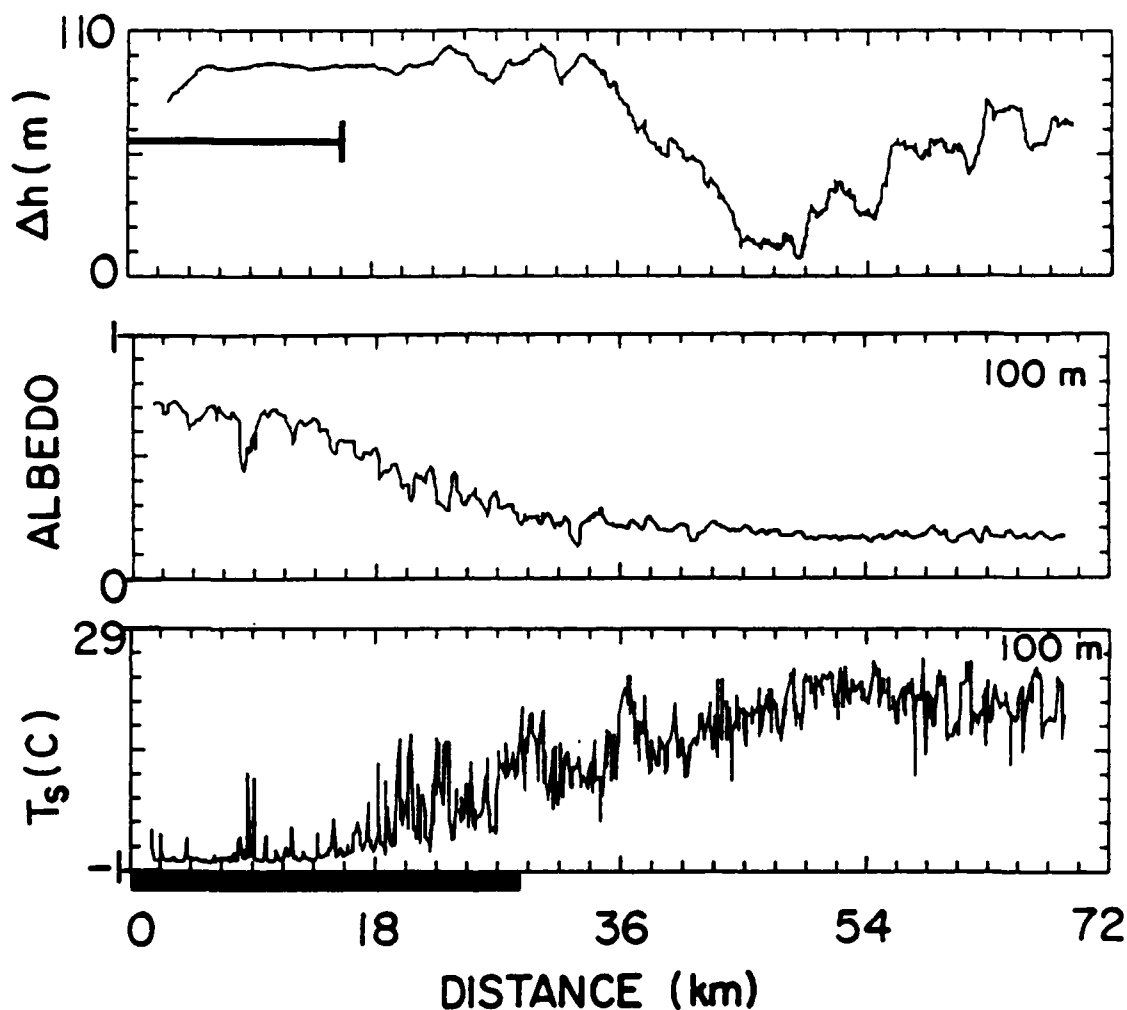


Figure 4.20: (a). Plotted aircraft measurements from flight #8 horizontal transects are shown in Figs. 4.20(a-i). 100 m data were measured from 13:14:00 - 13:27:05 CST. 180 m data were measured from 13:29:04-13:42:10. 270 m data were measured from 13:45:08 - 13:59:15. 450 m data measured from 14:01:25 - 14:14:35 CST. Dark line indicates snow-covered portion of transect. Relative terrain height plot (Δh) is based upon measured air pressure. The location of the vertical profile measurements over the snow (partially depicted by the bar and arrow in profile measurements location begins 4 km beyond the right-hand side of the figure and extends another 32 km beyond that point. Tick mark interval for Δh is 11m; for albedo it is 0.1; for T_s is 3°C.

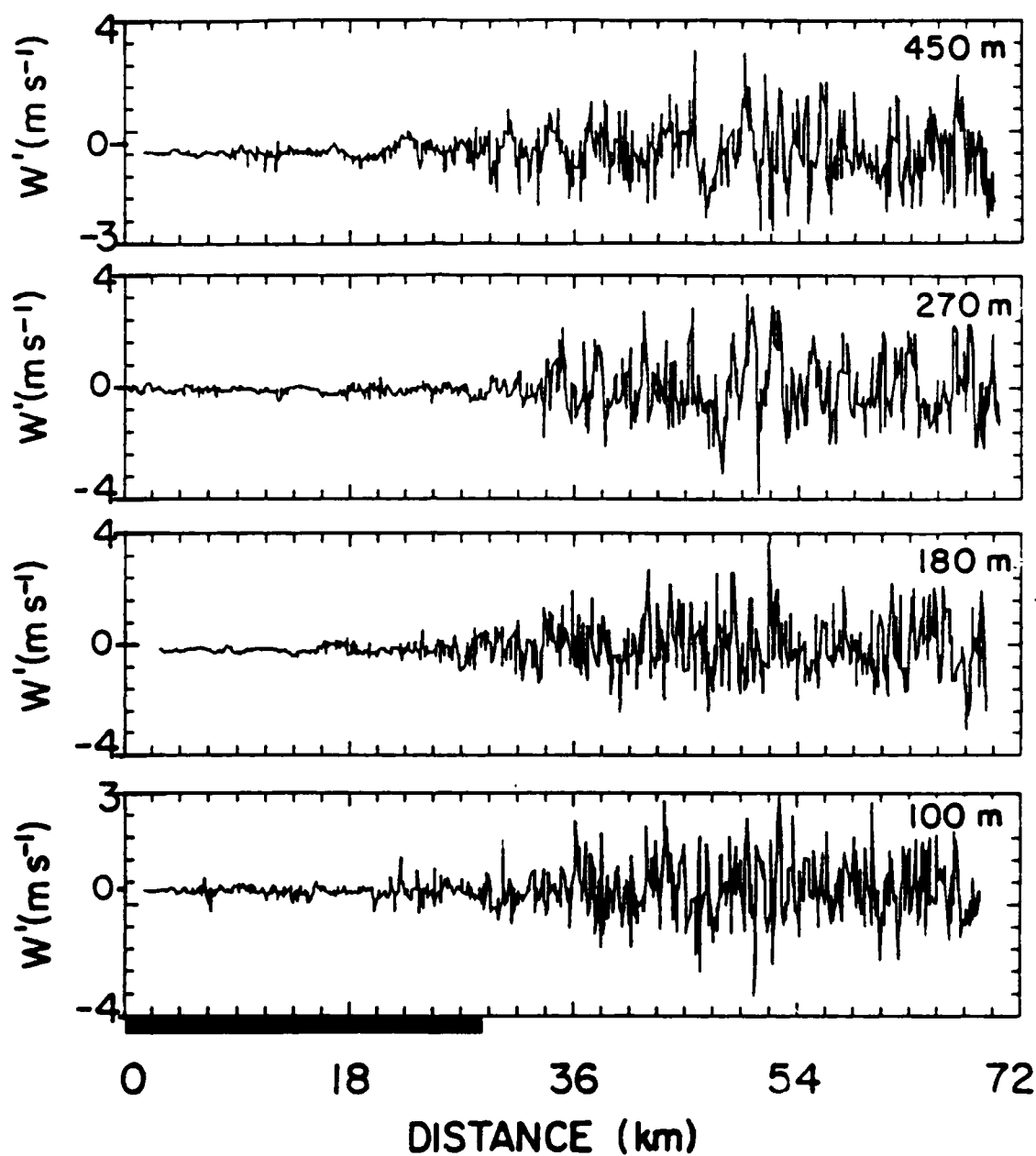


Figure 4.20: (b). Tick mark interval for w' at 100 m and 450 m is 0.7 m s^{-1} at 180 m and 270 m it is 0.8 m s^{-1} .

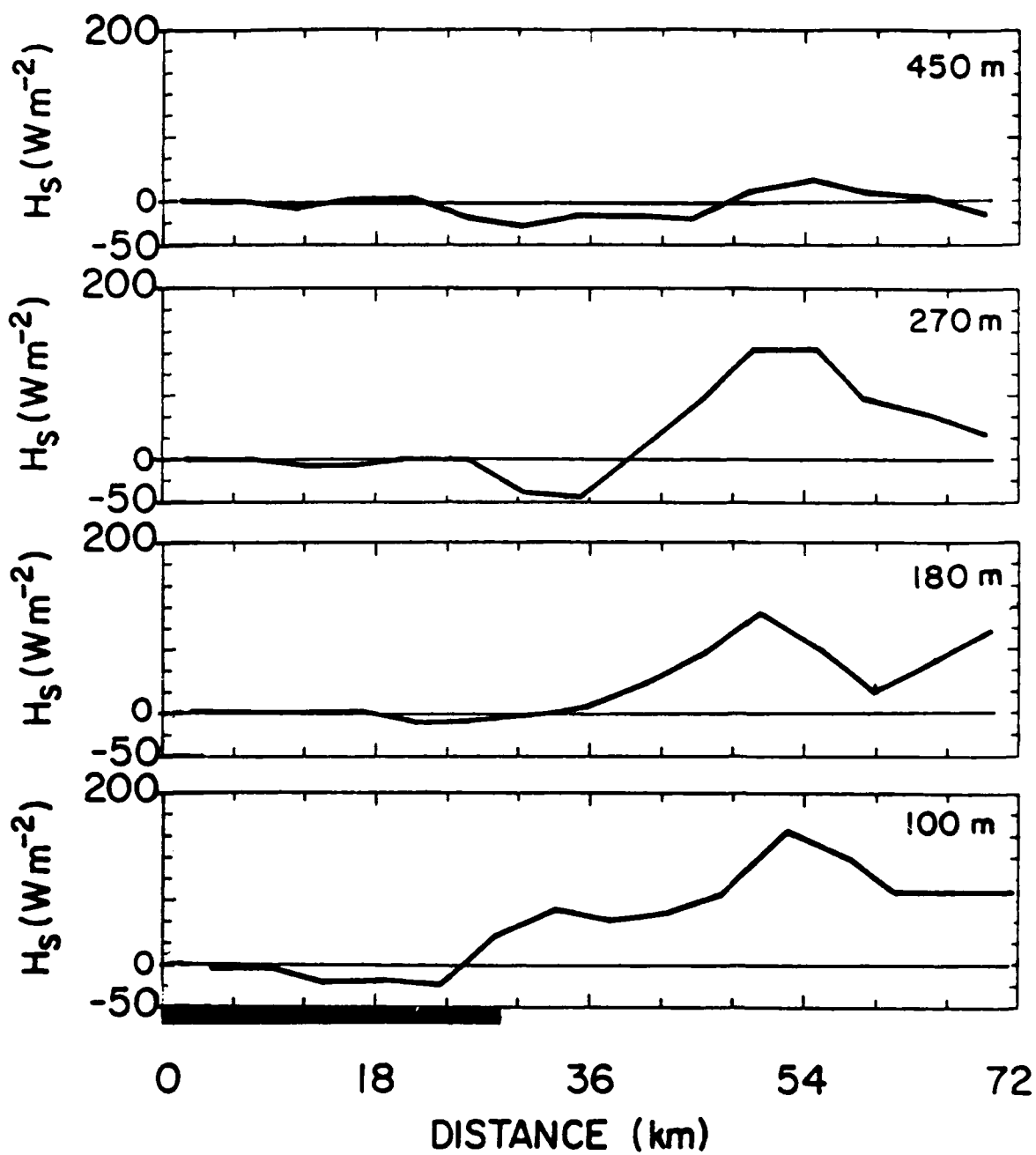


Figure 4.20: (c). Tick mark interval for H_S is 25 W m^{-2} .

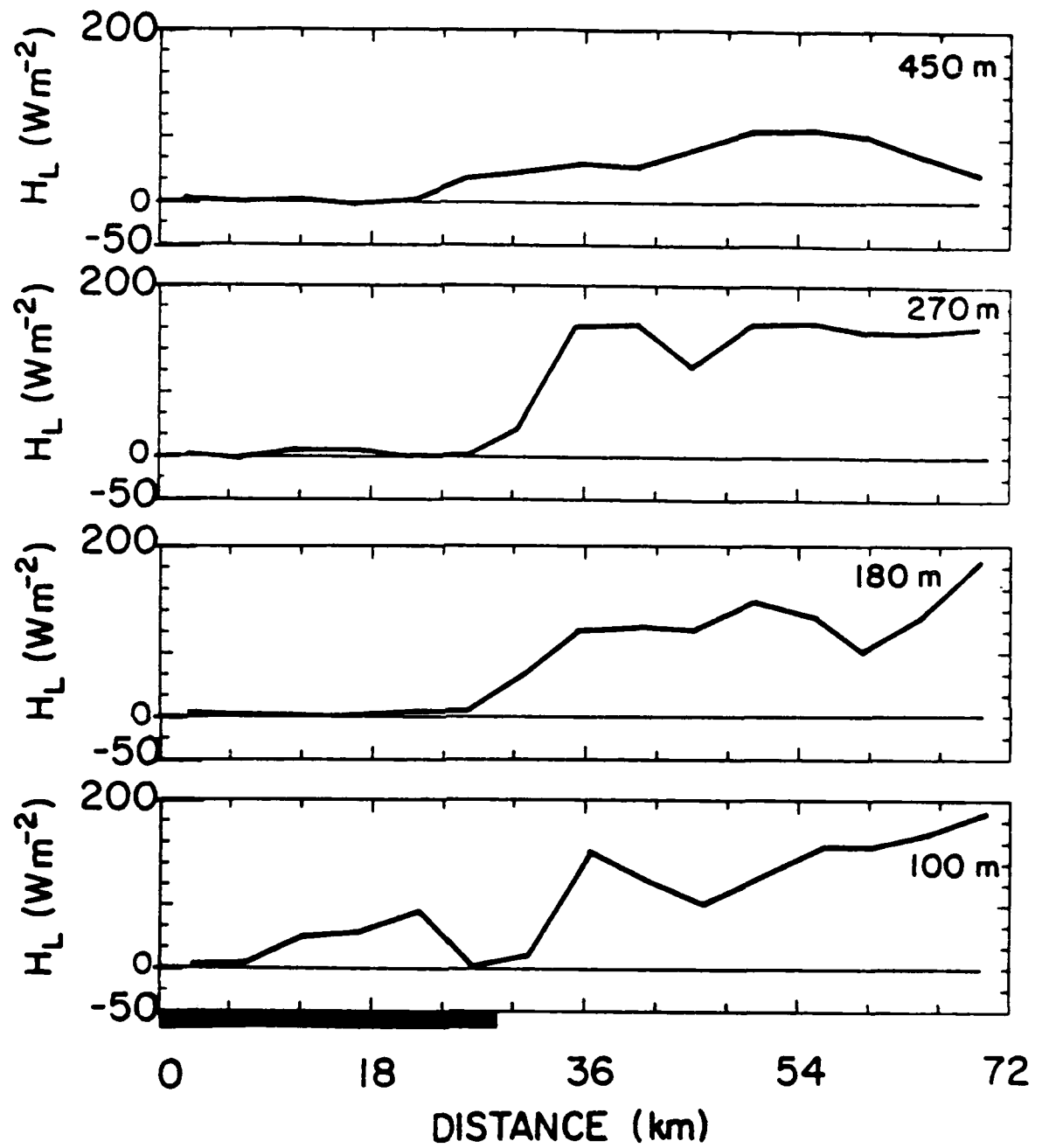


Figure 4.20: (d). Tick mark interval for H_L is 35 W m^{-2} .

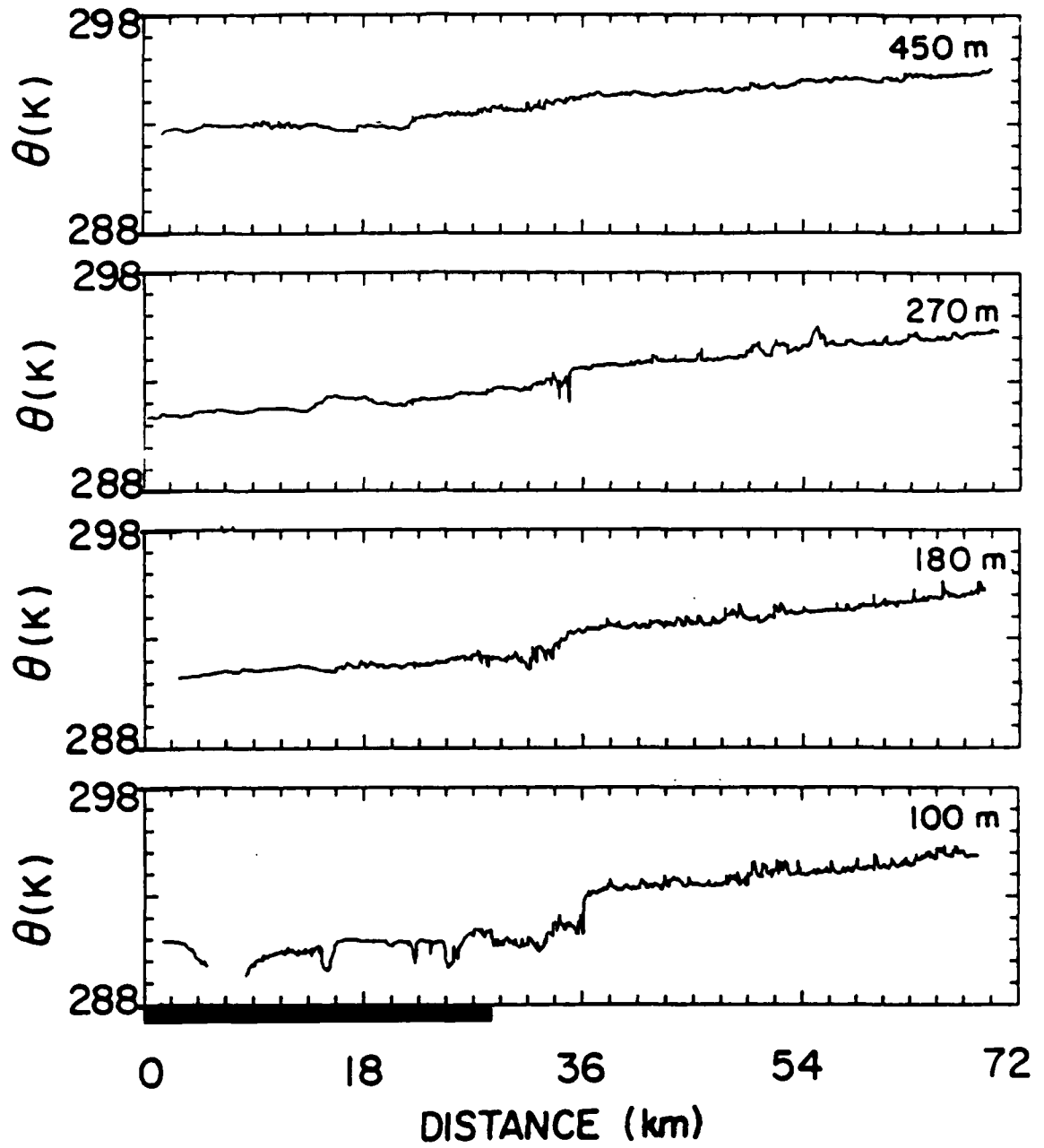


Figure 4.20: (e). Tick mark interval for θ is 1 K.

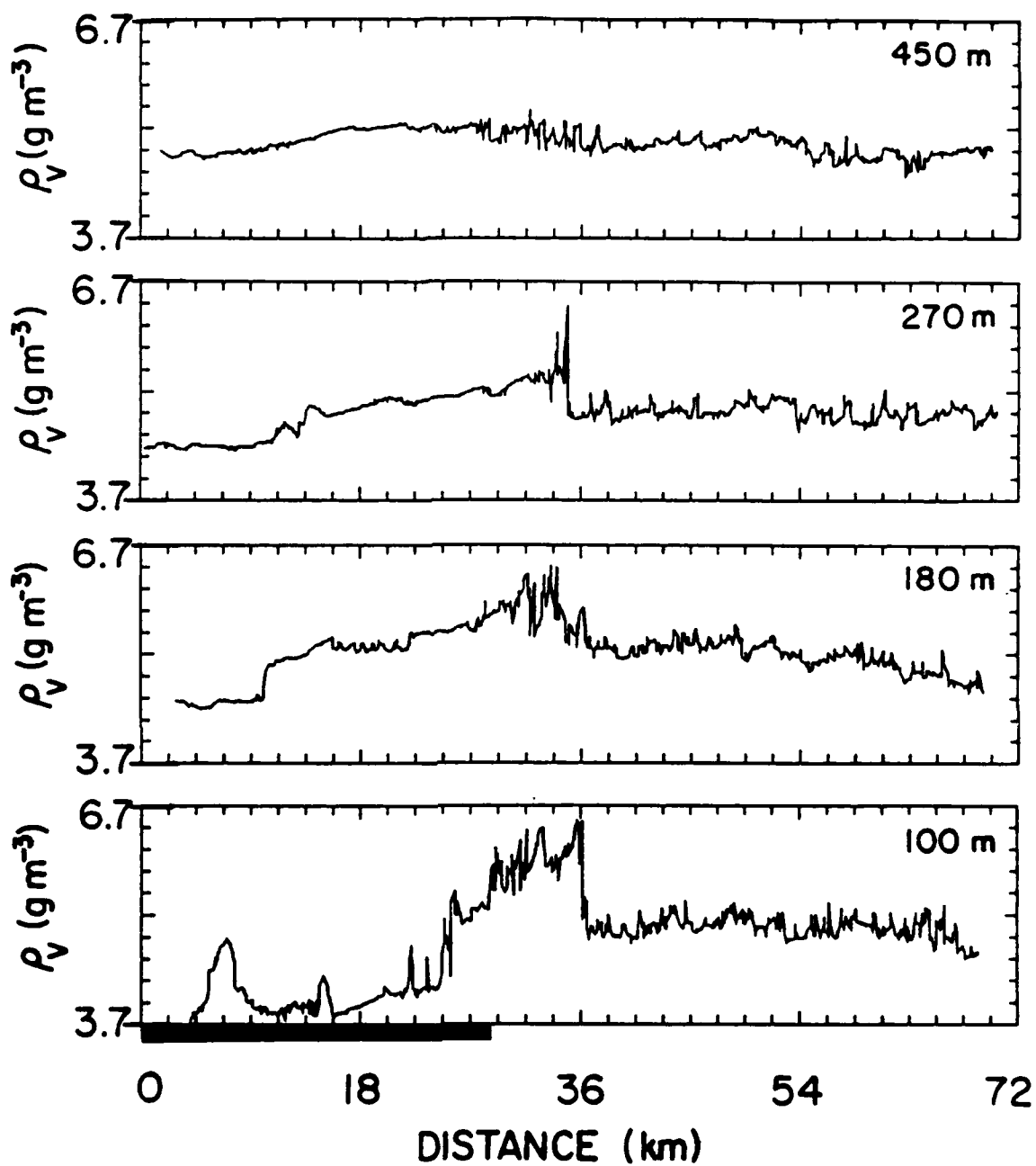


Figure 4.20: (f). Tick mark interval for ρ_v is 0.3 g m^{-3} .

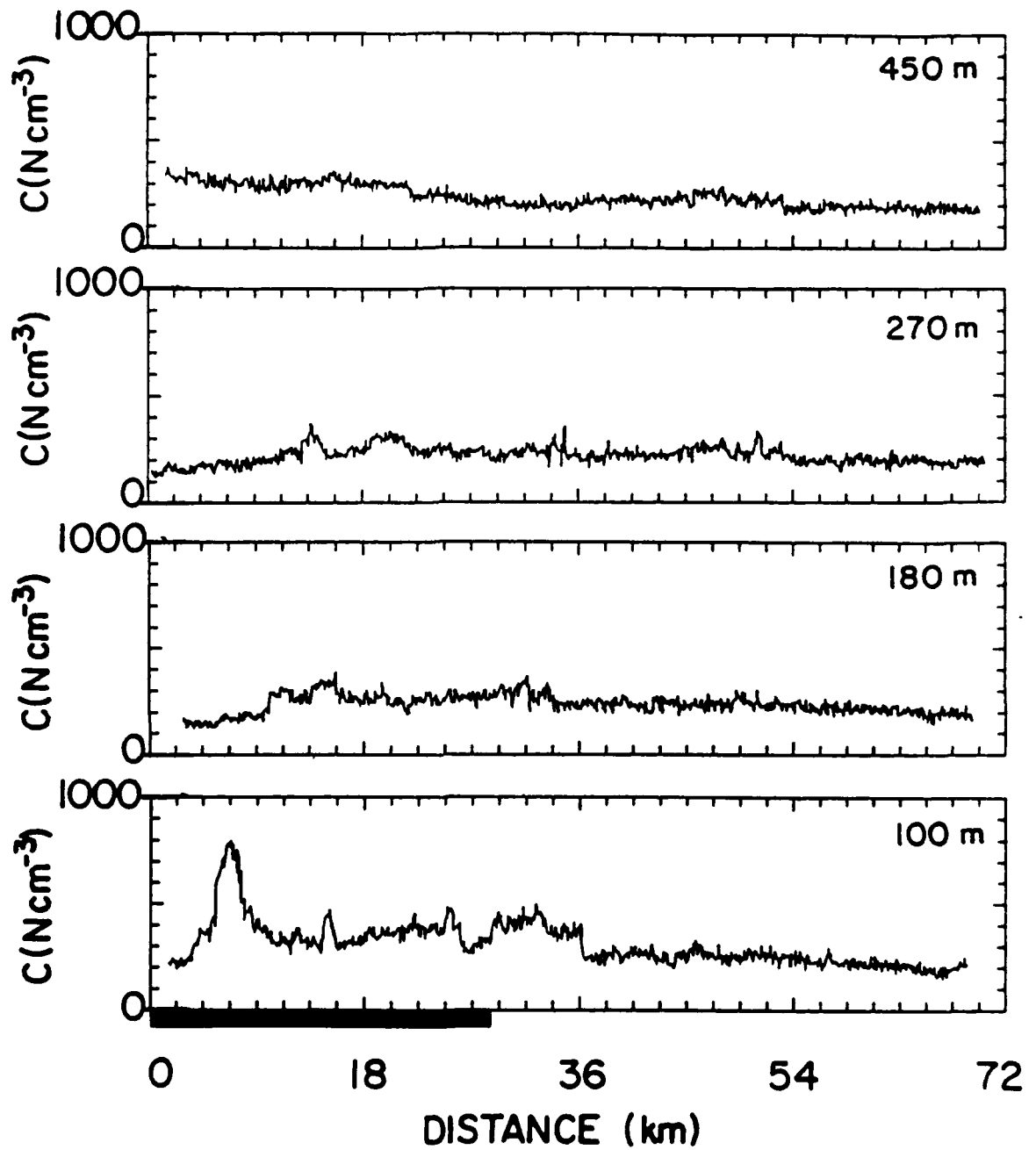


Figure 4.20: (g). Tick mark interval for C is 100 N cm^{-3} .

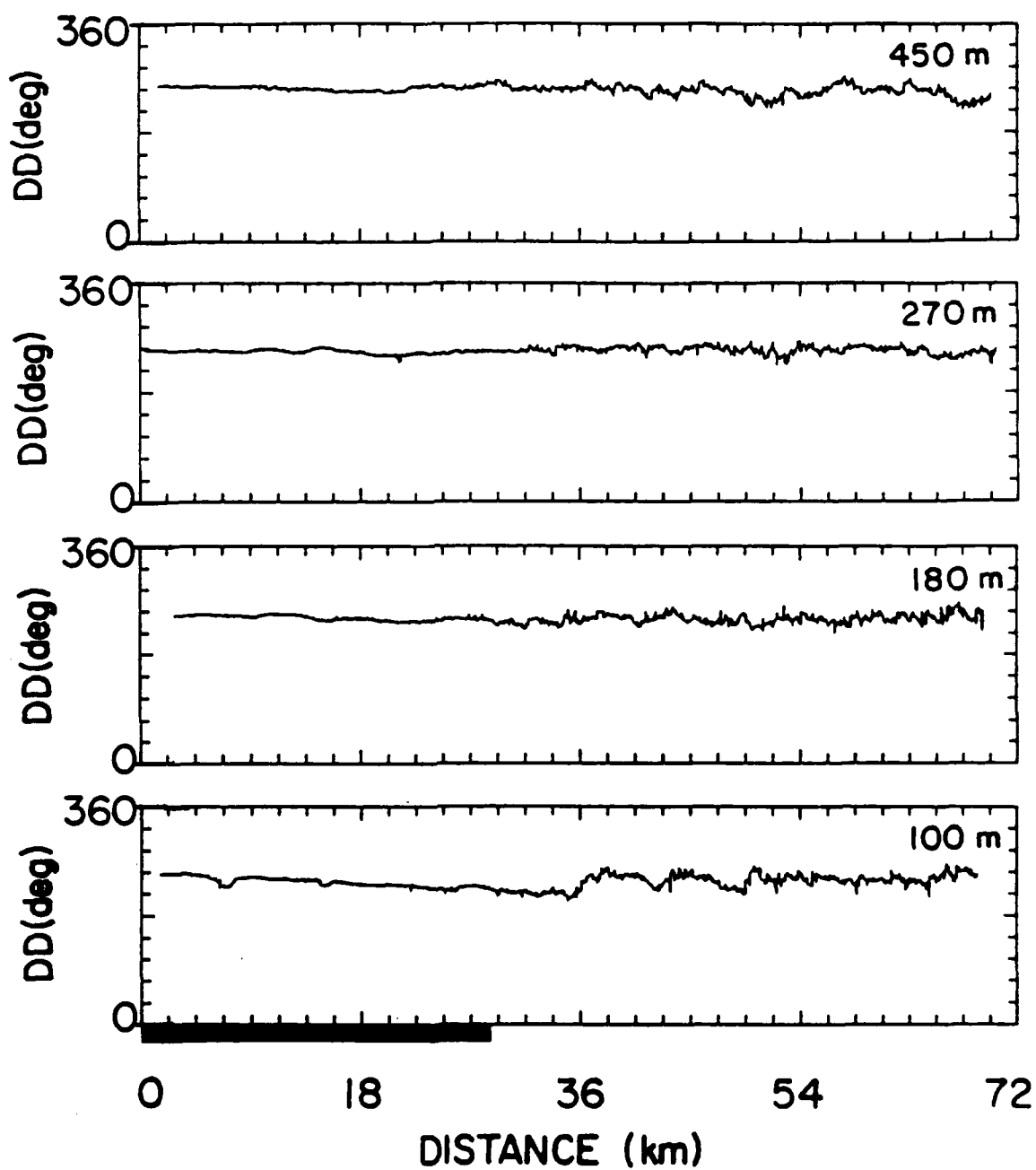


Figure 4.20: (h). Tick mark interval for DD is 36° .

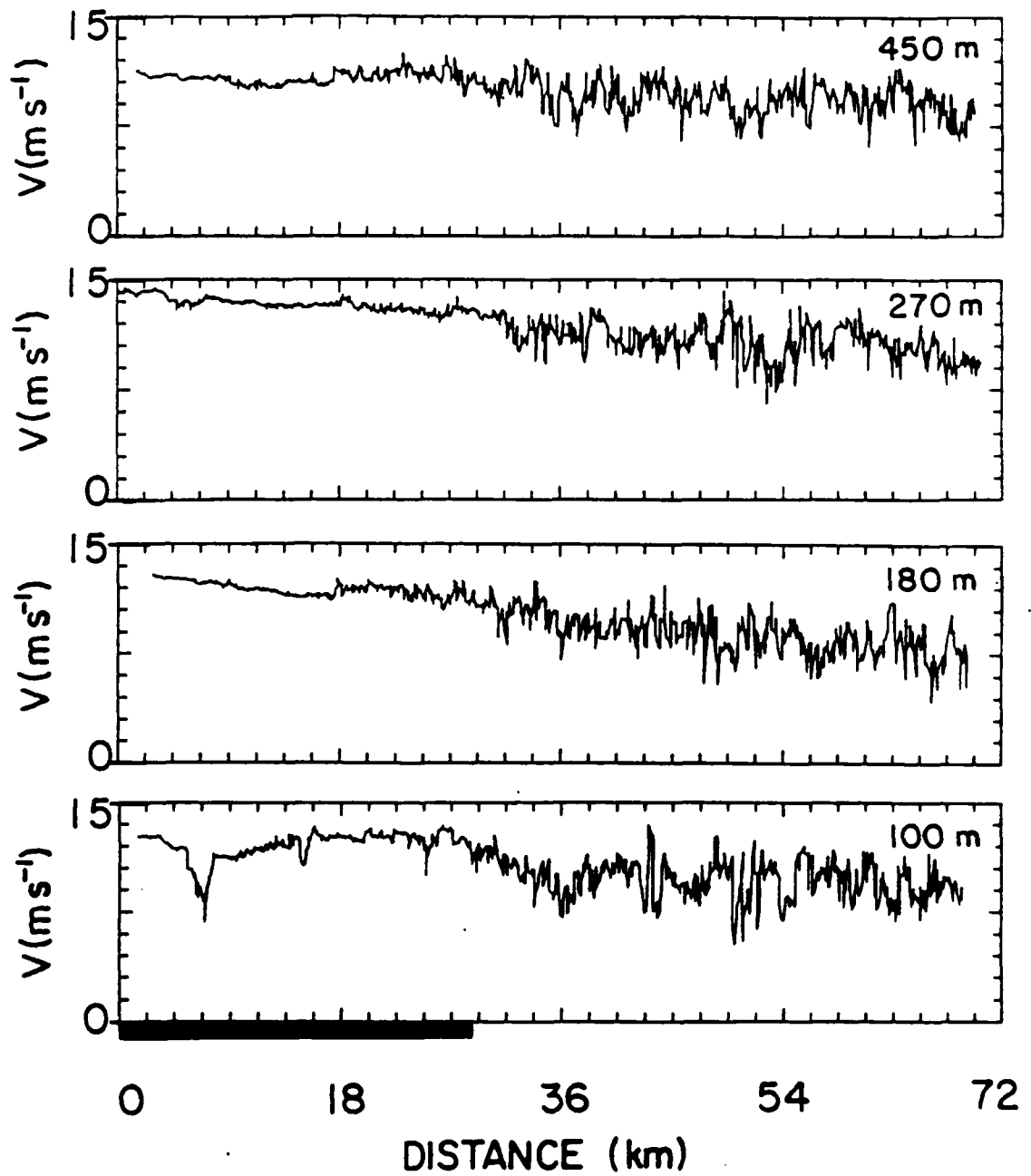


Figure 4.20: (i). Tick mark interval for V is 1.5 m s^{-1} .

Before discussing the snow cover's atmospheric effects, it is important to note that this was a windy day. The background flow was southwesterly (nearly perpendicular to the transect and parallel to the snow boundary) at about 13 m s^{-1} .

As should be expected on a windy day, sensible and latent heat fluxes are substantial over the melting and bare regions (Figs. 4.20c-d). Over the snow, the sensible heat flux is zero or small and directed downward. The latent heat flux over the snow is also relatively small, but directed upward. Over the bare region (including a large portion of presumably wet soil), both sensible and latent heat fluxes are substantial. Since the wind is strong most of the atmospheric changes are less noticeable than in the two previously presented cases.

The potential temperature plot shows an abrupt increase as the aircraft proceeds from the snow toward the bare soil. The increase is only about 2 K, however, and the change is much less noticeable at a height of 180 m. Over the entire transect, however, the potential temperature change is significant (about 3-5 K) at all levels. The wind does, apparently, help evaporate a large amount of water.

Along the transect, from the snow covered region to the region associated with strong melting, the absolute humidity increases at all levels (from 3.9 to 6.3 g m^{-3} at 100 m). Presumably, this change is due the evaporation and upward mixing of melted snow. More discontinuous changes occur as the aircraft proceeds out over the bare soil. At about 8 km away from the snow boundary absolute humidity sharply decreases (from 6.3 to 5.1 g m^{-3} at 100 m). Some decrease in moisture is noticed near that point at all measured flight levels.

It appears that the relatively strong synoptic flow (Fig. 4.20h-i) strongly modifies the snow-breeze deflection in this case. The only observable snow breeze effect is that the wind near the snow - no snow boundary on the snow side is slightly stronger and more southerly than elsewhere. The fact that this is looks like snow breeze effect becomes clearer in the cross section analysis (Fig. 4.21).

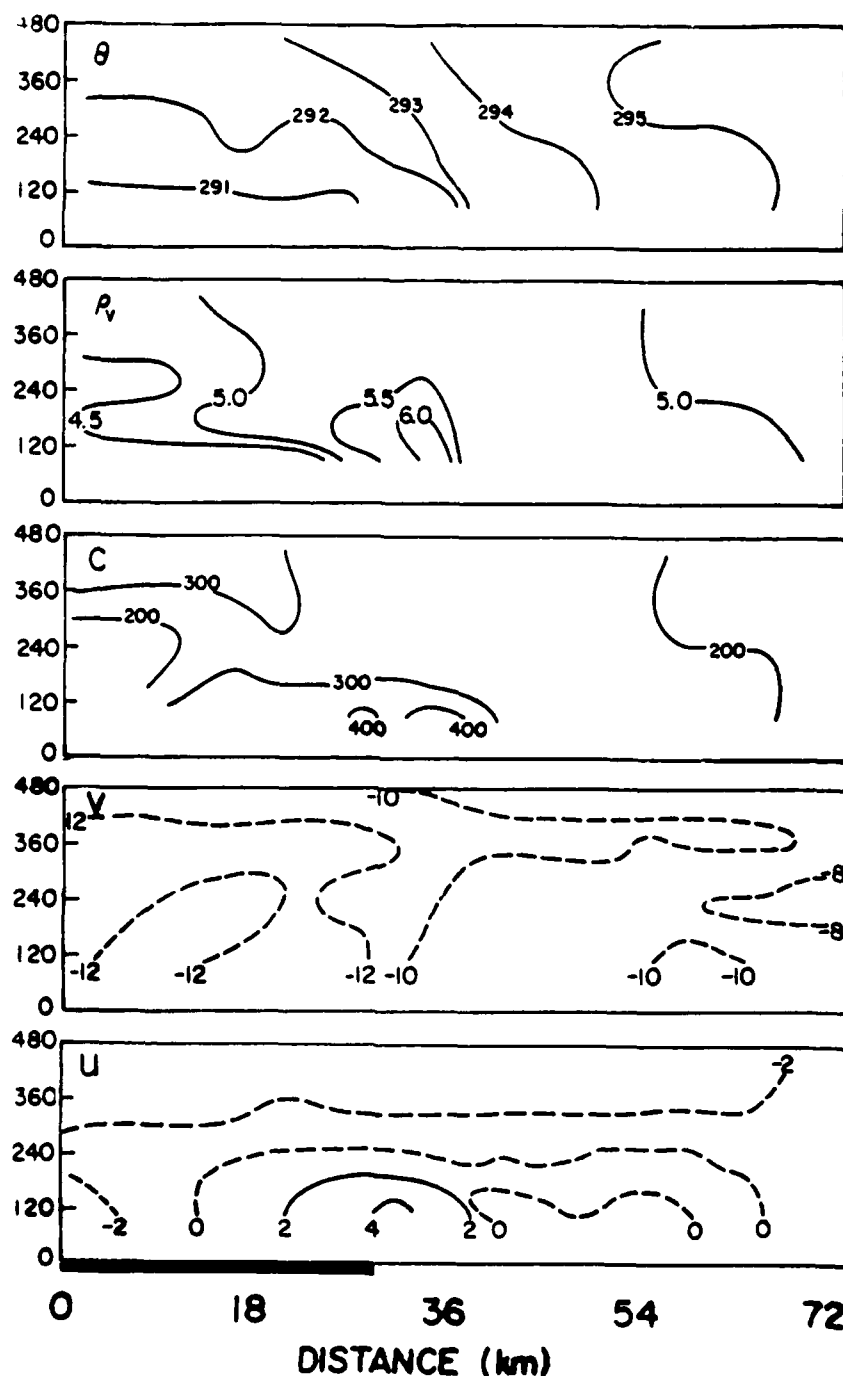


Figure 4.21: Cross section analyses for flight #8 based on plotted measurements in Fig. 4.20. For θ , the contour interval is 1 K; for ρ_v , the contour interval is 0.5 g m^{-3} ; for C , the contour interval is $100 \text{ particles cm}^{-3}$; and for u and v , the contour interval is 2 m s^{-1} . Dashed lines indicate flow in the negative x and y directions and the vertical-axes indicate height (m). The distance scale, and the x -axis, lies along the flight transect with the positive (x) direction pointing toward 330° measured clockwise from the north. The positive y -axis points toward 240° . Dark line indicates snow-covered portion of transect.

4.5.3 Cross section analysis and summary

The cross sectional analyses (Fig. 4.21) show similar features to the other flights, despite the strong background flow. The atmosphere is stable over the snow and near neutral over the bare ground. Some shallow trapping of aerosols (C) occurs over the snow (ρ_v) and moisture is mixed upward near the snow boundary from rapid melting and snow breeze convergence effects.

Although this case was certainly not ideal, it is useful in that it demonstrates the ability of snow cover to modify wind flow even in conditions of relatively strong synoptic wind.

Since the flow is predominantly perpendicular to the flight transect in this case, the cross sectional plots of both u and v are included in Fig. 4.21. Note that the u -field is supportive of snow breeze deflection.

4.6 Flight #9

4.6.1 Situation

Although the Texas panhandle snowband was significantly melted by 20 March, 1988, the CSU researchers decided to use the final SSBLIM flight hours to measure the boundary layer over what was left. The geostrophic flow over the region had weakened considerably (Fig. 4.22). Fig. 4.23a shows what was left of the snowband at about the time of the aircraft observations. The chosen transect is also shown. Considerable melting occurred this warm afternoon (note the average 95 m ambient temperature of about 23°C) and airborne scientists noticed pools of water where the snow had melted.

4.6.2 Measurements

Due to the time constraints on this final flight, vertical profile measurements were not made. Figs. 4.23b and 4.24 show the satellite-observed surface temperature gradient along the transect. This case is different from the previously presented flights in that the modified surface region is relatively small. Rather than crossing a boundary between relatively large areas of snow cover and bare soil, the transect passed over a small band

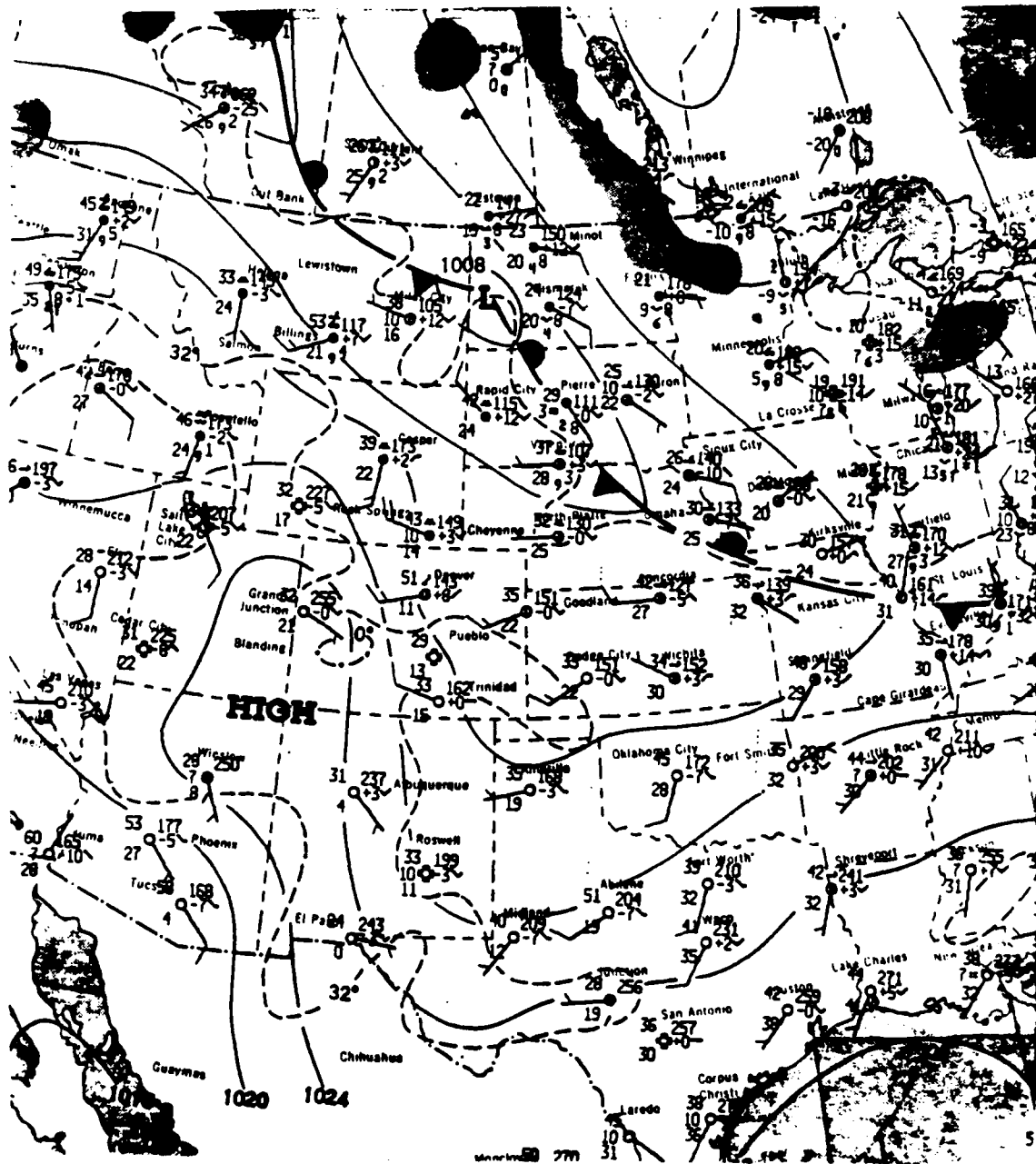


Figure 4.22: As in Fig. 4.3 except for 20 March, 1988.

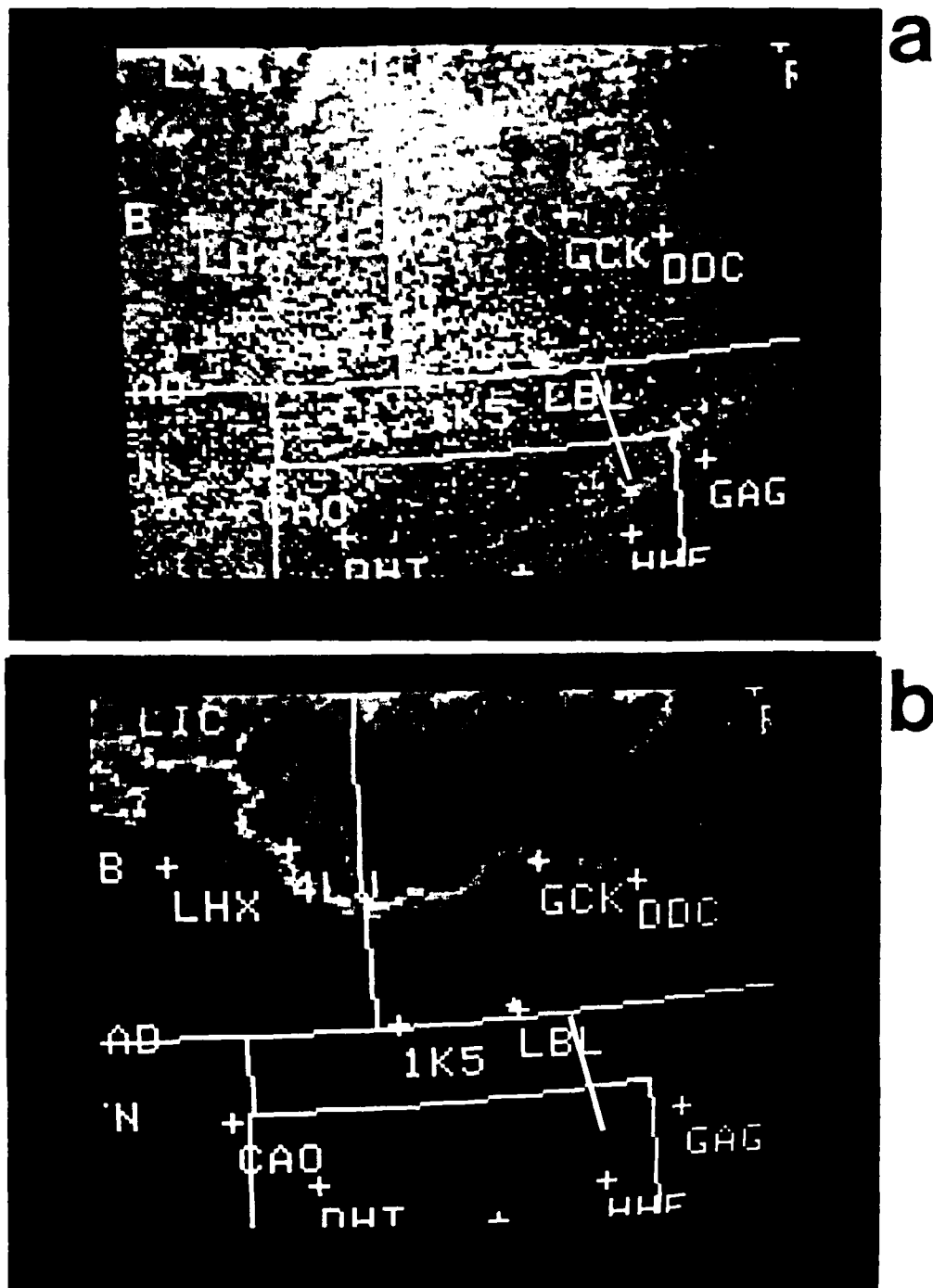


Figure 4.23: As in Fig. 4.2 except for 20 March, 1988, 1501 CST. Also, (a) visible image is for 1617 CST; and (b) IR image is for 1615 CST.

of melting snow with bare ground north and south of the band. Even so, the sharper gradients near the edges of the melting snow region are $\sim 1^{\circ}\text{C km}^{-1}$. Based on Fig. 4.24, the strongest surface temperature gradient exists about 10 km west of the chosen transect. Fig. 4.25 shows the plotted measurements from the flight transects. The wet soil and snow-covered portions of the transect were identified using surface temperatures, albedos, flight videotapes, and the airborne scientists' log. The wind plots (Fig. 4.25h-i) indicate that the background flow is north-northwesterly at about 4 m s^{-1} (note that the flow is generally from right to left looking at the figures in this case).

The surface data measured show substantial surface temperature gradients, however limited in horizontal extent. Beginning with the upwind bare region (right-hand side of the figures), it is seen that the surface temperature is around 28°C . Over the wet soil the temperature drops to near 22°C , and further decreases to a minimum of about 14°C over the northern portion of the patchy snow. Even within the patchy snow region the temperature begins to rise again, and over the downwind bare soil region the surface temperature is around 26°C . Note the relatively low snow albedo, indicative of the patchiness of the snow.

Figs. 4.25b-d display the turbulence characteristics along the transect at the various altitudes. Both the sensible and latent heat fluxes follow a similar pattern at all levels; upward heat transfer over the upwind bare region (right hand side of the figures), decreasing fluxes over the very wet soil, minimum values over the snow (in fact negative), and then increasing fluxes over the downwind bare region. At all levels, the upward transfer of latent heat was larger than that of sensible heat.

Changes in the atmosphere across the boundary above 95 m occur gradually. At 95 m changes are more discontinuous. The changes appear to be associated with the advection of the background flow over the moist, modified surfaces. This modified air is apparently advected over the downwind bare region; no significant atmospheric gradients are found between the snow region and the downwind bare region.

At 95 m the potential temperature drop from near 305.5 K over the upwind bare region to a minimum of 303.5 K over the snow. The absolute humidity increases quickly over the

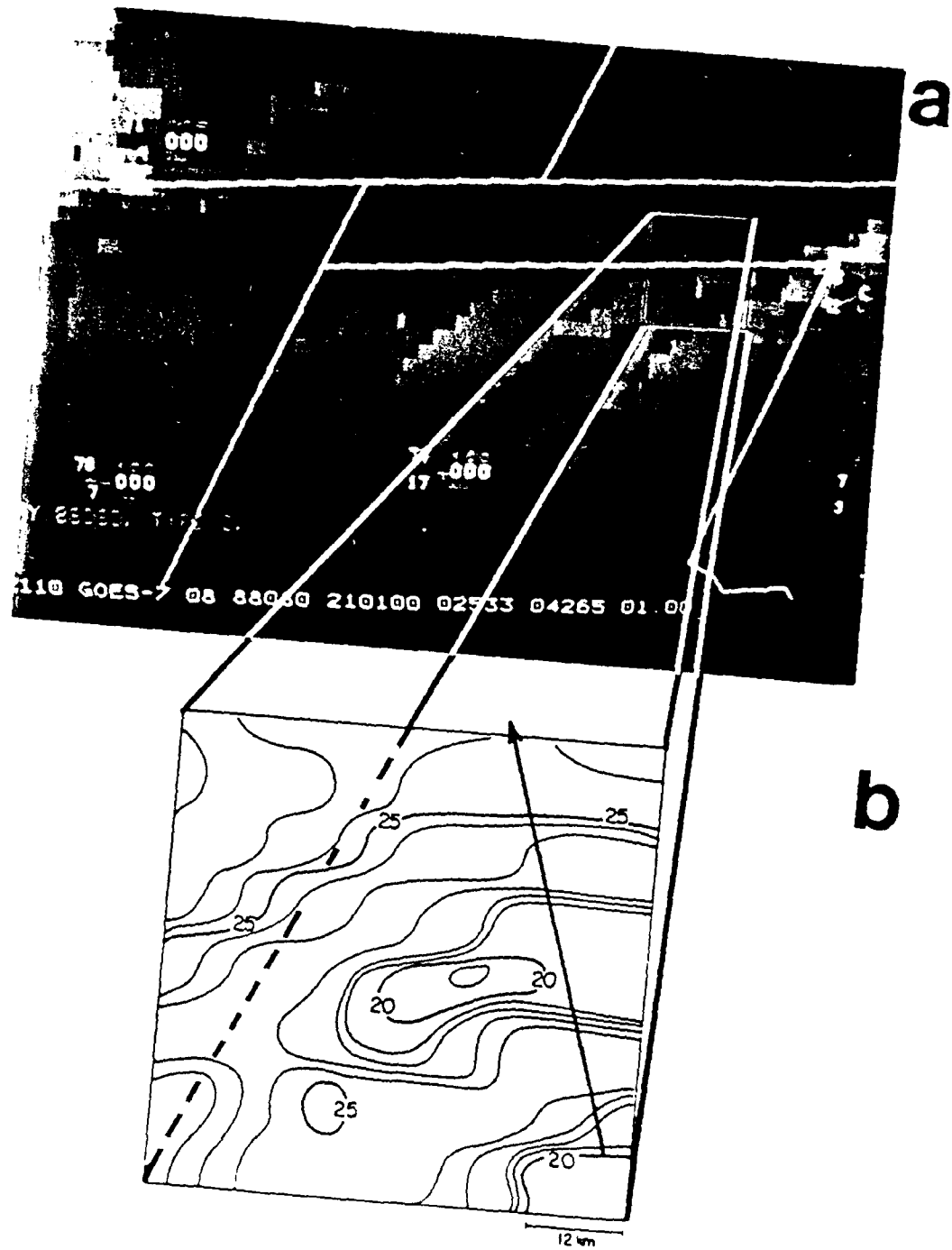


Figure 4.24: A, in Fig. 4.1 except for 20 March, 1988, 1501 CST. Heaviest line indicates location of flight transect.

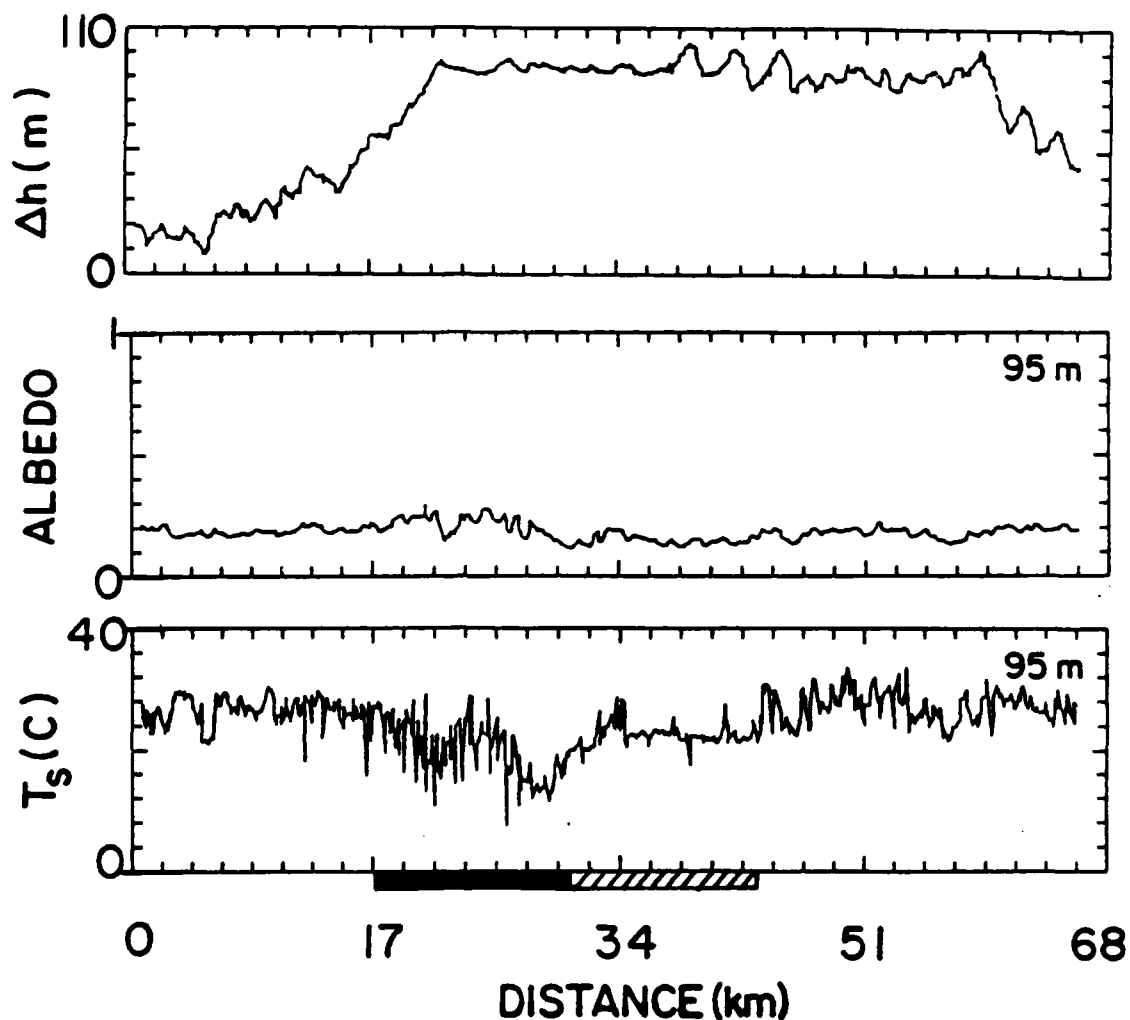


Figure 4.25: (a). Plotted aircraft measurements from flight #9 horizontal transects are shown in Fig. 4.25(a-i). 95 m data were measured from 15:10:07 - 15:22:09 CST. 180 m data were measured from 14:39:33 - 14:51:35 CST. 270 m data were measured from 14:54:30 - 15:07:20 CST. Dark line indicates snow cover; hatched region indicates wet soil. The relative terrain height plot (Δh) is based upon the measured air pressure. Tick mark interval for Δh is 11 m; for albedo it is 0.1; and for T_s is 4°C.

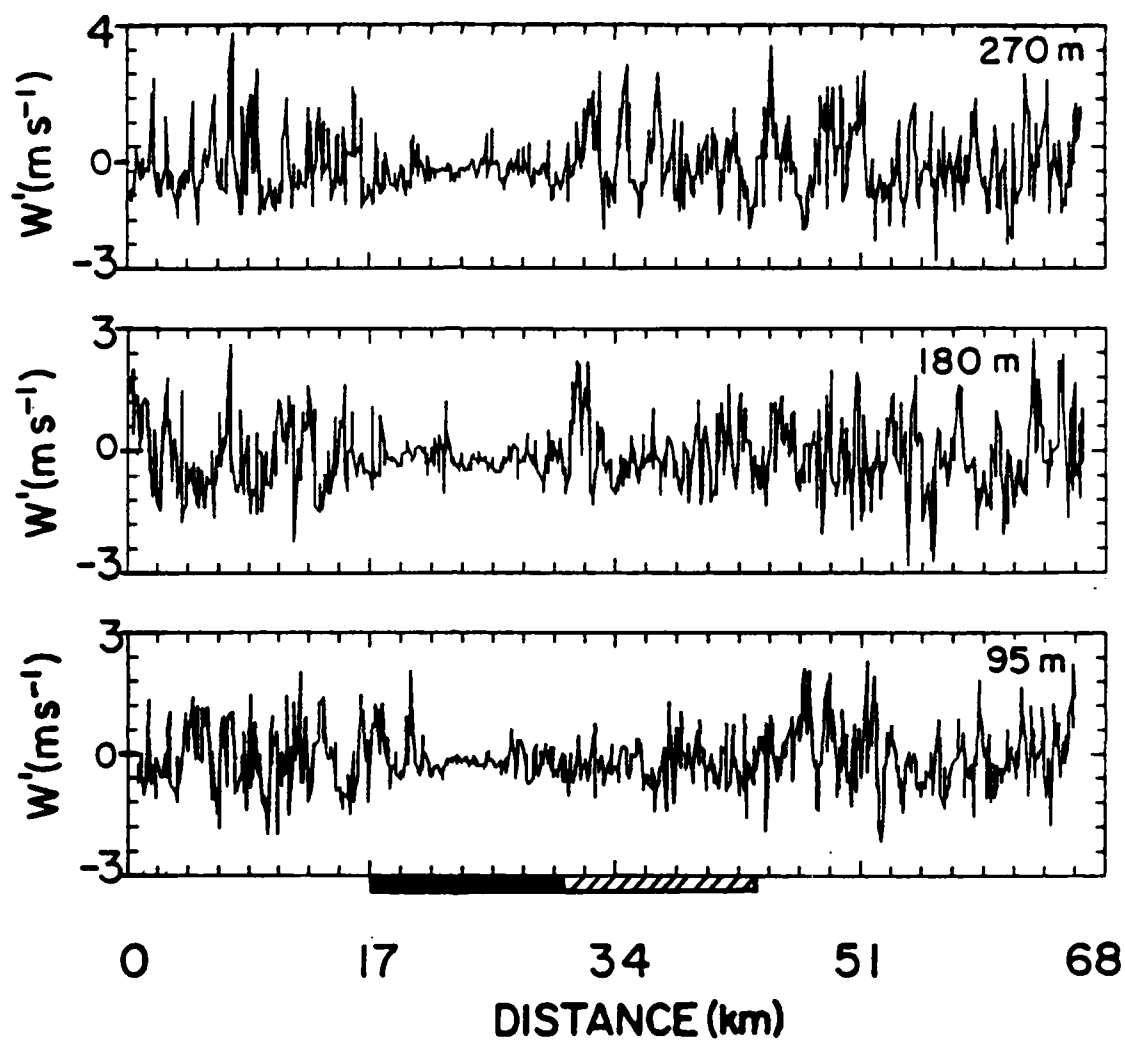


Figure 4.25: (b). Tick mark interval for w' at 95 m and 180 m is 0.6 m s^{-1} ; and at 270 m it is 0.7 m s^{-1} .

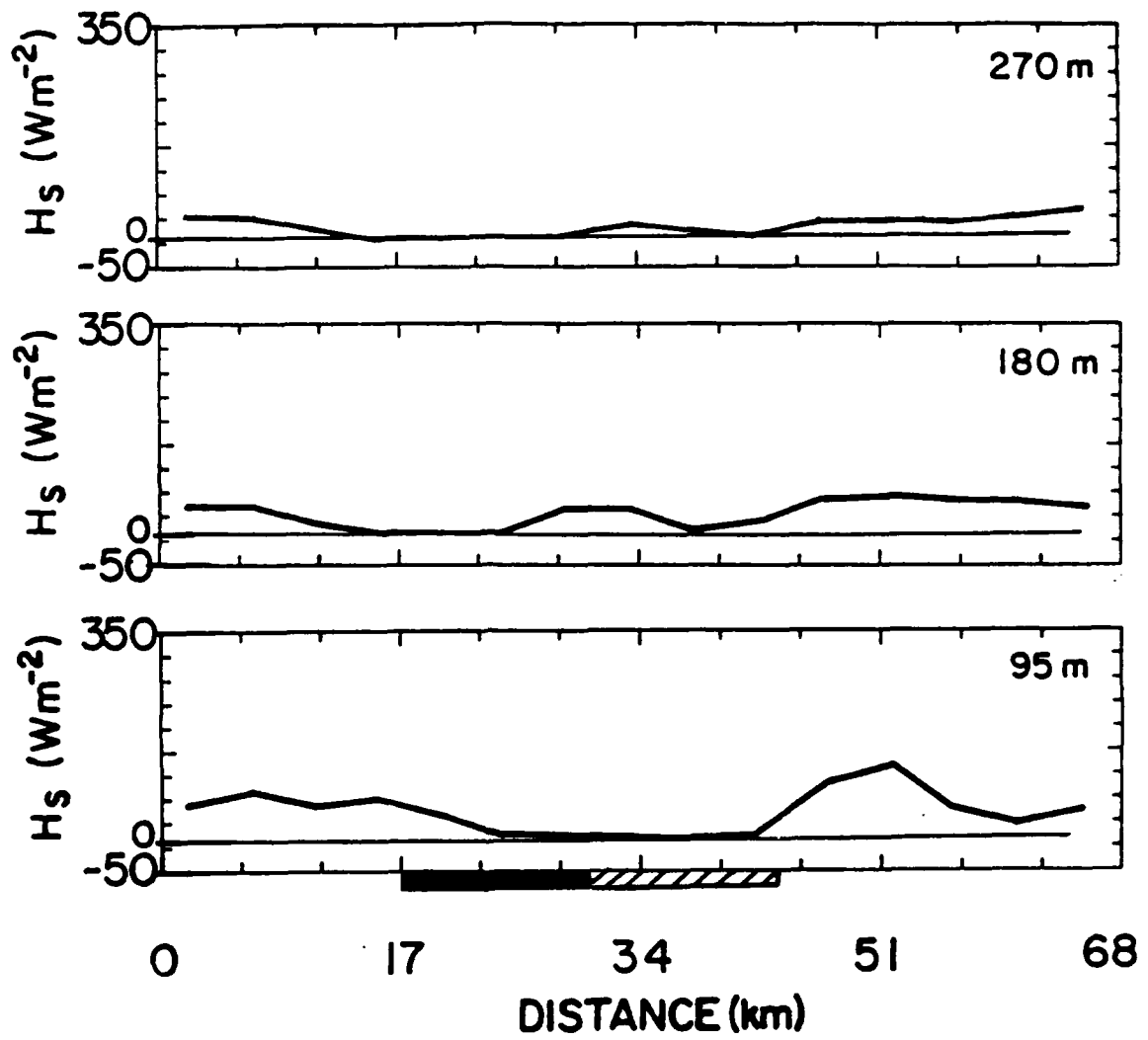


Figure 4.25: (c). Tick mark interval for H_S is 40 W m^{-2} .

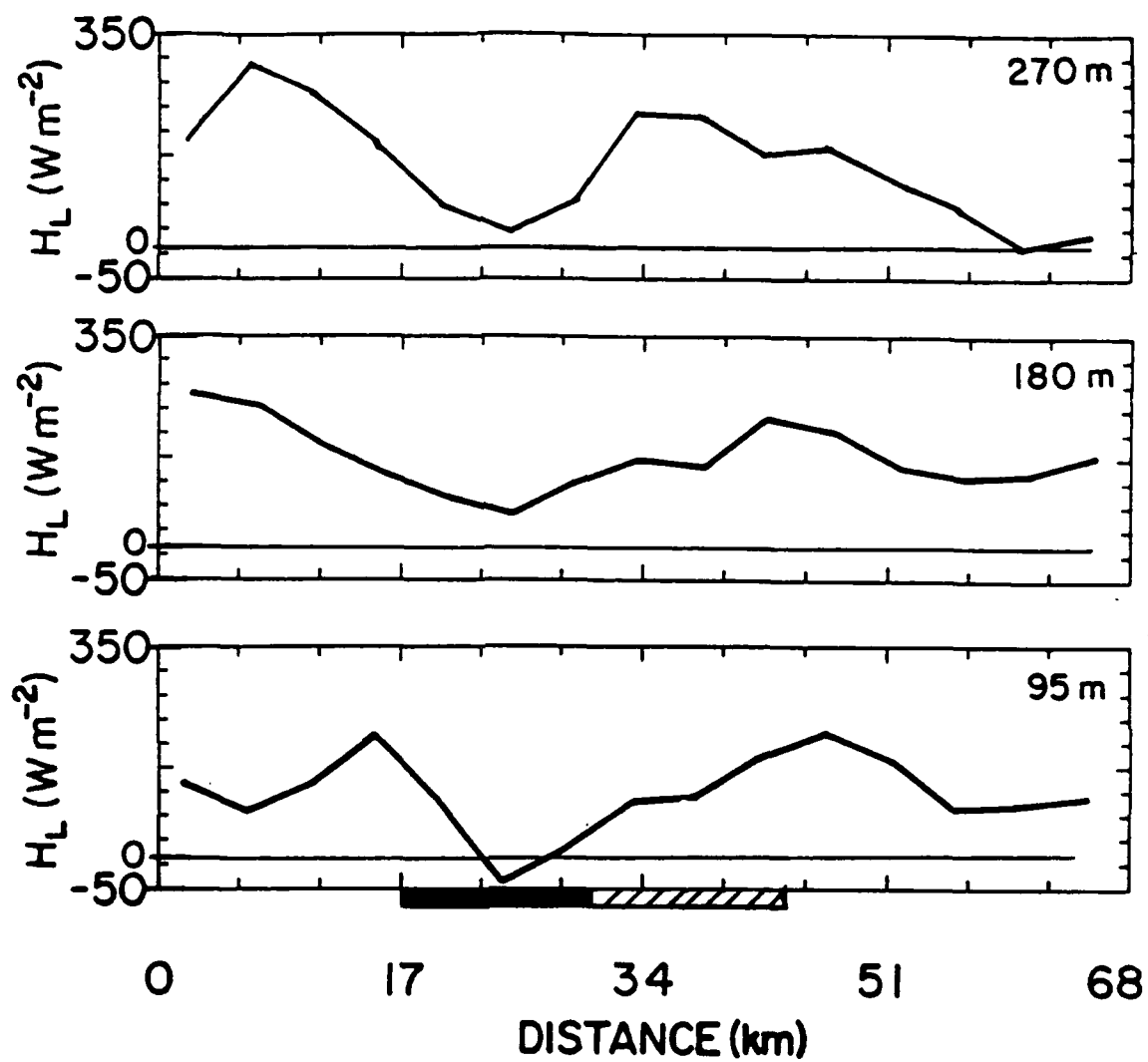


Figure 4.25: (d). Tick mark interval for H_L is 40 W m^{-2} .

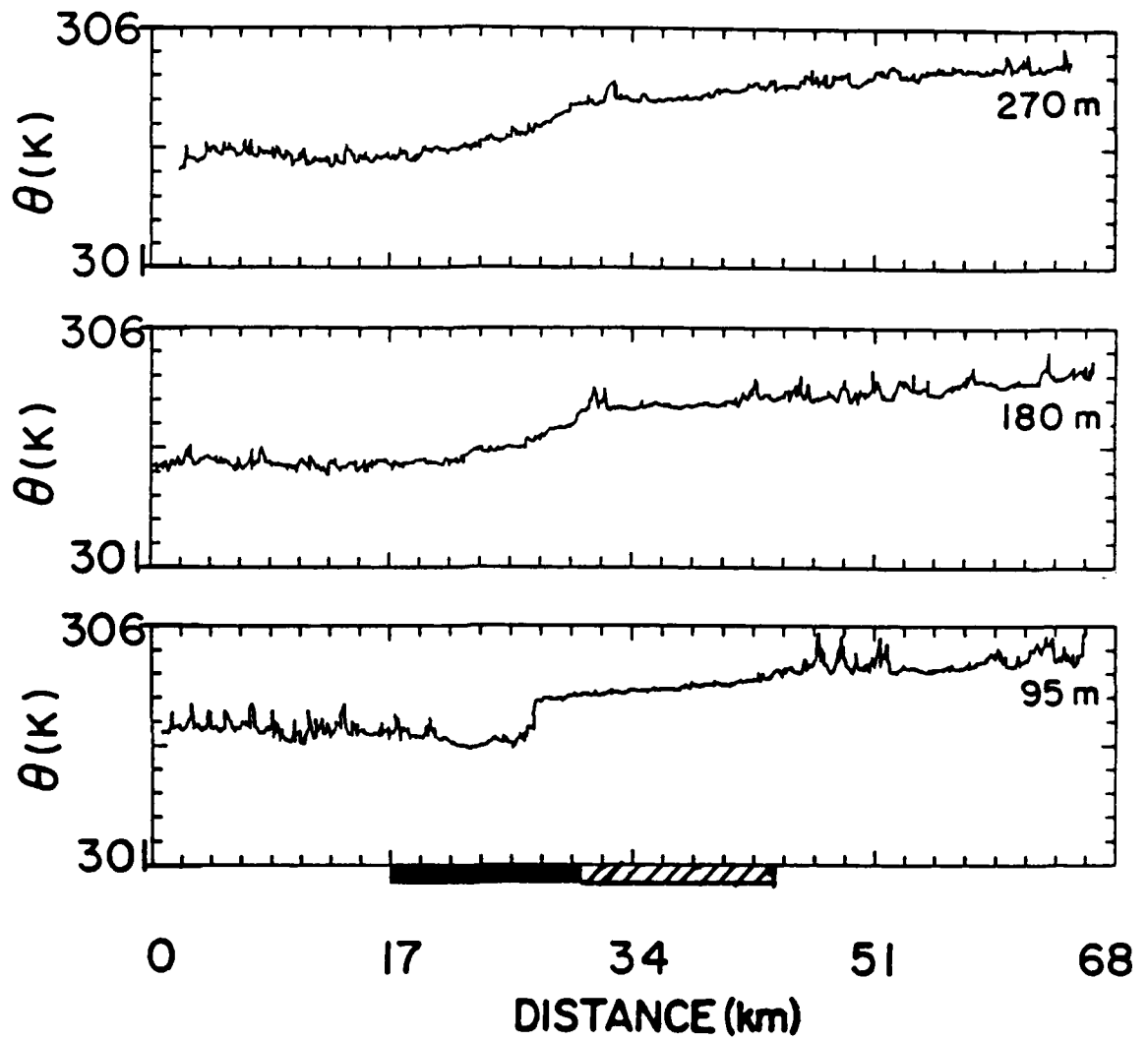


Figure 4.25: (e). Tick mark interval for θ is 0.5 K.

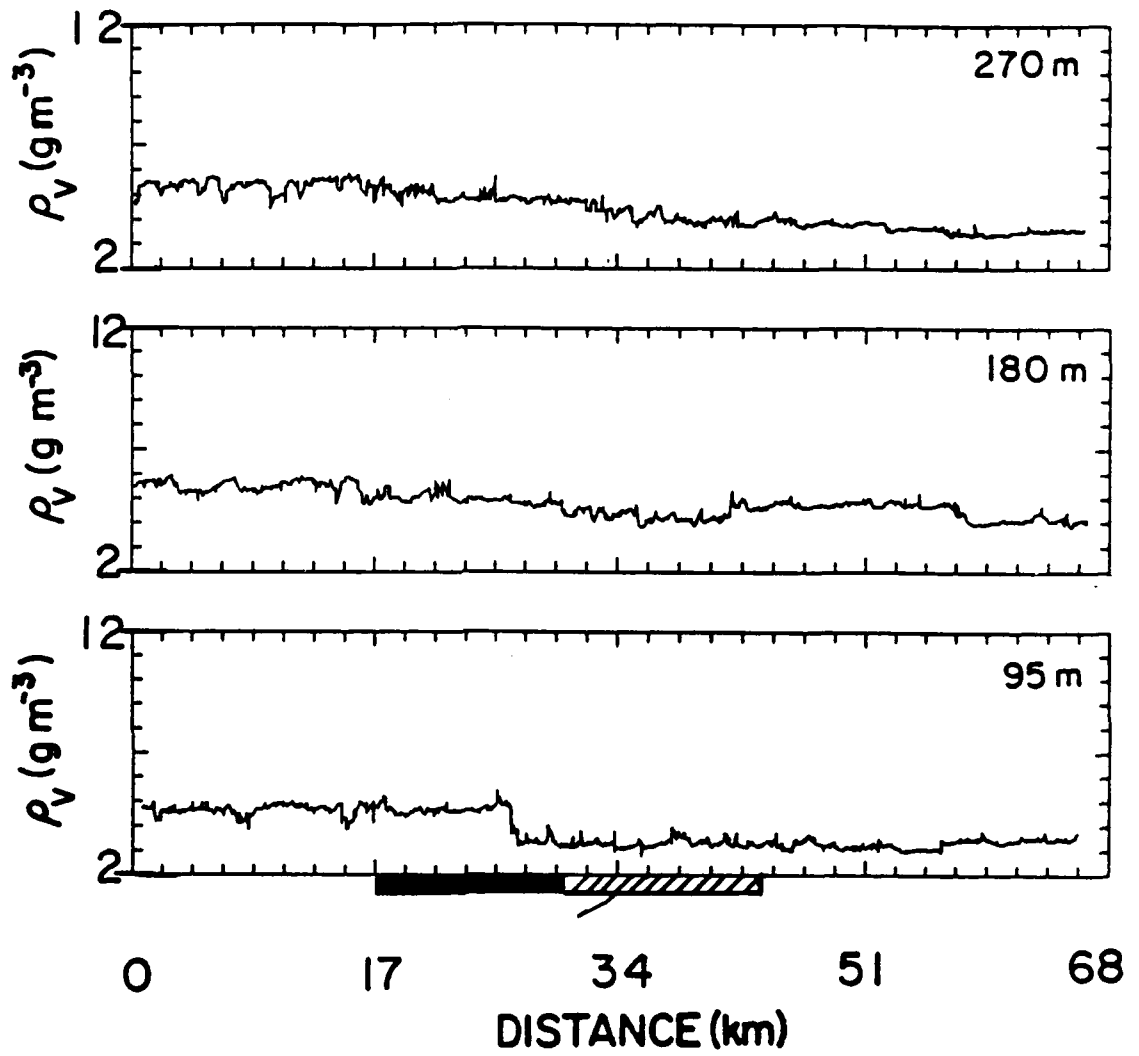


Figure 4.25: (f). Tick mark interval for ρ_v is 1 g m^{-3} .

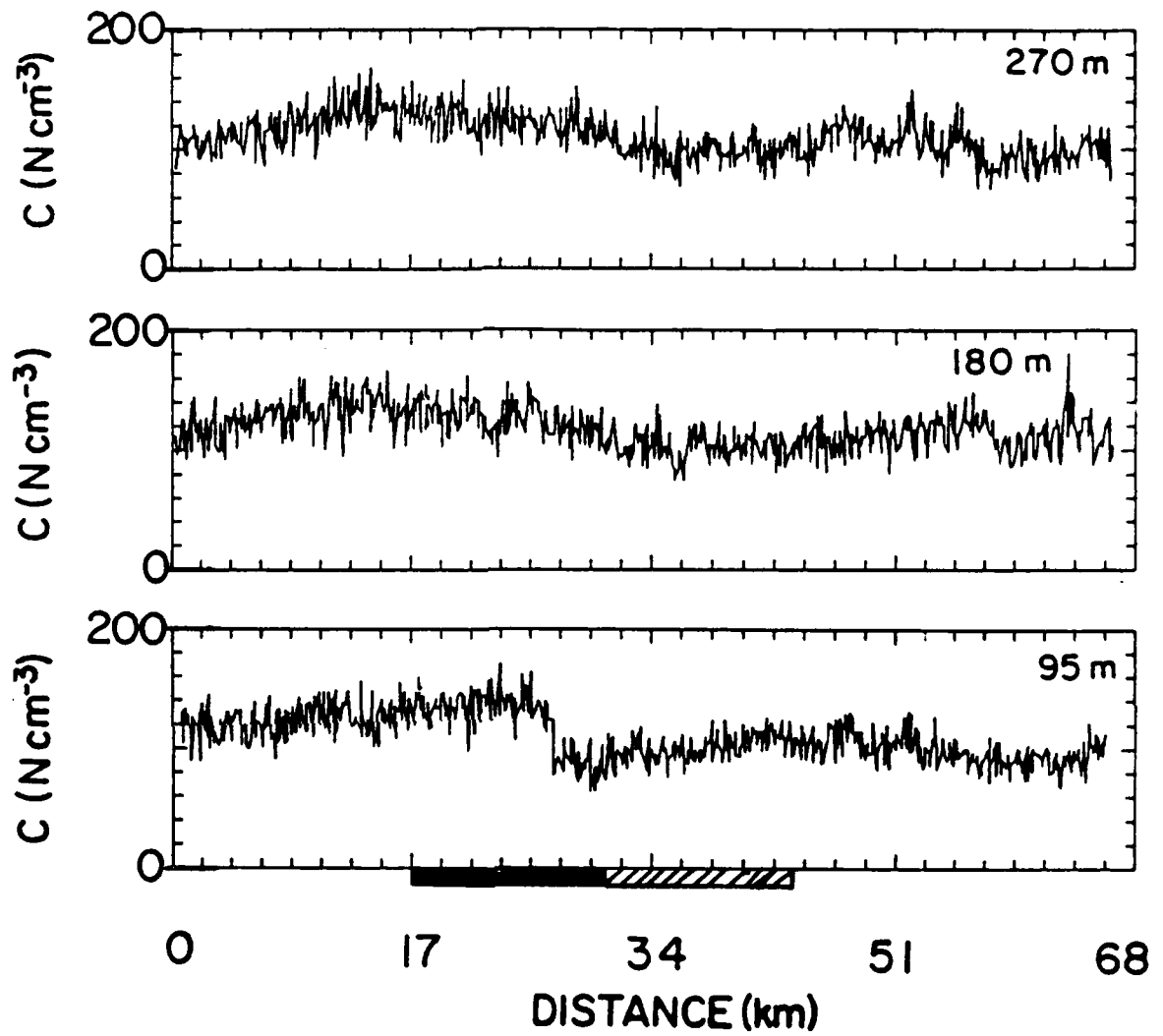


Figure 4.25: (g). Tick mark interval for C is 20 M cm^{-3} .

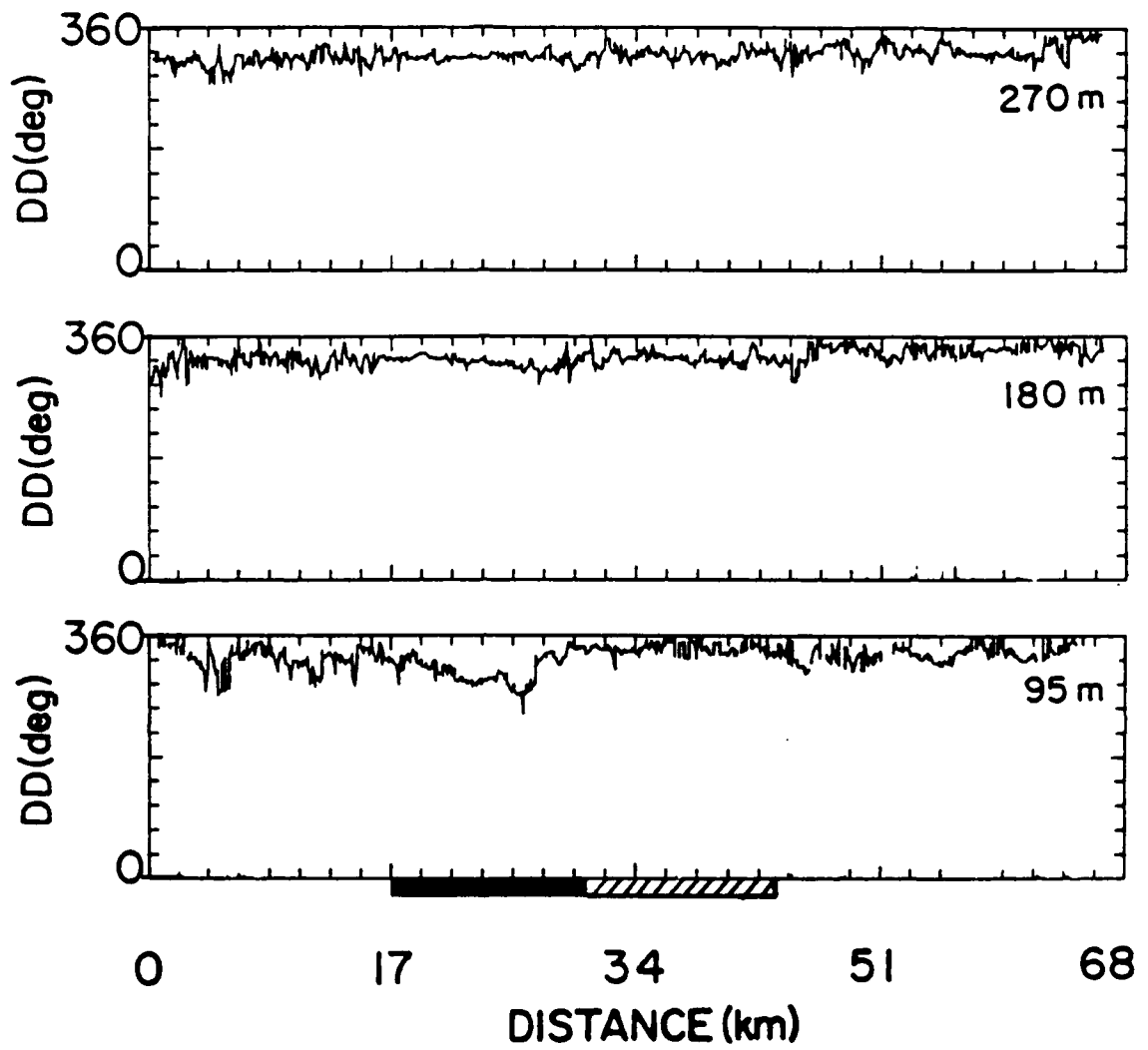


Figure 4.25: (h). Tick mark interval for DD is 36° .

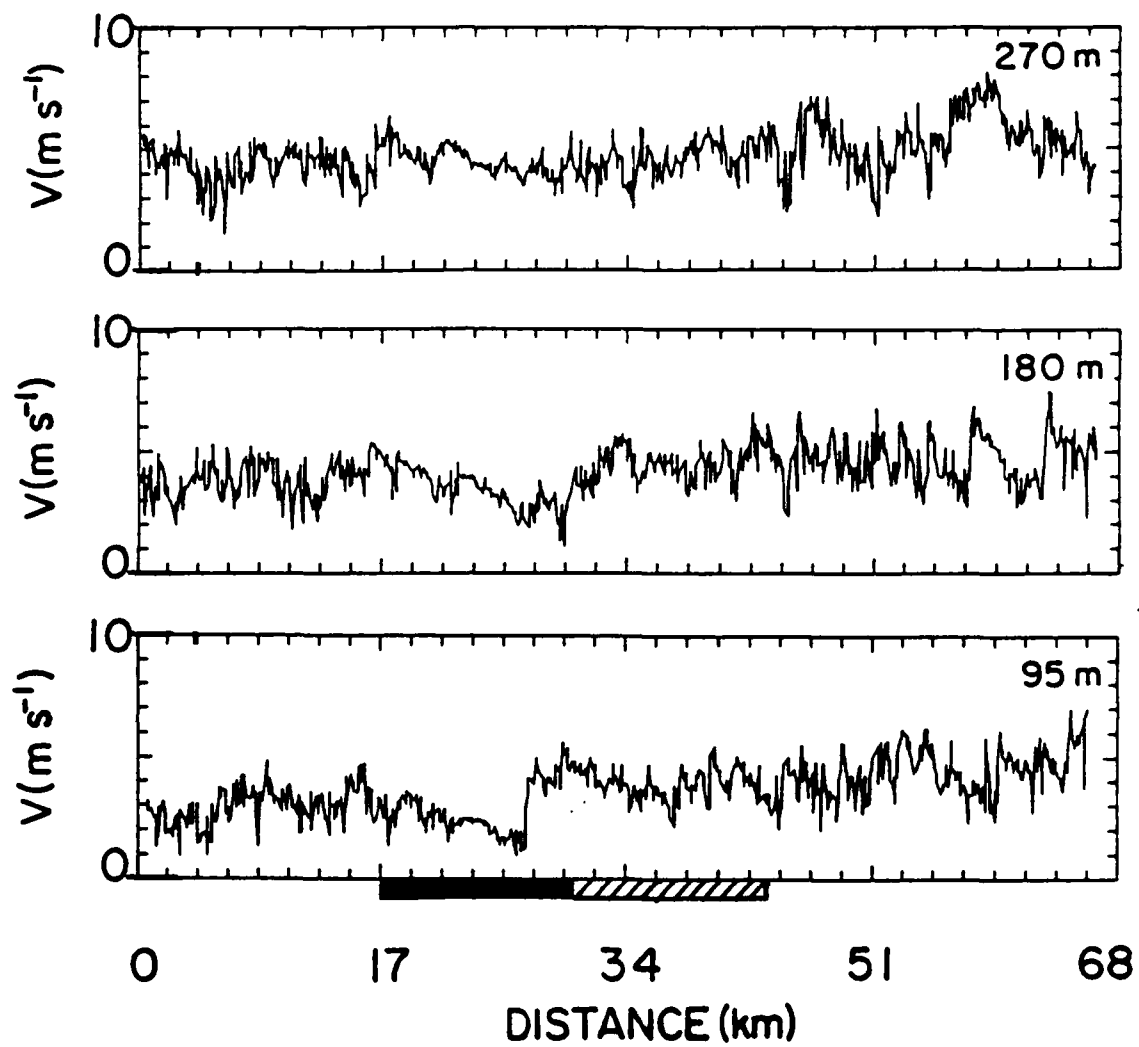


Figure 4.25: (i). Tick mark interval for V is 1 m s^{-1} .

snow from the upwind bare region value of 3.5 g m^{-3} to 6 g m^{-3} . Smaller but noticeable gradients exist at 200 and 300 m. Wind responses to these thermal modifications are noticed.

At the same locations the potential temperature and absolute humidity change, the wind also changes. At 95 m the speed decreases from 4 m s^{-1} to about 1.5 m s^{-1} and the direction changes from 340° to about 320° . A speed decrease is also noticed at 180 m, but not at 260 m. The changes are abrupt but small in horizontal extent. The flow returns to the background speed and direction over the downwind bare region.

4.6.3 Cross section analysis and summary

Although the surface modifications involved with this flight were small in horizontal extent, the cross section analyses show atmospheric responses similar to those seen in the other flights, though smaller in magnitude (Fig. 4.26). A horizontal temperature gradient is established, and thermally-induced modification results. There is a general increase in low-level moisture and aerosol concentration over the snow region.

4.7 Summarization and Generalization of the Field Experiment

Four of the eight SSBLIM flights involved with measurements across snow – no snow boundaries were presented in this Chapter. The third SSBLIM flight inconclusively attempted to measure suppression of daytime upslope flow on a snow-covered slope. Flights #2, 4, 5, and 6, were omitted since they were involved with unfavorable combinations of strong synoptic flow, ill-defined snow regions, and/or irregular terrain. Even for the flights presented, none of the situations were very nearly what the CSU research team considered to be ideal for snow breeze development, yet data supportive of the hypothesis presented in Section 2.2.3 were found.

Flights #1 and #7 were described subjectively by the team as just “reasonably good” in terms of synoptic wind and quality and areal extent of snow cover, and snow-breeze effects, as well as other major modifications, were clearly observed. Even for flights #8 and #9 which were quite non-ideal (due to a high synoptic wind speed and a small snow

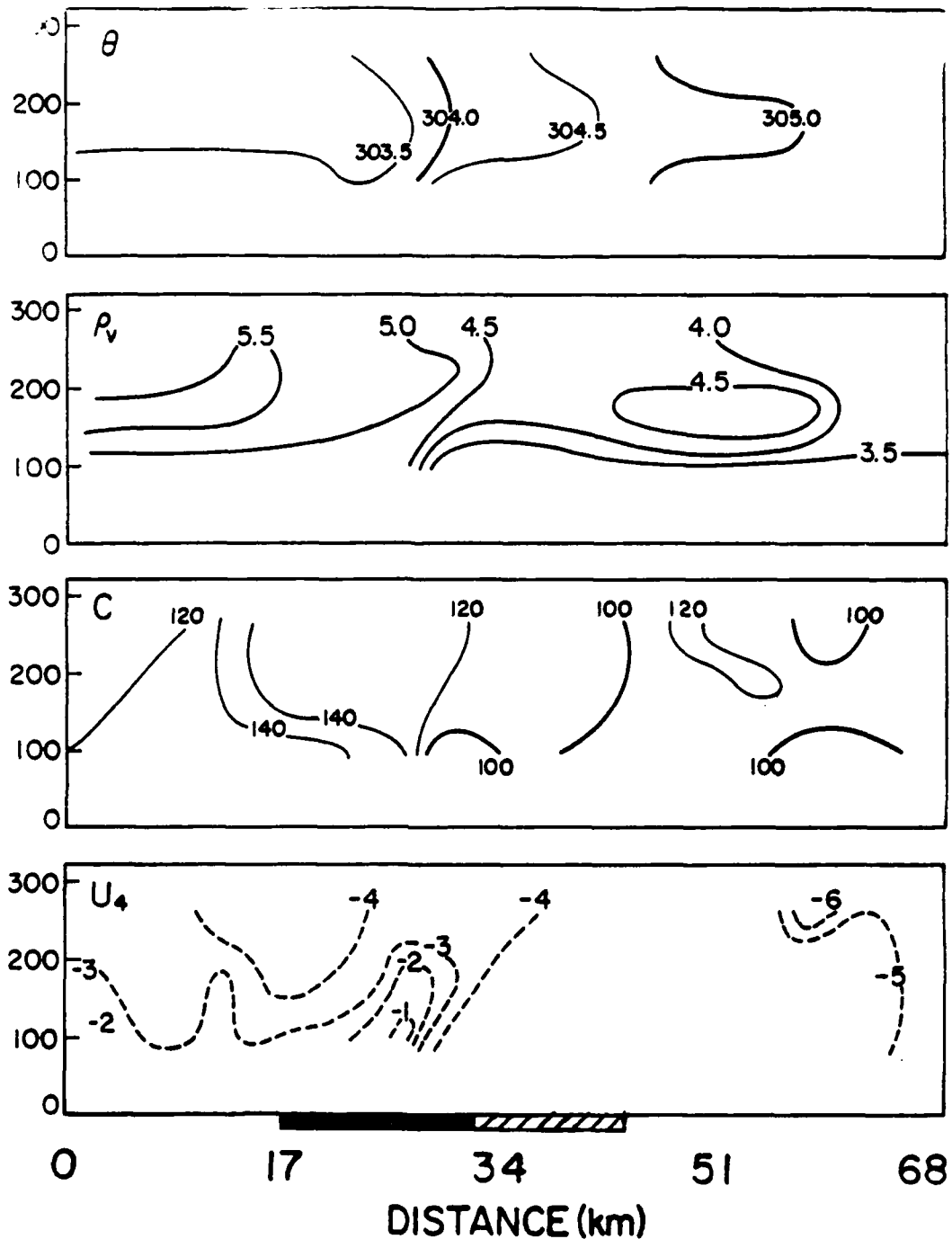


Figure 4.26: Cross section analyses for flight #9 based on plotted measurements in Fig. 4.25. For θ , the contour interval is 0.5 K; for ρ_v , the contour interval is 0.5 g m⁻³; for C , the contour interval is 20 particles cm⁻³; and for u , the contour interval is 1 m s⁻¹. All lines indicate flow in the negative- x direction and the vertical-axes indicate height (m). The distance scale, and the x -axis, lies along the flight transect with the positive (x) axis pointing toward 340° as measured clockwise from the north. The dark line and hatched regions are as in Fig. 4.25.

atch, respectively), atmospheric modifications caused by the snow, including snow-breeze wind modifications, were observed.

Table 4.2 summarizes the results, in terms of the snow breeze, for the four case studies presented in this chapter. The table attempts to concisely relate the case situations (described by snow extent, snow quality, terrain, and background flow) to the resulting mesoscale circulations (described by Δu , L , and h). Note the wide range of situations and results. The length scales of the observed circulations ranged from ~ 10 km to >30 km, and their vertical depths ranges from ~ 200 m to ~ 700 m. Though the results varied, each of the cases, even the highly non-ideal cases #8 and #9, showed snow breeze effects.

The model 1 and model 2 cases in Table 4.2 are included for comparison. Model 1 refers to the same simulation discussed and presented in Section 3.3 and Fig. 3.11. The model 2 case simulation is identical to model 1 except for the inclusion of a 3 m s^{-1} background flow opposing the snow breeze. The only SSBLIM case which resembles either of the model cases is #7, which resembles model 2. Both involve extensive snow, relatively flat terrain, and an opposing background flow. The primary differences between the cases are the dates, the snow quality, and the magnitude of the background flow. Based solely on the dates (using the scale analysis results from Table 2.1), the magnitude of the case #7 circulation should be about 25% larger than the model 2 circulations. The model 2 circulation is, however, noticeably larger (note the differences in Δu and L). This is probably due to the better snow quality and weaker background flow associated with the model 2 simulation. Also, the roughness length (Z_0) included in the model 2 simulations was quite small; 4 cm over the soil and a dynamic formulation similar to that applied over water was used for the snow. Perhaps some interpolation between the case #7 and case model 2 results provides a more realistic speculation on the scale and intensity of a favorable February-March snow breeze. Note that the depths of both circulations are ~ 700 m.

A generalization of the snow breeze is difficult based on four cases, especially since the results were varied. The model comparisons in Table 4.2 help in that they provide at least some qualitative insight as to how far away the SSBLIM cases were from the "ideal" snow

Table 4.2: Summarization of case studies. Snow extent refers to the horizontal extent in the transect direction. The u refers to the component of the flow parallel to the transect, as in the previously presented cross section figures. L is the length scale of the snow breeze circulation, and h is its depth; that is, the height at which u over the snow breeze roughly equals the background u . (Model results courtesy of M. Segal and R.A. Pielke.)

CASE	DATE	SNOW EXTENT	SNOW QUALITY	TERRAIN	BACKGROUND FLOW	PEAK CHANGE IN u DUE TO SNOW BREEZE	L	h
#1	12 Feb	~80 km	Excellent for 20 km of transect; patchy for another 20 km	Complicated (see Fig. 4.6a)	4-6 m s ⁻¹ opposing the snow breeze	~6 m s ⁻¹	-	200 m
#7	18 Mar	~60 km	Deep, but melting rapidly. Patches of soil and vegetation showing	Relatively gentle slope (Fig. 4.12a)	4-6 m s ⁻¹ opposing the snow breeze	~6 m s ⁻¹	>30 km	700 m
#8	19 Mar	~50 km	Good	~100 m elevation drop on bare side (Fig. 4.20a)	~12 m s ⁻¹ parallel to the snow boundary	~4 m s ⁻¹	~30 km	250 m
#9	20 Mar	~15 km (~10 km wet soil)	Poor, very patchy	Much of transect elevated ~100 m from endpoints (Fig. 4.25a)	~5 m s ⁻¹ across snow patch, roughly parallel to the transect	~4 m s ⁻¹	~10 km	200 m
Model 1	12 Feb	54 km (to model boundary)	Ideal	Flat	~Calm	~7 m s ⁻¹	~80 km	1000 m
Model 2	12 Feb	54 km (to model boundary)	Ideal	Flat	3 m s ⁻¹ opposing the snow breeze	~9 m s ⁻¹	~50 km	700 m

breeze simulations. The data allow that the hypothesis stated in Section 2.2.3, that snow breezes exist on the same scale and intensity as sea breezes, may be true. In other words, for lack of a more precise generalization following this research, the generic snow breeze appears to be very similar (given the same radiational forcing) in scale and intensity to the generic sea breeze.

Chapter 5

SUMMARY AND CONCLUDING REMARKS

Recent data from northeast Colorado has reinforced previous understanding that snow cover has a cooling and stabilizing effect on the lower atmosphere. Furthermore, examples of daytime upslope suppression have supported previous observations of such suppression by Ohata *et al.*, (1981). In addition to demonstrating daytime upslope suppression with surface observations due to snow cover, this research extended the previous observations by demonstrating the effect through a 300 m layer.

It should be noted that whereas Ohata *et al.*, (1981) found the daytime upslope circulation to be a stable feature throughout the year in the Khumbu Himal, East Nepal (measurements taken on a slope of $\sim 330 \text{ m km}^{-1}$ elevation change), good examples of daytime mesoscale upslope flow in the PROFS region of northeast Colorado (Fig. 3.6), where the slopes are much milder ($\sim 7 \text{ m km}^{-1}$ elevation change), are the exception, not the rule, during the winter. Most of the days, whether the region is snow covered or bare, involve the influence of large-scale pressure gradients and render thermally-induced mesoscale flow comparisons inappropriate. It will be stated here, without statistical backing, that on days associated with weak large-scale pressure gradients, daytime upslope flow appeared to be generally anomalously weak in intensity and/or short in duration when snow cover prevailed as opposed to bare ground. There were, however, isolated examples of surface upslope flow associated with weak synoptic pressure gradients and general snow cover, and weak upslope flow associated with bare ground and slight pressure gradients, that could not be explained. The few favorable examples shown in Chapter 3 are intended only to show that snow cover apparently does suppress the daytime upslope flow in certain situations.

Results from the aircraft measurements taken during the SSBLIM project are also consistent with the previous understanding that the daytime atmosphere over snow cover is generally cool and stable, with little upward vertical transfer of sensible heat.

The SSBLIM flight results presented in Chapter 4 are, to the author's knowledge, the first direct comprehensive set of measurements of the snow breeze. The main conclusion of the SSBLIM project is that mesoscale gradients of snow cover/bare soil, given a favorable environment, cause noticeable thermally-induced circulation effects on the mesoscale flow. Even though none of the presented cases closely approximated ideal snow-cover and back-ground flow conditions, the data are supportive of a conjectured generalization that the snow breeze, given a favorable snow - no snow boundary, is of similar scale and intensity as the sea breeze, under the same environmental conditions.

Considering the "success rate" of the SSBLIM project and the belief of the CSU research team that several potentially good opportunities were missed during the project, it is suggested that clearly observable snow breeze effects are not the infrequent result of combinations of clear skies, very light synoptic flow, and well-defined boundaries of deep snow. Rather, such effects should be anticipated whenever variable snow cover exists in moderately favorable environments.

The results of this study should enhance awareness of potentially important short-range mesoscale forecasting considerations. The importance of the sea breeze is well recognized. Sea breezes (and lake breezes) are important to the mesoscale weather of affected regions regularly (especially during the warm months) due to the permanence of the water-land boundaries. Snow breezes should be similarly important late in the snow season (around early spring), though less frequently. Furthermore, snow breeze effects should be significant to a lesser degree throughout the fall and winter months.

The most important mesoscale weather impacts of the snow breeze should occur during the spring. It is in the spring that atmospheric moisture content is often substantial, bare soil sensible heat fluxes are large (under clear skies), and the snow breeze may initiate or enhance moist convection (Pielke, personal communication, 1988). Concerning the practicability of anticipating snow breeze effects, it has been shown in the SSBLIM project

that significant snow - no snow boundaries can be identified shortly after sunrise in GOES satellite imagery. The CSU researchers found the interactive workstation (the PROFSERS and the VDUC) extremely valuable in accurately locating the snow boundaries and monitoring the associated surface temperature gradients.

The data in Chapter 4 show higher aerosol concentrations over the snow cover due to the relative lack of vertical mixing. The stable daytime temperature profiles over the snow render snow cover an important factor when considering pollution dispersion (Segal *et al.*, 1988b). Additionally, the accuracy of any dispersion forecast or model simulation involving variable snow cover is limited if it does not include snow breeze considerations.

In order to more fully understand the snow breeze and the potential differences that may exist between it and other thermally-induced mesoscale circulations, more observational and modeling study is required. Case studies (in addition to the case presented by Johnson *et al.*, 1984) showing the initiation or enhancement of moist convection would underscore the statements made in this thesis concerning the potential importance of the snow breeze. It is suggested that case study modeling simulations be attempted based on the data presented in Chapter 4. Such efforts may lead to the improvement of snow - atmosphere interaction formulations in mesoscale models.

REFERENCES

- Anderson, Eric A., 1976: A point energy and mass balance model of snow cover. NOAA Technical Report NWS 19, U.S. Dept. of Commerce, 150 pp.
- Anthes, Richard A., 1984: Enhancement of convective precipitation by mesoscale variations in vegetative covering in semiarid regions. *J. Clim. Appl. Meteor.*, **23**, 541-554.
- Atkinson, B.W., 1981: *Meso-scale Atmospheric Circulations*. Academic Press, 495 pp. (See chpts. 5-6).
- Bailey, M.J., K.M. Carpenter, L.R. Lowther and C.W. Passant, 1981: A mesoscale forecast for 14 August 1975 - the Hampstead Storm. *Meteor. Mag.*, **110**, 147-161.
- Beran, D.W. and C.G. Little, 1979: Prototype regional observing and forecasting service: From concept to implementation. *Natl. Wea. Dig.*, **4**, 2-5.
- Berry, M.O., 1981: *Handbook of Snow*, Gray, D.M. and D.H. Male, (Eds.), Pergamon Press, 32-59.
- Bluestein, H.B., 1982: A wintertime mesoscale cold front in the Southern Plains. *Bull. Amer. Meteor. Soc.*, **63**, 178-185.
- Bryson A. and F.K. Hare, 1974: Climates of North America. *World Survey of Climatology*, Vol. 11, Elsevier Scientific Publishing Company.
- Dunkel, M., L. Hasse, L. Krügermeyer, D. Schriver and J. Wucknitz, 1974: Turbulent fluxes of momentum, heat, and water vapor in the atmospheric surface layer at sea during ATEX. *Bound.-Layer Meteor.*, **6**, 81-106.

- Dzerdzeevskii, B.L., 1963: Meteorological parameters of the surface air layer over humid and dry sectors of the Trans-Volga Steppe. In *Sukhoveis and Drought Control*, Dzerdzeevskii, B.L., Ed., Israel Program for Scientific Translations, Jerusalem, 162-180.
- Estoque, M.A., 1962: The sea breeze as a function of the prevailing synoptic situation. *J. Atmos. Sci.*, **19**, 244-250.
- Granger, R.J. and D.H. Male, 1978: Melting of a prairie snowpack. *J. Appl. Meteor.*, **17**, 1833-1842.
- Halberstam, I.M. and R. Melendez, 1979: A model of the planetary boundary layer over a snow surface. *Bound.-Layer Meteor.*, **16**, 431-452.
- Halberstam, I.M. and J.P. Schieldge, 1981: Anomalous behavior of the atmosphere over melting snowpack. *J. Appl. Meteor.*, **20**, 255-265.
- Hicks, B.B. and H.C. Martin, 1972: Atmospheric turbulent fluxes over snow. *Bound.-Layer Meteor.*, **2**, 496-502.
- Johnson, R.H., and J.J. Toth, 1982: A climatology of the July 1981 surface flow over northeast Colorado. Atmos. Sci. Paper No. 342, Colorado State University, Fort Collins, CO, 80523, 52 pp.
- Johnson, R.H., G.S. Young, J.J. Toth and R.M. Zehr, 1984: Mesoscale weather effects of variable snow cover over northeast Colorado. *Mon. Wea. Rev.*, **112**, 1141-1152.
- Kaimal, J.C. and J.E. Gaynor, 1983: The Boulder Atmospheric Observatory. *J. Climate Appl. Meteor.*, **22**, 863-880.
- Kuzmin, P.P., 1961: *Melting of Snow Cover*. [Translated from Russian by Israel Program for Scientific Translations (1972).] 290 pp.
- Lenschow, D.H. and P. Spyers-Duran, 1987: Measurement techniques: Air motion sensing. *NCAR RAF Bulletin No. 23*, NCAR, Boulder, CO 80307.

- Mahfouf, J.F., E. Richard and P. Mascart, 1987: The influence of soil and vegetation on the development of mesoscale circulations. *J. Climate Appl. Meteor.*, **26**, 1483-1495.
- Mahrer, Y. and R.A. Pielke, 1977: A numerical study of the airflow over irregular terrain. *Contrib. Atmos. Phys.*, **50**, 98-113.
- Mahrer, Y. and R.A. Pielke, 1978: The meteorological effect of the change in surface albedo and moisture. *Isr. Meteor. Res. Pap.*, **2**, 55-70.
- McCumber, M.C., 1980: A numerical simulation of the influence of heat and moisture fluxes upon mesoscale circulations. Ph.D. dissertation, Department of Environmental Science, University of Virginia, Charlottesville, 255 pp.
- McKay, D.C. and G.W. Thurtell, 1978: Measurements of the energy fluxes involved in the energy budget of a snow cover. *J. Appl. Meteor.*, **17**, 339-349.
- McNider, R.T. and R.A. Pielke, 1981: Diurnal boundary layer development over sloping terrain. *J. Atmos. Sci.*, **38**, 2198-2212.
- McNider, R.T., G.J. Jedlover and G.S. Wilson, 1984: Data analysis and model simulation of convection on April 24, 1982. *Tenth Conf. on Weather Forecasting and Analysis*, Tampa, Florida. Amer. Meteor. Soc., 543-549.
- Miller, E.R. and R.B. Freisen, 1987: Standard output data products from the NCAR Research Aviation Facility. *NCAR RAF Bulletin No. 9*, NCAR, Boulder, CO 80307, 70 pp.
- Müller-Glewe, J. and H. Hinzpeter, 1974: Measurements of the turbulent heat flux over the sea. *Bound.-Layer Meteor.*, **6**, 47-52.
- NCAR RAF, 1988: The King Air: Overview and summary of capabilities. *NCAR RAF Bulletin No. 2*, NCAR, Boulder, CO 80307-3000.

- Ohata, T., K. Higuchi and K. Ikegami, 1981: Mountain-valley wind system in the Khumbu Himal, East Nepal. *J. Meteor. Soc. Japan*, **59**, 753-762.
- Ookouchi, Y., M. Segal, R.C. Kessler and R.A. Pielke, 1984: Evaluation of soil moisture effects on the generation and modification of mesoscale circulations. *Mon. Wea. Rev.*, **112**, 2281-2292.
- Physick, W.L., 1980: Numerical experiments of the inland penetration of the sea breeze. *Quart. J. Roy. Meteor. Soc.*, **106**, 735-746.
- Pielke, R.A., 1974: A three-dimensional numerical model of the sea breezes over south Florida. *Mon. Wea. Rev.*, **102**, 115-139.
- Pielke, R.A., 1984: *Mesoscale Meteorological Modeling*. Academic Press, 612 pp.
- Pielke, R.A. and Y. Mahrer, 1978: Verification analysis of the University of Virginia three-dimensional mesoscale model prediction over south Florida for July 1, 1973. *Mon. Wea. Rev.*, **106**, 1568-1589.
- Pond, S., G.T. Phelps, J.E. Paquin, G. McBean and R.W. Stewart, 1971: Measurements of the turbulent fluxes of momentum, moisture, and sensible heat over the ocean. *J. Atmos. Sci.*, **28**, 901-917.
- Reynolds, D.W., 1983: Prototype workstation for mesoscale forecasting. *Bull. Amer. Meteor. Soc.*, **64**, 264-273.
- Schlatter, T.W., 1972: The local surface energy balance and sub-surface temperature regime in Antarctica. *J. Appl. Meteor.*, **11**, 1048-1062.
- Schlatter, T.W., V.D. Barker and J.F. Henz, 1983: Profiling Colorado's Christmas Eve blizzard. *Weatherwise*, **36**, 60-66.
- Schneider, S.H. and T. Gal-Chen, 1973: Numerical experiments in climatic stability. *J. Geophys. Res.*, **78**, 6182-6194.

- Segal, M. and R.A. Pielke, 1981: Numerical mode simulation of human biometeorological heat load conditions - summer day case study for the Chesapeake Bay area. *J. Appl. Meteor.*, **20**, 735-749.
- Segal, M. Y. Mahrer and R.A. Pielke, 1982: Application of a numerical mesoscale model for the evaluation of seasonal persistent regional climatological patterns. *J. Appl. Meteor.*, **21**, 1754-1762.
- Segal, M., J.F.W. Purdom, J.L. Song, R.A. Pielke and Y. Mahrer, 1986: Evaluation of cloud shading effects on the generation and modification of mesoscale circulations. *Mon. Wea. Rev.*, **114**, 1201-1212.
- Segal, M., R. Avissar, M.C. McCumber and R.A. Pielke, 1988: Evaluation of vegetation effects on the generation and modification of mesoscale circulations. *J. Atmos. Sci.*, **45**, 2268-2392.
- Segal, M., W. Schreiber, G. Kallos, R.A. Pielke, J.R. Garratt, J. Weaver, A. Rodi and J. Wilson, 1988: Evaluation of the impact of crop areas in northeast Colorado on the mid-summer atmospheric boundary layer. *Mon. Wea. Rev.*, (in revision).
- Segal, M. and R.A. Pielke, 1988a: Evaluation of snow covered ground effect on the generation and modification of daytime mesoscale circulations. Part I: Theoretical and numerical model considerations. *J. Atmos. Sci.*, (to be submitted).
- Segal M., J.R. Garratt, R.A. Pielke, J. Cramer, P. Hildebrand and Frank Rogers, 1988b: On the impact of snow covered ground on daytime pollutants dispersion conditions. *Atmos. Environ.*, (to be submitted).
- Sellers, W.D., 1965: *Physical Climatology*. The University of Chicago Press, Chicago, 272 pp.
- Thorntwaite, C.W. and B. Holzman, 1939: The determination of evaporation from land and water surfaces. *Mon. Wea. Rev.*, **67**, 4-11.

U.S. Army Corps of Engineers, 1956: *Snow Hydrology*. Summary report of the snow investigations. North Pacific Division, Corps of Engineers, Portland, Oregon, 437 pp.

Wash, C.H., D.A. Edman and J. Zapotocny, 1981: GOES observation of a rapidly melting snowband. *Mon. Wea. Rev.*, **109**, 1353-1356.

Williams, J., 1975: The influence of snow cover on the atmospheric circulation and its role in climate change. *J. Appl. Meteor.*, **14**, 137-152.

Yan, H. and R.A. Anthes, 1988: The effect of variations in surface moisture on mesoscale circulations. *Mon. Wea. Rev.*, **116**, 192-208.

APPENDIX A

SNOW COVER CLIMATOLOGY

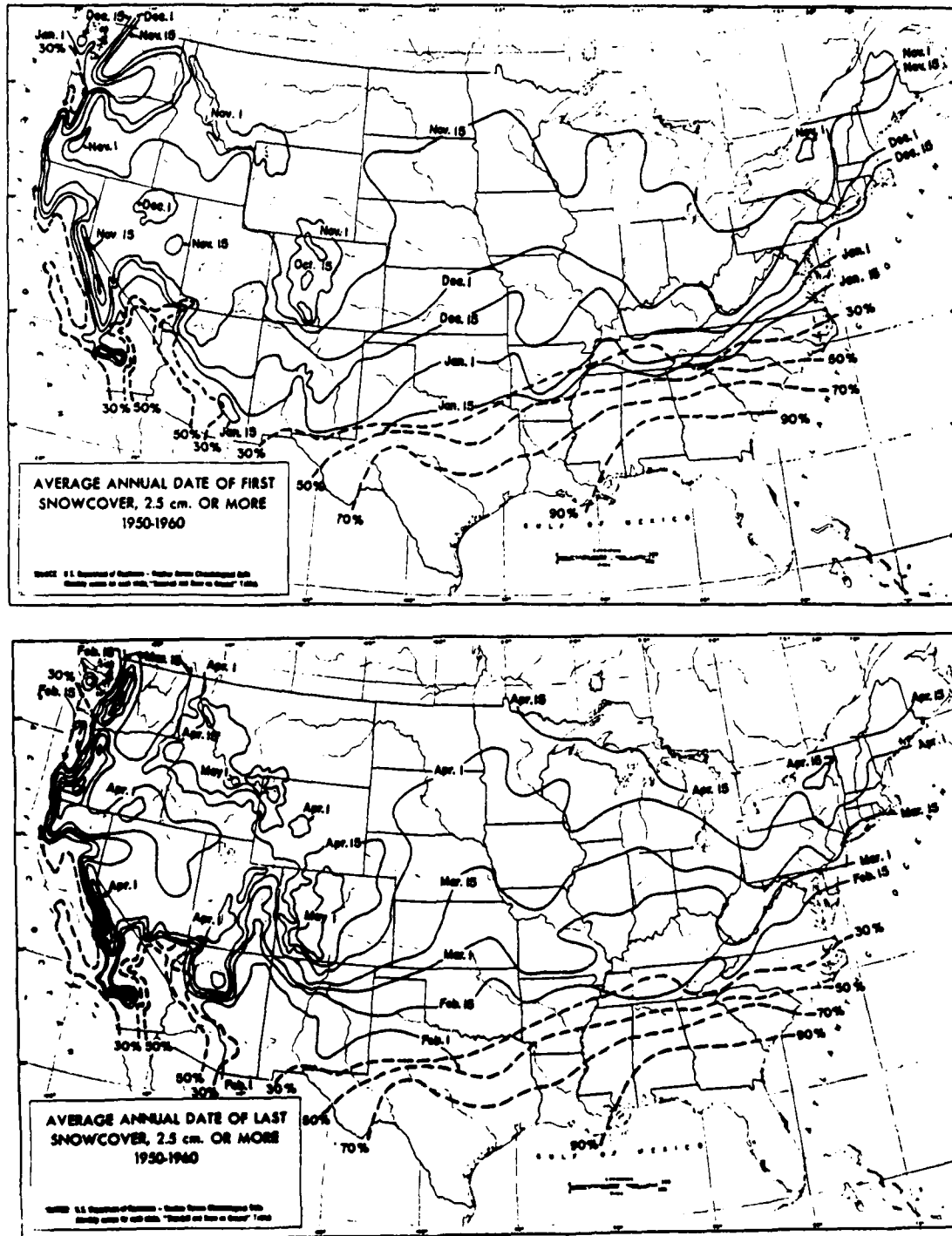


Figure A.1: Average annual date of first and last snow cover of 2.5 cm or more, 1950-1960. Dashed lines give percent of years without snow cover. (Prepared by Donald Larson, reproduced from Bryson and Hare, 1974.)

APPENDIX B

SYNOPTIC MAPS

This appendix contains synoptic weather analyses involved with the examples of mesoscale flow variations presented in Chapter 3 (Figs. B.1 through B.9).

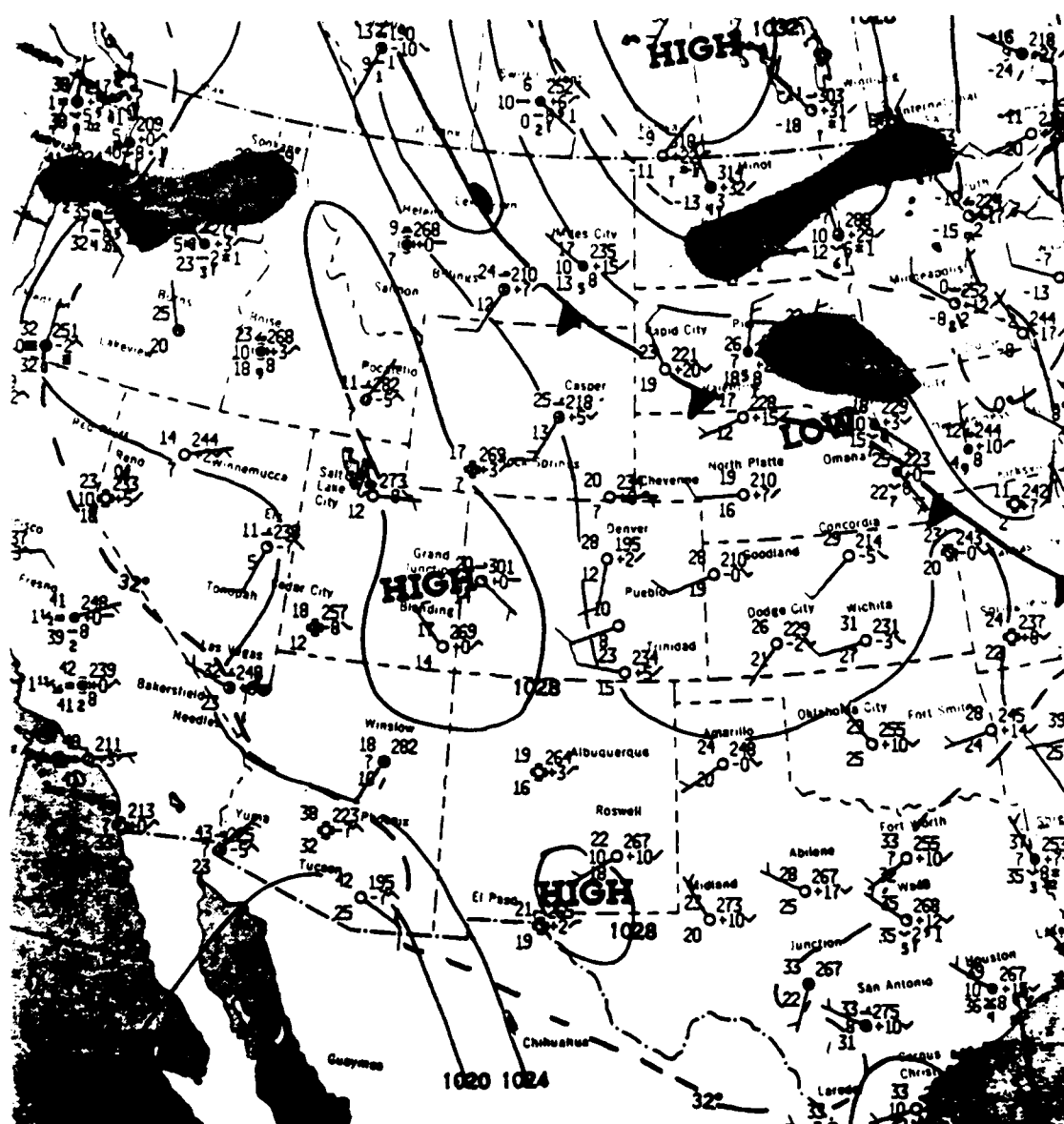


Figure B.1: Surface synoptic weather analysis for 0500 MST, 12 December, 1986. (Reproduced from "Daily Weather Maps", Climate Analysis Center.)

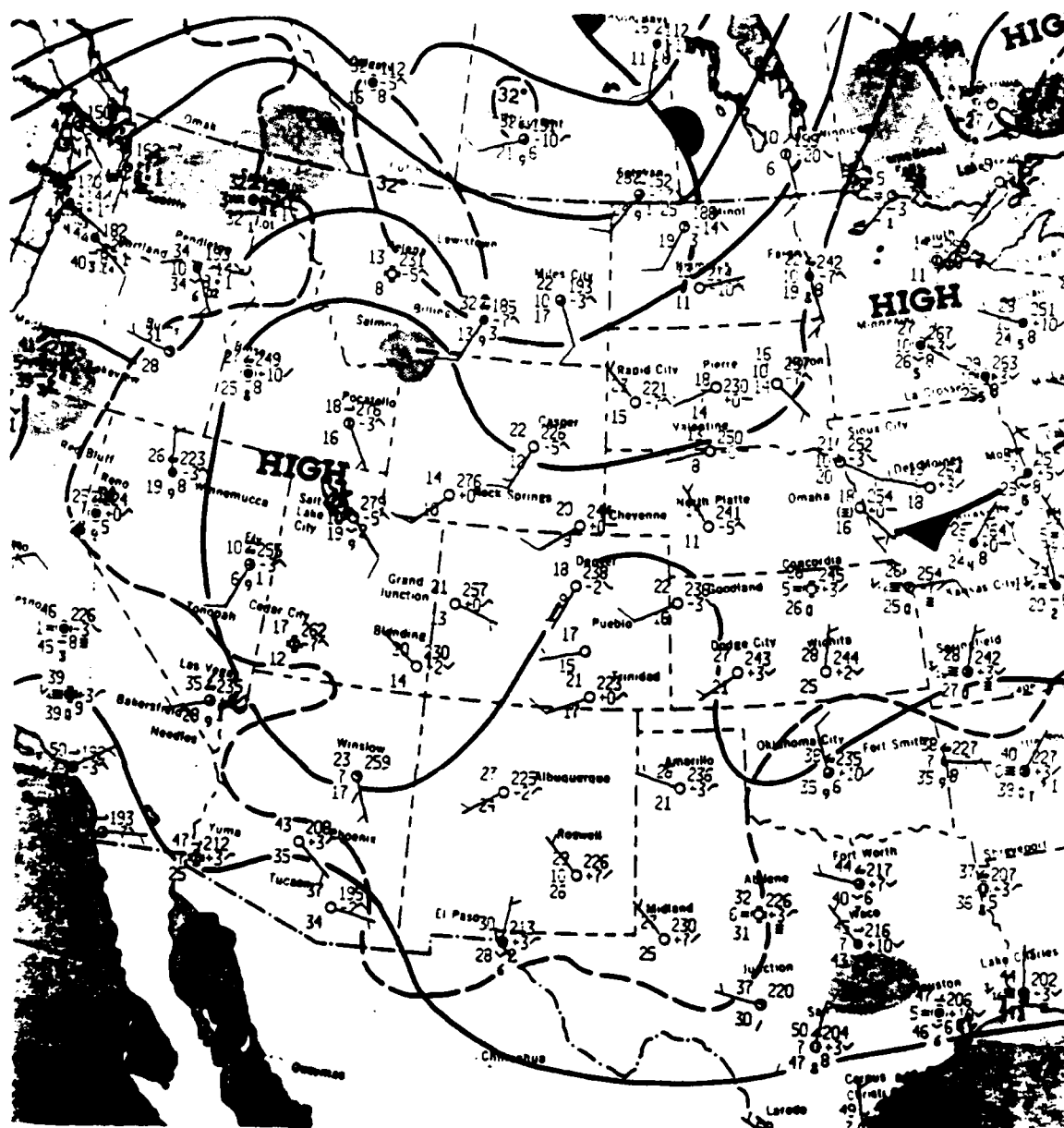
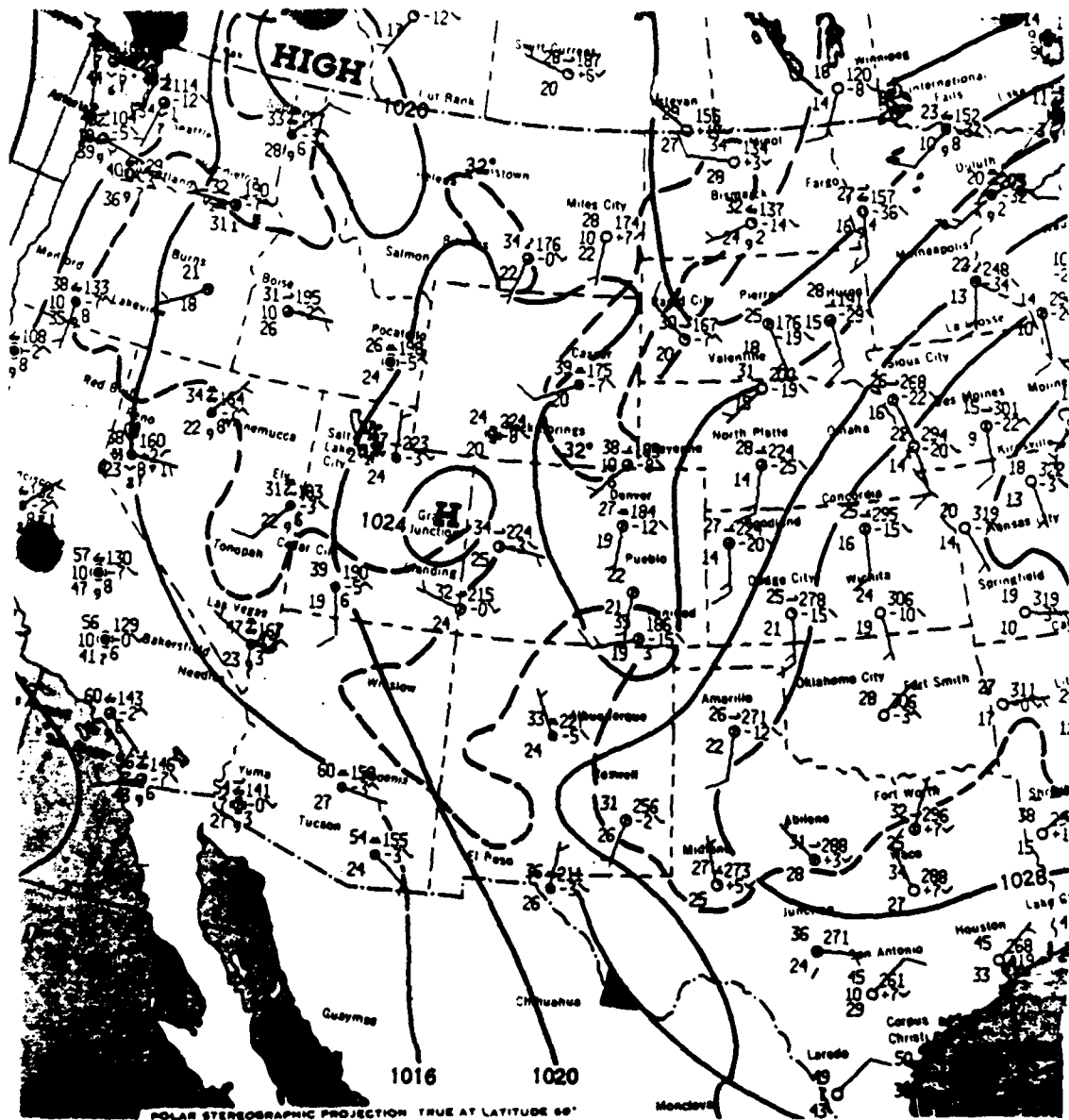


Figure B.2: As in Fig. B-1 except for 26 December, 1986.



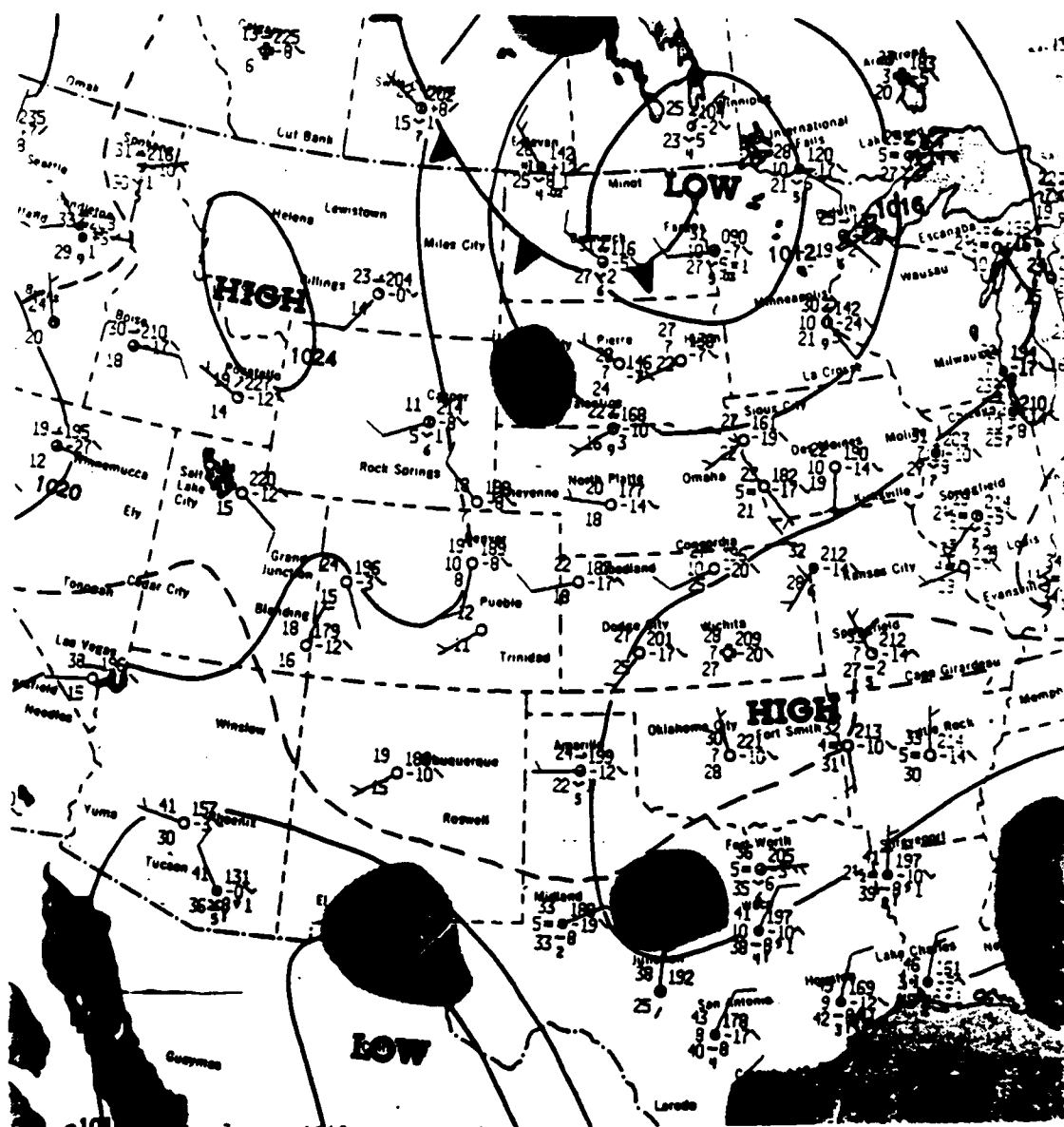


Figure B.4: As in Fig. B-1 except for 21 February, 1987.

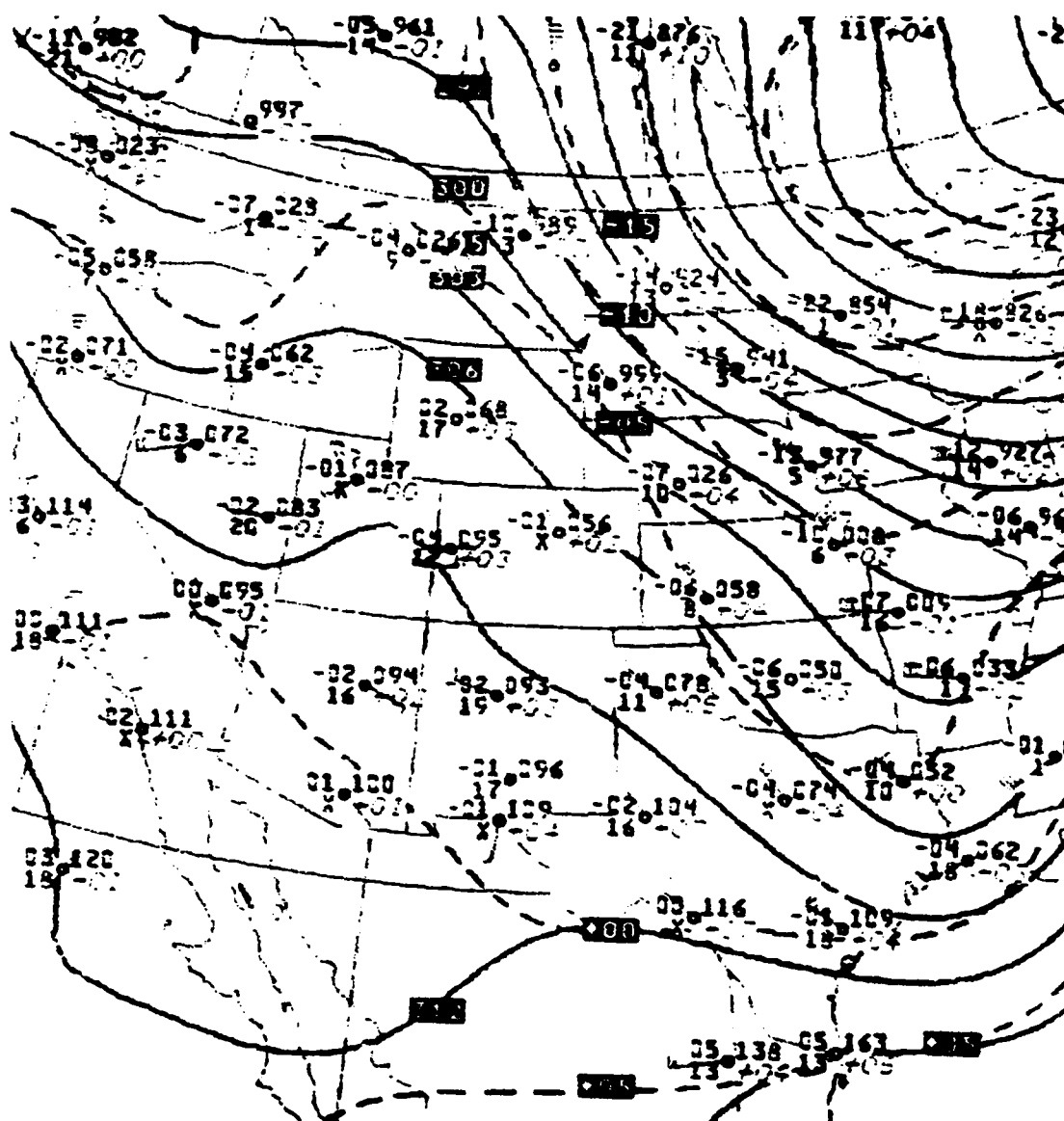


Figure B.5: 70 kPa analysis valid at 0500 MST, 12 December, 1986. (NMC real-time analysis courtesy of the CSU Weather Laboratory.)

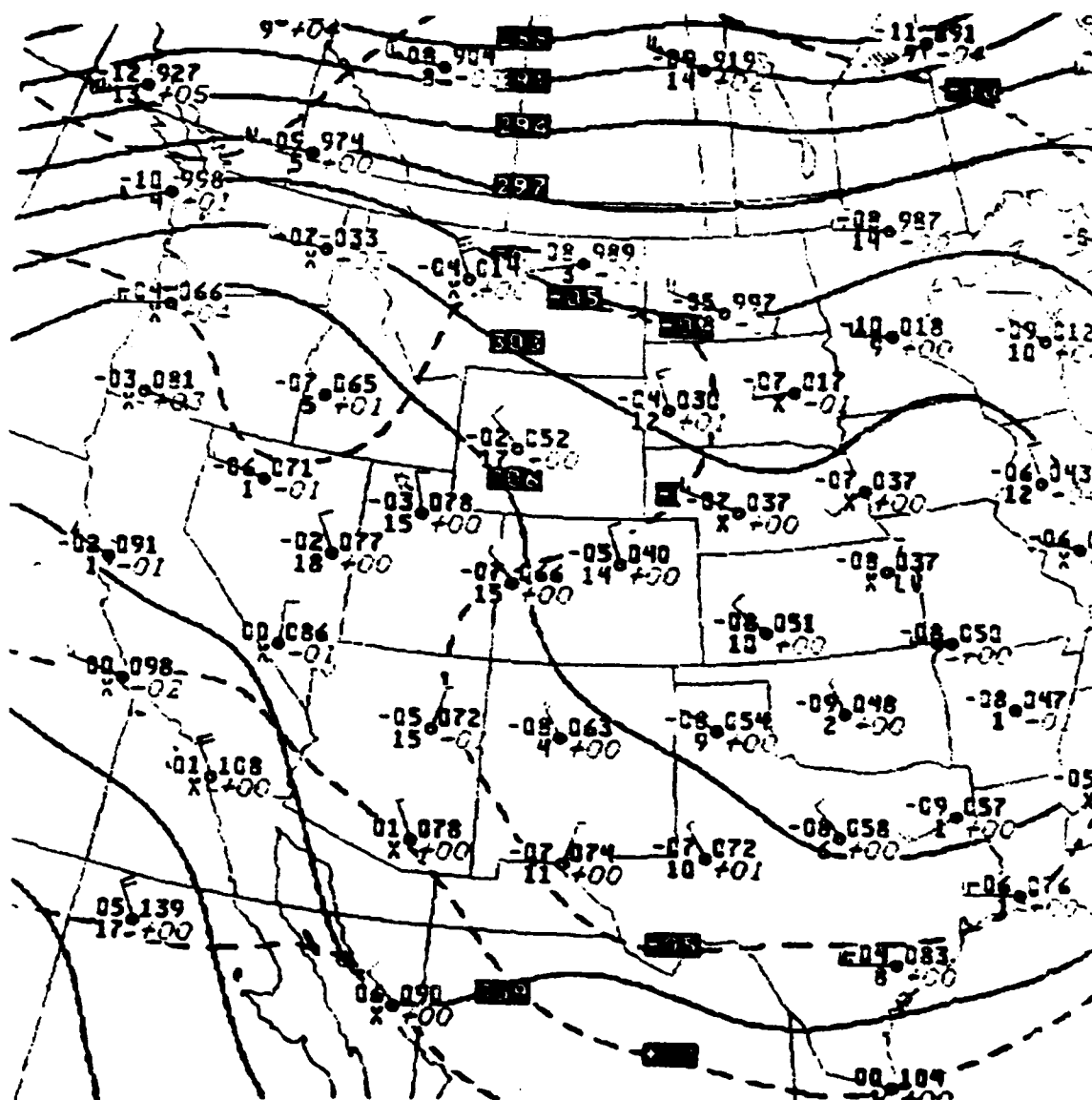


Figure B.6: As in Fig. B-5 except for 1700 MST, 26 December, 1986.

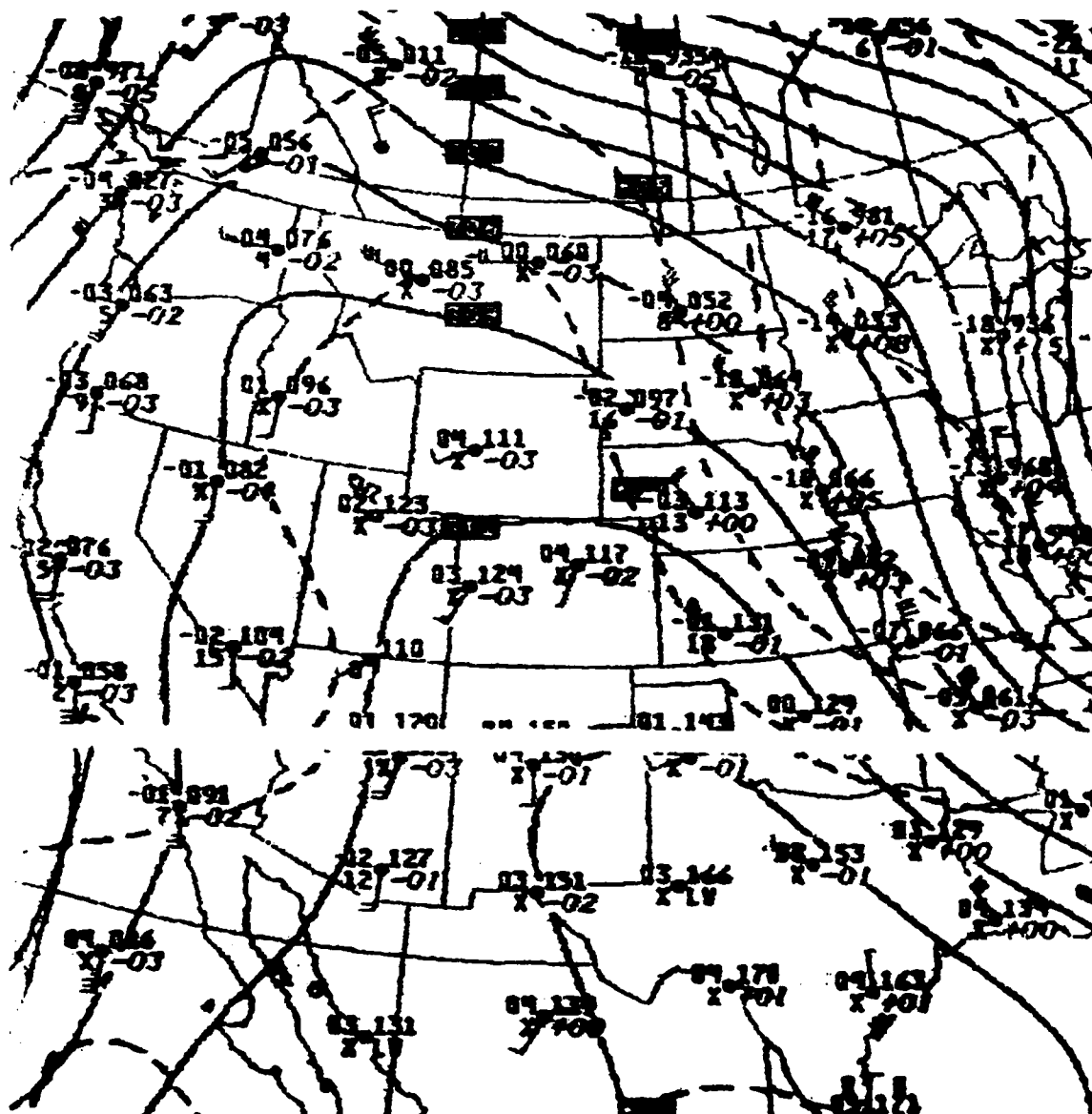


Figure B.7: As in Fig. B-5 except for 1700 MST, 8 February, 1987.

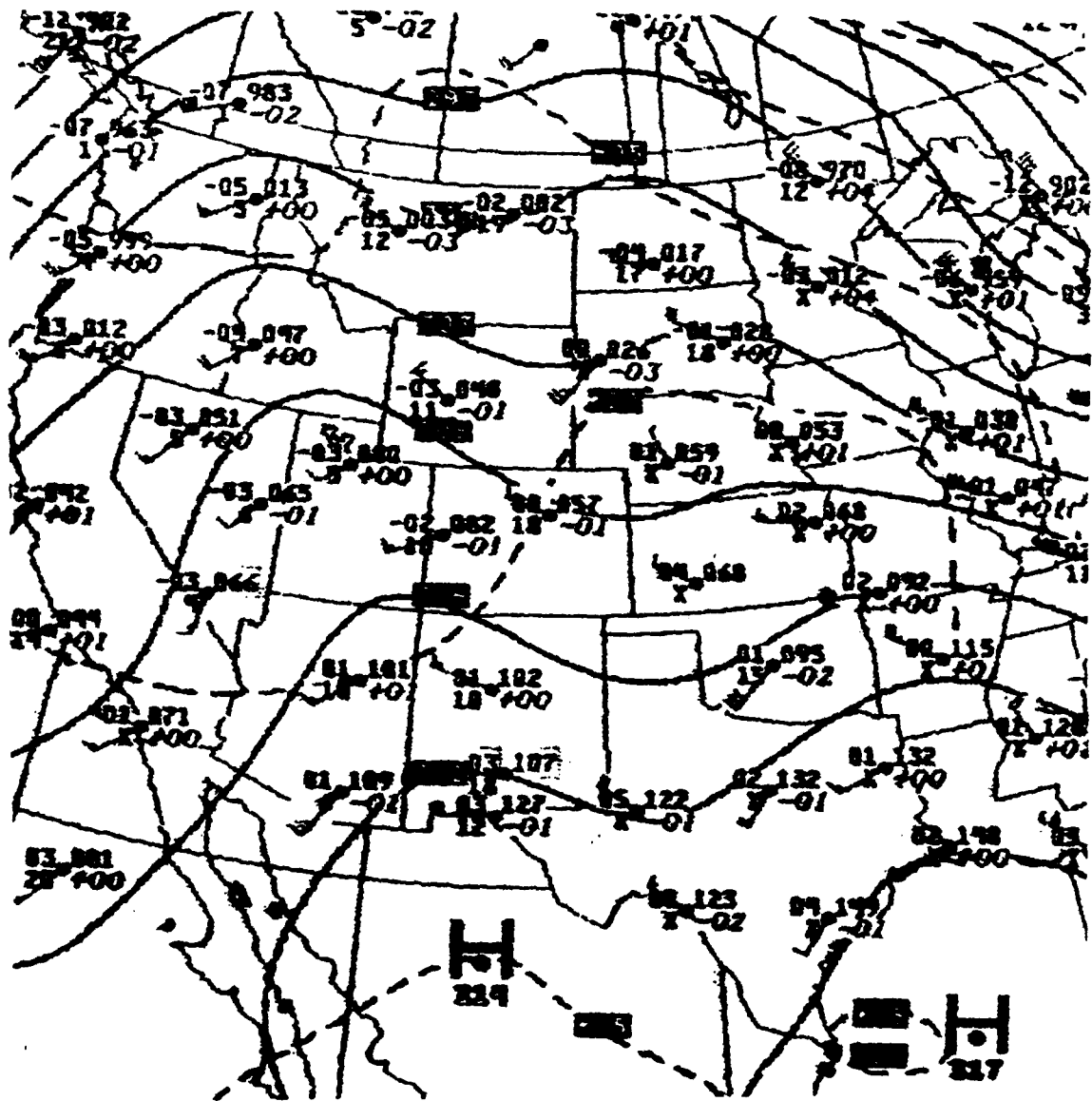


Figure B.8: As in Fig. B-5 except for 0500 MST, 10 February, 1987.

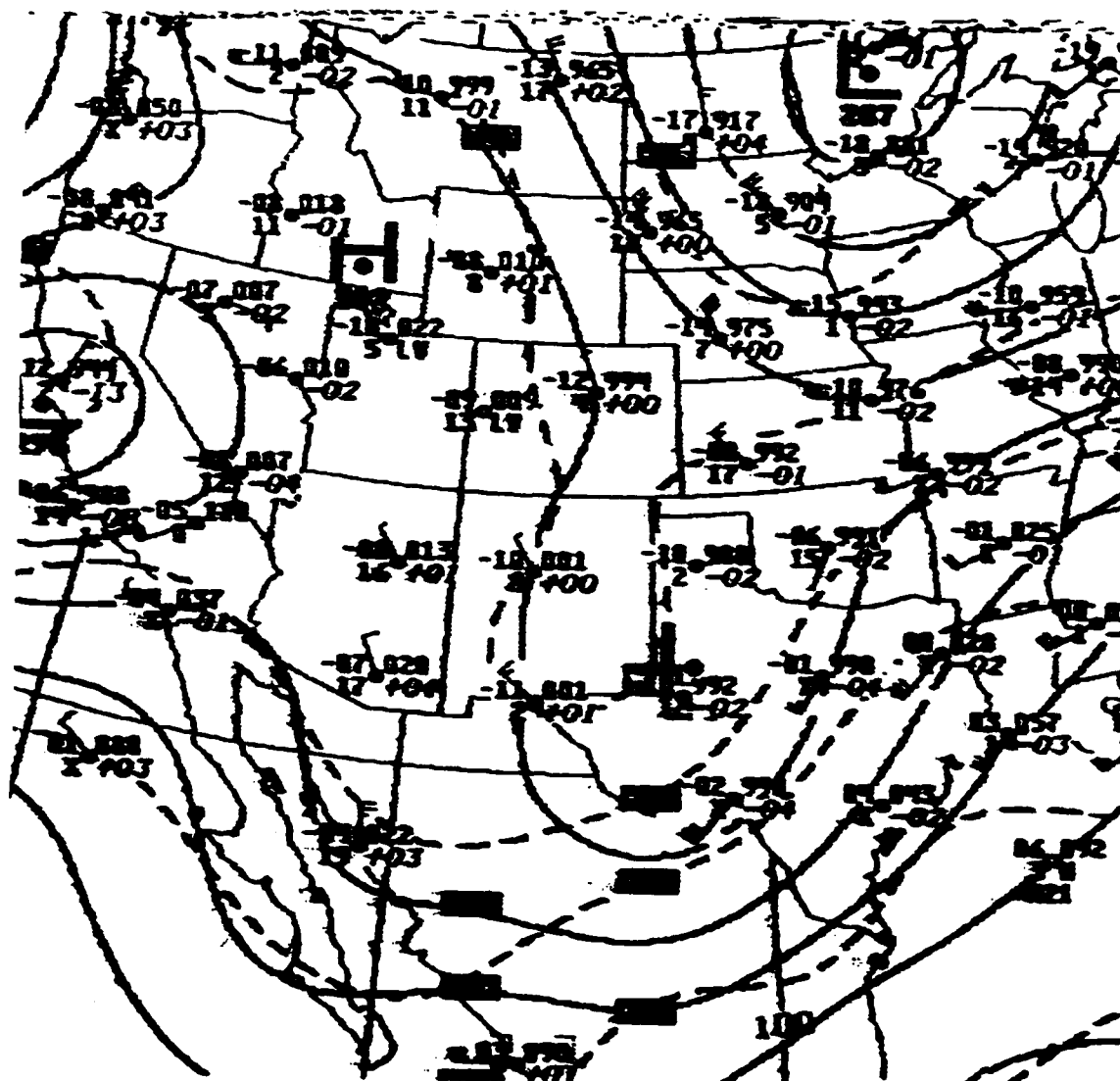


Figure B.9: As in Fig. B-5 except for 1700 MST, 21 February, 1987

APPENDIX C

SNOW COVER MAPS

This appendix contains the snow cover maps related to the observed mesoscale flow variations presented in Chapter 3 (Figs. C.1 through C.4).

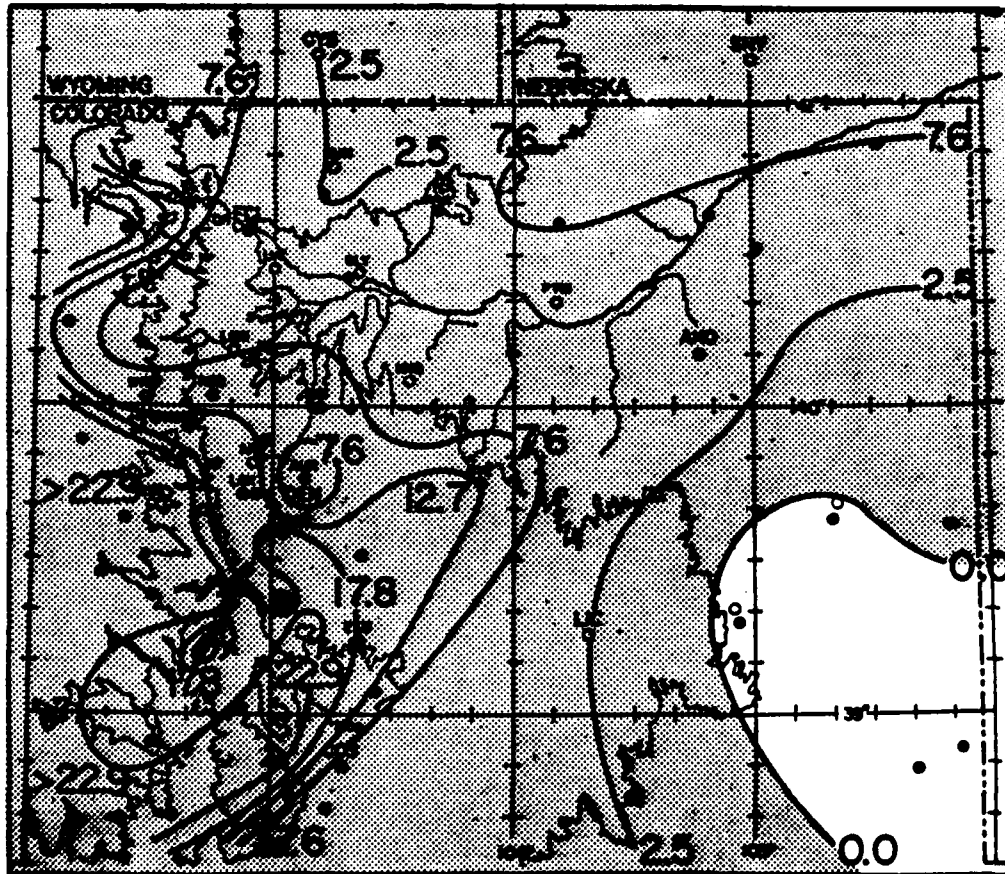


Figure C.1: Observed snow depth (cm) for 12 December, 1986. Snow depth is contoured at an irregular interval. (Data are courtesy of the Colorado Climate Center located at CSU.)

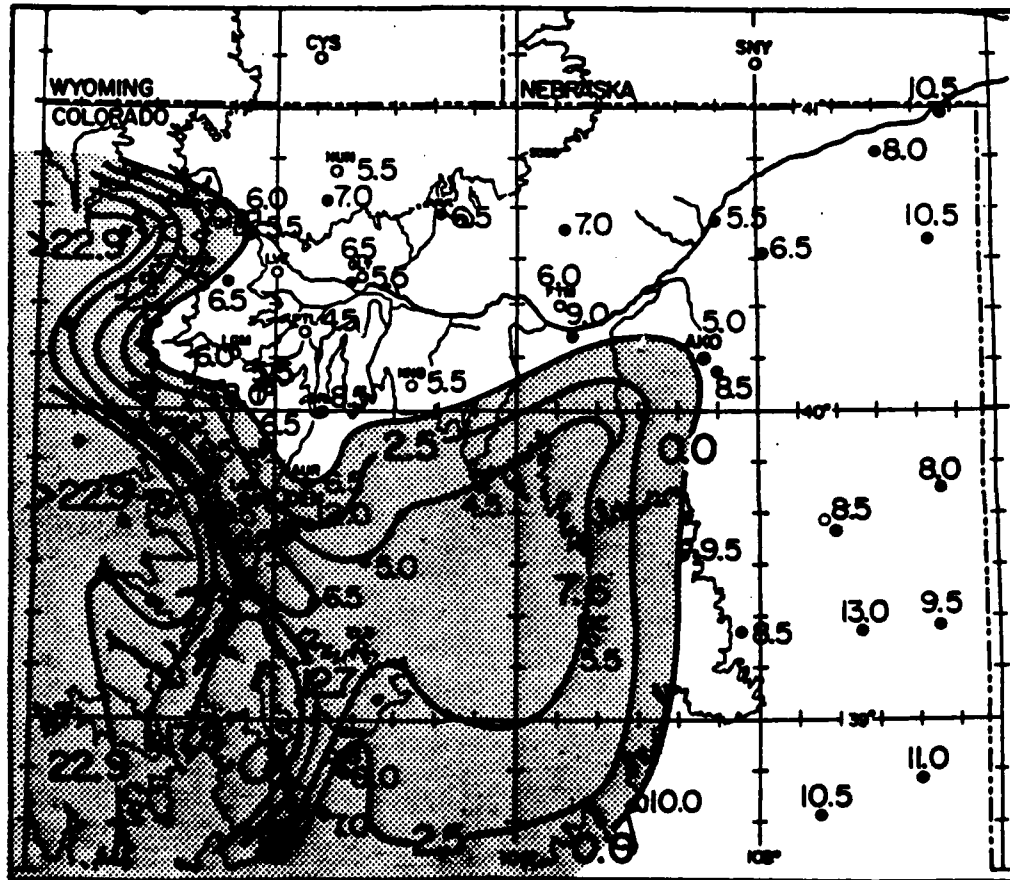


Figure C.2: As in Fig. C-1 except for 20 December, 1986. Analyzed with the aid of GOES visible imagery from 23 December, 1986. Note the period 20 December through 26 December, 1986 was without snowfall for this region.

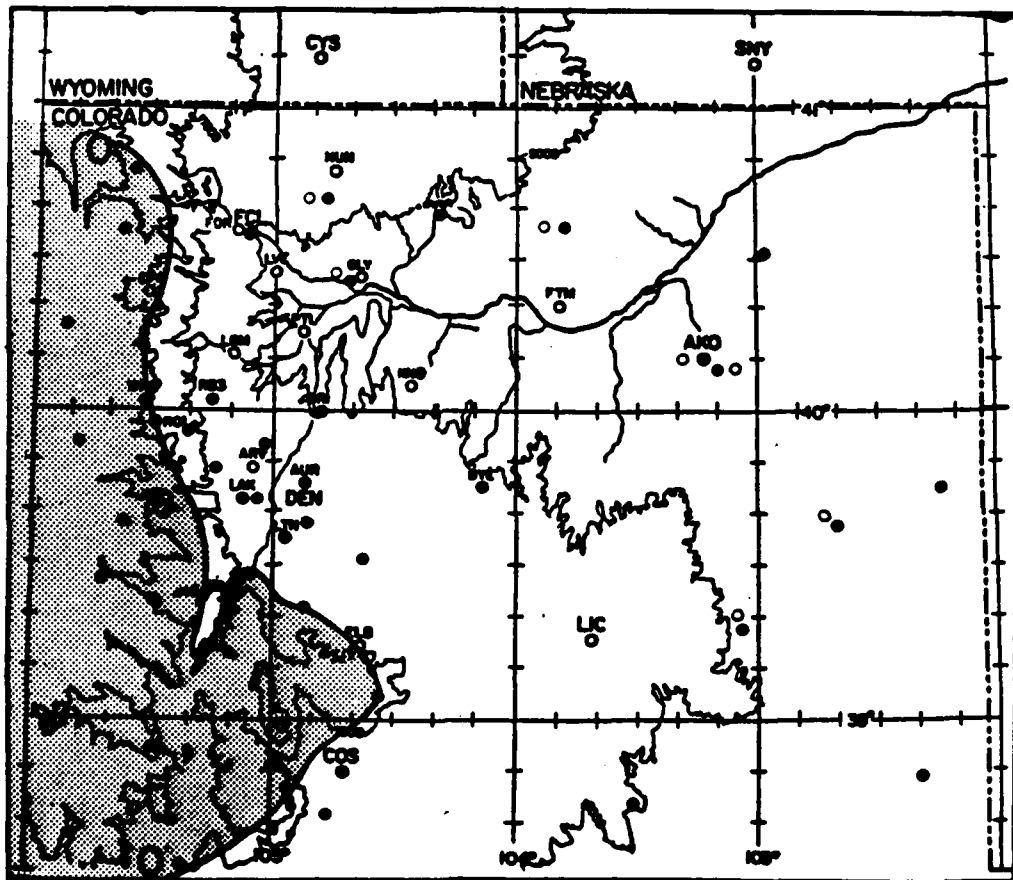


Figure C.3: As in Fig. C-1 except for 9 February, 1987.

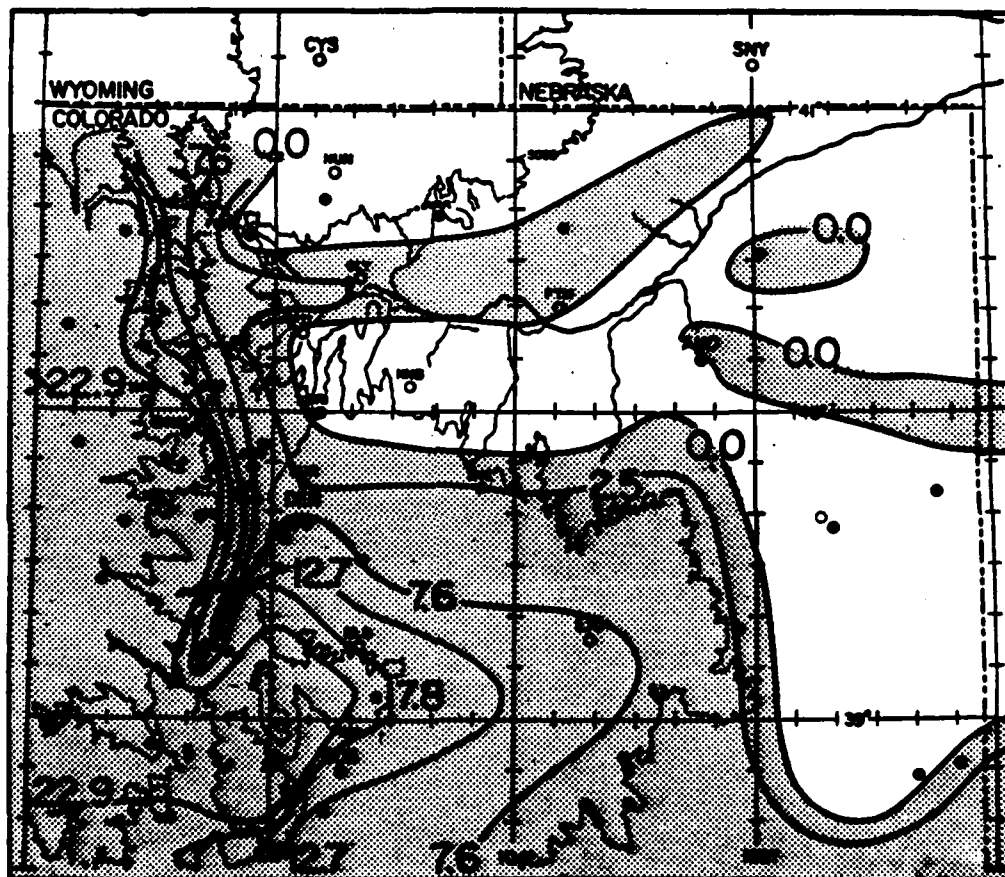


Figure C.4: As in Fig. C-1 except for 21 February, 1987.

APPENDIX D

PROCEDURE TO PRODUCE THE HEAT FLUX PLOTS IN CHAPTER 4

Sensible (H_S) and latent (H_L) heat fluxes were calculated for fifteen points along each horizontal flight transect to produce the heat flux plots presented in Chapter 4. All of the heat flux processing was performed using an NCAR RAF flux program generally following procedures previously established by Dr. Peter Hildebrand.

Each transect was divided into fifteen subsegments, with each overlapping the adjacent subsegments by 50%. Using the 20 sps data from magnetic tapes, average values for $w'T'$ and $w'q'$ were calculated for each subsegment and assigned to each subsegment centerpoint where w is the vertical wind speed, T is the air temperature, and q is the specific humidity. The prime symbol denotes perturbation, or fluctuating, quantities. A high-pass filter with a filter width of 120 s was used for the averaging.

From these averages, sensible and latent heat fluxes were calculated using

$$\begin{aligned}H_S &= w'T'\rho C_p \\H_L &= w'q'\rho L\end{aligned}$$

where ρ is the air density, C_p is the specific heat of air at constant pressure, and L is the latent heat of vaporization.